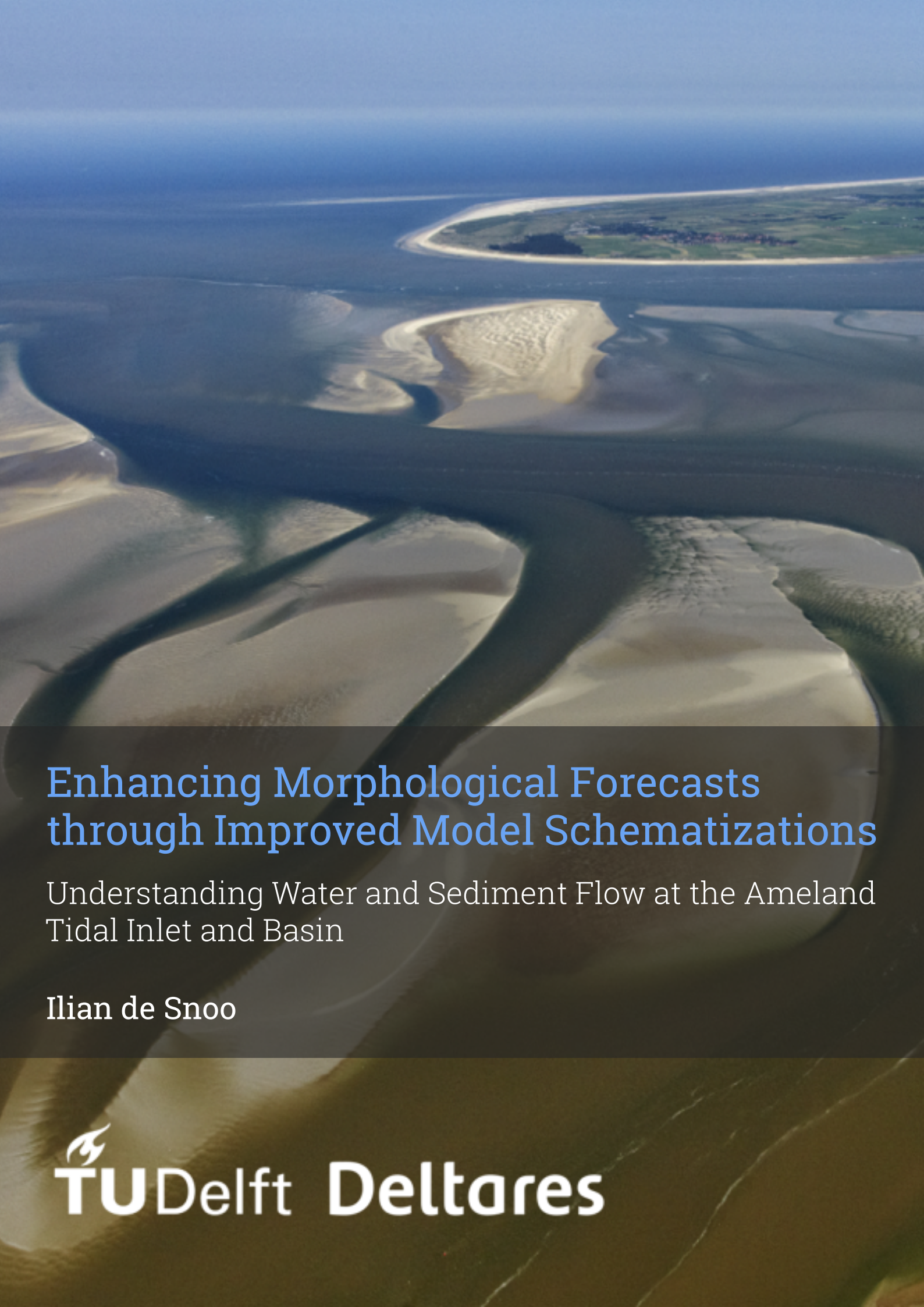

Enhancing Morphological Forecasts through Improved Model Schematizations

Understanding Water and Sediment Flow at the Ameland Tidal Inlet and Basin

Ilian de Snoo

TU Delft Deltares

Enhancing Morphological Forecasts through Improved Model Schematizations

Understanding Water and Sediment Flow at the Ameland Tidal Inlet and Basin

by

Ilian de Snoo

to obtain the degree of Master of Science
at the Delft University of Technology,
to be defended publicly on November 13th 2023.

Student number:	4718534	
Project duration:	December, 2023 – November, 2024	
Thesis committee:	Dr. ir. B.C. van Prooijen	TU Delft, chair
	Dr. ir. A.J.H.M. Reniers	TU Delft
	Dr. ir. A.P. Luijendijk,	TU Delft & Deltares
	Dr. ir. E. Elias	Deltares

Cover: Tidal inlet near Ameland, The Netherlands by Theo Stolk (Media bank Deltares)

An electronic version of this thesis is available at http://repository.tudelft.nl/.

Acknowledgements

This thesis concludes my study towards the degree of Master of Science in Hydraulic Engineering at Delft University of Technology. This research was conducted at the research institute Deltares and it has been an honour for me to work on such an intricate project with the esteemed experts of Deltares. I am very grateful for the opportunity to work on this thesis and will cherish this experience. This study would not have been possible without the support of my graduation committee. I would like to thank the committee members, Bram van Prooijen, Ad Reniers, Arjen Luijendijk and Edwin Elias for their time, effort and guidance throughout the research. My sincere gratitude is especially directed towards Arjen Luijendijk and Edwin Elias, who provided consistent feedback and engaged in constructive discussions on a weekly basis. I would finally like to thank Laura Brakenhoff from Rijkswaterstaat for supporting this research.

I am also grateful to my friends and family for their support and encouragement throughout this journey. While I am proud of the work presented here, I acknowledge that there are limitations and much work remains to be done on the subject of morphological forecasting of tidal inlets. I am eager to continue building upon what I have learned during this research, not only in a theoretical sense but also in terms of mental fortitude and approach to research projects in general.

Ilian de Snoo
Delft, September 2023

Abstract

The Wadden Sea serves multiple roles: it acts as a protective barrier against severe wave conditions, is a natural habitat for diverse flora and fauna and has recreational purposes. This research provides a comprehensive analysis of the intricate morphological dynamics of the Wadden Sea. By implementing various model schematizations, the study aims to enhance understanding of complex interactions between tidal inlets and basins, sediment transport dynamics, the influence of forcing actors and the importance of grid resolution. The ultimate goal is to improve the process-based models that are used to perform morphological forecasts, serving as a valuable tool for efficient coastal management and ensuring the preservation of this unique tidal ecosystem.

The study incorporates several schematizations, including the spatial extent of the modelling grid (domain schematization), grid resolution and various forcing components applied to the model boundaries and grid. Analysing water and sediment exchange between basins and through the Ameland tidal inlet has revealed distinct differences in hydrodynamics and morphodynamics across the model schematizations.

The single-inlet domain schematization encompassed only the Ameland tidal inlet region, while the more expansive multi-inlet schematization captured the entire Wadden Sea area. The single-inlet schematization does not account for hydrodynamic interactions between the Ameland basin and neighboring basins. This impacts sediment transport and morphological development in the Ameland inlet. A multi-inlet approach, encompassing the entire Wadden Sea, grants a more comprehensive model. The model with Wadden Sea domain schematization is essential for obtaining accurate results, as it showed significant differences in sediment transport compared to the single-inlet model. Modeling practices that exclude transport dynamics between tidal basins risk misrepresenting the natural processes in play.

Around the Ameland inlet, ebb dominance is observed in most regions, but there are exceptions in the marginal flood channel and at the outer side of the ebb-tidal delta. The Ameland model shows more ebb-dominance than the Wadden Sea model. Sediment transport during ebb periods exceed than during flood periods and differences in sediment transport between model schematizations are more pronounced during ebb than during flood.

Regarding the drivers of change, the spring-neap tidal cycle is particularly indicative of periods with meaningful residual sediment transport. Wind, especially from southwesterly directions, has a significant impact on water transport dynamics and a limited impact on sediment transport through the inlet.

Two grid schematizations are used, one with a base resolution of 60 by 60 meter and another with a high-resolution grid of 30 by 30 meter near the inlet. An enhanced grid resolution results in marginal changes in simulation outcomes, offering limited advantages for the conducted short-term morphological forecasts.

Overall, enhanced model schematizations can significantly improve short-term morphological forecasts of the Ameland tidal inlet, providing a more accurate and comprehensive representation of the complex hydrodynamic and sediment transport processes. Leveraging high-performance computing (HPC) for executing Delft3D-FM models has been central in this research, offering possibilities to enhance model resolution and reduce computational time.

The benefits of HPC come with the added challenge of mastering new software, handling larger models and interpreting more extensive data sets. A deep understanding of the physical processes and careful cost-benefit consideration is crucial, as increased computational power does not automatically resolve all modeling limitations. As such, the effective use of HPC in coastal modeling requires a balance between its sophisticated capabilities and the complexity it introduces.

Contents

Acknowledgements i

Summary ii

Table of Contents iii

List of Figures v

List of Tables xi

1 Introduction 1
- 1.1 Study area . . . 1
- 1.2 Relevance and context . . . 2
- 1.3 Previous studies . . . 4
- 1.4 Aim and research questions . . . 6
- 1.5 Reader guide . . . 6

2 Theoretical background 8
- 2.1 Inlet classification . . . 8
- 2.2 Morphological features . . . 9
  - 2.2.1 Present-day situation . . . 10
- 2.3 General principles and definitions of relevant hydrodynamic processes . . . 14

3 Research methodology 17
- 3.1 General research methodology . . . 17
- 3.2 Process-based modelling using Delft3D-FM . . . 18
- 3.3 Incorporation of high-performance computing . . . 19
- 3.4 Model setup . . . 19
  - 3.4.1 Grid and initial bathymetry . . . 19
  - 3.4.2 Grid resolution . . . 21
  - 3.4.3 Forcing components . . . 22
  - 3.4.4 Map file data management . . . 23
- 3.5 Model scenarios . . . 24

4 Results and analysis 25
- 4.1 Baseline simulation: Wadden Sea with tide-only forcing . . . 25
  - 4.1.1 Cross-sectional hydrodynamic analysis . . . 25
  - 4.1.2 Spatial maxima of ebb and flood transport . . . 30
  - 4.1.3 Spatial distribution and transect analysis of bed level change . . . 31
- 4.2 Variation in model domain (tide-only forcing) . . . 33
  - 4.2.1 Cross-sectional hydrodynamic analysis . . . 34
  - 4.2.2 Spatial maxima of ebb and flood transport . . . 38
  - 4.2.3 Spatial distribution and transect analysis of bed level change . . . 41
- 4.3 Variation in forcing processes (Wadden Sea domain) . . . 43
  - 4.3.1 Cross-sectional hydrodynamic analysis . . . 44
  - 4.3.2 Spatial distribution and transect analysis of bed level change . . . 49
- 4.4 Variation in grid resolution (Wadden Sea domain, tide-only forcing) . . . 53
  - 4.4.1 Cross-sectional hydrodynamic analysis . . . 53
  - 4.4.2 Spatial distribution and transect analysis of bed level change . . . 55

5 Synthesis and discussion 58
- 5.1 Synthesis . . . 58
  - 5.1.1 Transport overview . . . 58

5.1.2 Transport dynamics . . . 60
5.1.3 Morphological change . . . 62
5.2 Discussion . . . 62
5.2.1 Reflections on using high-performance computing . . . 63
5.2.2 Recommendations for future research . . . 63

6 Conclusions **65**
6.1 Main conclusion . . . 65
6.2 Sub-conclusions . . . 65

A Spatial transport asymmetry **68**

B Variation in domain **69**
B.1 Tide-only forcing . . . 70
B.2 Wind-inclusive forcing . . . 72

C Variation in resolution **79**

D Temporal and spatial visualization of wind flow **84**

E DelftBlue configuration **91**

List of Figures

1.1 An overview of the islands and inlets that form the Wadden Sea (based on picture from www.waddensea-secretariat.org). Top panel shows the 5 most westerly inlets of the Dutch Wadden Sea (Elias, 2020). . . . 2
1.2 A cascade of scales and relevant processes to describe the chang in inlet dynamics over various time and spatial scales for Ameland Inlet (Elias et al., 2020). . . . 3
1.3 Flowchart illustrating the structure and progression of this report. The figure outlines the major sections of the report and highlights the subdivisions within the ”Results and analysis” chapter. . . . 7

2.1 Graphical representation of tidal influence versus wave height, defining the regions of tide-dominated, mixed-energy and wave-dominated conditions. The position of Ameland Inlet is highlighted and falls into the mixed energy domain (Davis and Hayes, 1984). . . . 8
2.2 Sketch of the most important features and processes of a tidal inlet system (De Swart and Zimmerman, 2009). . . . 9
2.3 Topographic maps of the Ameland tidal inlet region showing in the top figure the broader geographical context and in the bottom figure a detailed overview of the ebb-tidal delta (Elias, 2020). . . . 11
2.4 Overview of ebb-tidal delta dynamics where (a) specifies the six distinct morphological zones; (b) determines the energy characteristics of the six zones; and (c) visualizes the interplay of wave-driven and tide-driven forces on sediment transport (Elias, 2021). . . . 13
2.5 Sketch of the various components of a tidal system (Stive and Wang, 2003). . . . 14
2.6 Approximate location of the tidal divides in the Wadden Sea over various years, based on the data from Vroom and Wang (2012). . . . 16

3.1 Flow diagram for Delft3D-FM, sourced from Hillen et al. (2009) and originally adapted from Roelvink (2006). . . . 18
3.2 Wadden Sea grid (base resolution). . . . 19
3.3 Visualization of the initial bathymetry (generated with Vaklodingen data from 2014 to 2018). 20
3.4 Location of thin dams on initial bathymetry to schematize multi-inlet Wadden Sea model as a single-inlet Ameland model. . . . 20
3.5 Naming and locations of cross-sections that are used for the cross-sectional hydrodynamic analysis. . . . 21
3.6 Base resolution grid and initial bathymetry at the inlet throat (grid cells are approximately 60 by 60 meters). . . . 21
3.7 High resolution grid and initial bathymetry at the inlet throat (grid cells are approximately 30 by 30 meters). . . . 22
3.8 Locations of the three sluices where inland water flows into the Wadden Sea basin. . . . 22
3.9 Selected partitions for base (left figure) and high (right figure) resolution grid to reduce data storage. . . . 23

4.1 Cumulative residual discharge for a 3-month simulation for five different cross-sections. The top Figure contains data for the tidal inlet, the middle for two cross-sections defined at the landside of the barrier island Terschelling and Ameland and the lower Figure for two cross-sections defined at the seaside of the barrier islands. . . . 26
4.2 Cumulative sediment transport for a 3-month simulation for five different cross-sections. The top figure contains data for the tidal inlet, the middle for two cross-sections defined at the landside of the barrier island Terschelling and Ameland and the lower figure for two cross-sections defined at the seaside of the barrier islands. . . . 27

4.3 Comparison of average flood and ebb velocities over time (top) for the tidal inlet cross-section and their difference (bottom) during the 3-month simulation period (positive difference meaning higher ebb velocity). 28
4.4 Comparison of average flood and ebb velocities over time (top) for the seaside Terschelling cross-section and their difference (bottom) during the 3-month simulation period (positive difference meaning higher ebb velocity). 29
4.5 Comparison of average flood and ebb velocities over time (top) for the seaside Ameland cross-section and their difference (bottom) during the 3-month simulation period (positive difference meaning higher ebb velocity). 29
4.6 Spatial representation of flow velocities (left column) and sediment transport (right column). Top row: averaged values per tidal cycle (12 hrs, 25 mins) for maximum ebb velocity/transport over a 7-day simulation; middle row: corresponding data for flood velocity/transport; bottom row: the difference between the ebb and flood values. 31
4.7 Top row: Ameland inlet initial bed level (left column) and bed level change (right column) after a 3-month simulation (Wadden Sea domain, water levels forcing, baseline grid resolution). Bottom row: Zoomed-in version of top row focusing on the ebb-tidal delta and highlighting the locations of Transect 1, Transect 2 and Transect 3. 32
4.8 Transect analyses of bed level change for three distinct transects. Figures 1A, 2A and 3A show the initial bed level with highlighted areas of sedimentation and erosion. Figures 1B, 2B and 3B provide quantified sedimentation and erosion values. The transect numbering is consistent with those presented in Figure 4.7. 33
4.9 Comparison of simulation results for the seaside Ameland cross-section for two different model domains: Ameland and Wadden Sea. The figure showcases five subplots: the topmost plot shows the cumulative discharge for both domains, followed by a plot on cumulative sediment transport. The third and fourth plots illustrate average velocities during flood and ebb periods, respectively. The lower plot highlights the difference between the average flood and ebb velocities (ebb-flood). 34
4.10 Comparison of simulation results for the seaside Terschelling cross-section for two different model domains: Ameland and Wadden Sea. The figure showcases five subplots: the topmost plot shows the cumulative discharge for both domains, followed by a plot on cumulative sediment transport. The third and fourth plots illustrate average velocities during flood and ebb periods, respectively. The lower plot highlights the difference between the average flood and ebb velocities (ebb-flood). 35
4.11 Comparison of simulation results for the tidal inlet cross-section for two different model domains: Ameland and Wadden Sea. The figure showcases five subplots: the topmost plot shows the cumulative discharge for both domains, followed by a plot on cumulative sediment transport. The third and fourth plots illustrate average velocities during flood and ebb periods, respectively. The bottom plot highlights the difference between the average flood and ebb velocities (ebb-flood). 36
4.12 Comparison of cumulative discharge (top figure) and sediment transport (lower figure) under tide-only forcing per tidal cycle (12 hrs, 25 mins) averaged over a 3-month simulation across the tidal inlet cross-section. Positive discharge and transport indicate westward and northward flow, while negative values represent southward and eastward flow. 37
4.13 Comparison of simulation results for two different model domains: Ameland and Wadden Sea. The graph represents average water flow velocities across the tidal inlet cross-section over a 3-day period. 38
4.14 Spatial representation of flow velocities comparing two different model domains: Ameland and Wadden Sea over the ebb-tidal delta. The left column (a) represents data from the Ameland simulation, while the right column (b) shows the difference in velocities between the Ameland and Wadden Sea simulations (Ameland-Wadden Sea). Top row: averaged values per tidal cycle (12 hrs, 25 mins) for maximum ebb flow velocity over a 7-day simulation; middle row: corresponding data for flood flow velocity; bottom row: the difference between the ebb and flood values. 39

4.15 Spatial representation of sediment transport comparing two different model domains: Ameland and Wadden Sea over the ebb-tidal delta. The left column (a) represents data from the Ameland simulation, while the right column (b) shows the difference in sediment transport between the Ameland and Wadden Sea simulations (Ameland-Wadden Sea). Top row: averaged values per tidal cycle (12 hrs, 25 mins) for maximum ebb sediment transport over a 7-day simulation; middle row: corresponding data for flood sediment transport; bottom row: the difference between the ebb and flood values. 40
4.16 Top row: Ameland inlet initial bed level (left column) and bed level change (right column) after a 3-month simulation (Ameland domain, tide-only forcing, baseline grid resolution). Bottom row: Zoomed-in version of top row focusing on the ebb-tidal delta. 41
4.17 Top row: Initial bed level of the Ameland inlet (left) and bed level change difference between the Ameland and Wadden Sea models after a 3-month simulation (right), under tide-only forcing and baseline grid resolution. Positive values indicate larger positive bed level changes in the Ameland simulation. Bottom row: Zoomed-in version of the top row focusing on the ebb-tidal delta. 42
4.18 Transect analyses of bed level change for three distinct transects. Comparison of simulation results for two different model domains: Ameland and Wadden Sea. Figures 1A, 2A and 3A show the initial bed level and bed level for the two simulations after 3 months. Figures 1B, 2B and 3B provide quantified sedimentation and erosion values. The transect numbering is consistent with those presented in Figure 4.7. 43
4.19 Temporal progression of cumulative water discharge for three different forcing scenarios at the landside Ameland (top figure) and Terschelling (bottom figure) cross-sections. . . 44
4.20 Comparison of simulation results for the tidal inlet cross-section for three different forcing processes: tide-only, water levels, wind. The figure showcases five subplots: the topmost plot shows the cumulative discharge for both domains, followed by a plot on cumulative sediment transport. The third and fourth plots illustrate average velocities during flood and ebb periods, respectively. The lowest plot highlights the difference between the average flood and ebb velocities (ebb-flood). 45
4.21 Comparison of simulation results for the seaside Ameland cross-section for three different forcing processes: tide-only, water levels, wind. The figure showcases five subplots: the topmost plot shows the cumulative discharge for both domains, followed by a plot on cumulative sediment transport. The third and fourth plots illustrate average velocities during flood and ebb periods, respectively. The lowest plot highlights the difference between the average flood and ebb velocities (ebb-flood). 46
4.22 Comparison of simulation results for the seaside Terschelling cross-section for three different forcing processes: tide-only, water levels, wind. The figure showcases five subplots: the topmost plot shows the cumulative discharge for both domains, followed by a plot on cumulative sediment transport. The third and fourth plots illustrate average velocities during flood and ebb periods, respectively. The lowest plot highlights the difference between the average flood and ebb velocities (ebb-flood). 47
4.23 Comparison of cumulative sediment transport for three forcing variations per tidal cycle (12 hrs, 25 mins) averaged over a 3-month simulation across the tidal inlet cross-section. Positive discharge and transport indicate westward and northward flow, while negative values represent southward and eastward flow. 48
4.24 Comparison of simulation results for three different forcing processes: tide-only, water levels, wind. The graph represents average water flow velocities across the tidal inlet cross-section over a 3-day period. 48
4.25 Top row: Ameland inlet initial bed level (left column) and bed level change (right column) after a 3-month simulation (Wadden Sea domain, water levels forcing, baseline grid resolution). Bottom row: Zoomed-in version of top row focusing on the ebb-tidal delta. 49
4.26 Top row: Initial bed level of the Ameland inlet (left) and bed level change difference between the tide-only and water levels forcing models after a 3-month simulation (right), with Wadden Sea domain and baseline grid resolution. Positive values indicate larger positive bed level changes in the tide-only simulation. Bottom row: Zoomed-in version of the top row focusing on the ebb-tidal delta. 50

4.27 Top row: Ameland inlet initial bed level (left column) and bed level change (right column) after a 3-month simulation (Wadden Sea domain, wind-inclusive forcing, baseline grid resolution). Bottom row: Zoomed-in version of top row focusing on the ebb-tidal delta. . 51
4.28 Top row: Initial bed level of the Ameland inlet (left) and bed level change difference between the tide-only and wind-inclusive forcing models after a 3-month simulation (right), with Wadden Sea domain and baseline grid resolution. Positive values indicate larger positive bed level changes in the tide-only simulation. Bottom row: Zoomed-in version of the top row focusing on the ebb-tidal delta. 52
4.29 Transect analyses of bed level change for three distinct transects. Comparison of simulation results for three different forcing variations. Figures 1A, 2A and 3A show the initial bed level and bed level for the three simulations after 3 months. Figures 1B, 2B and 3B provide quantified sedimentation and erosion values. The transect numbering is consistent with those presented in Figure 4.7. 53
4.30 Comparison of simulation results for the tidal inlet cross-section for two different grid resolution: 30x30 m cells and 60x60 m cells. The figure showcases five subplots: the topmost plot shows the cumulative discharge for both domains, followed by a plot on cumulative sediment transport. The third and fourth plots illustrate average velocities during flood and ebb periods, respectively. The lower plot highlights the difference between the average flood and ebb velocities (ebb-flood). 54
4.31 Comparison of cumulative discharge (top figure) and sediment transport (lower figure) for simulations with different grid resolution under tide-only forcing averaged per tidal cycle (12 hrs, 25 mins) over a 3-month simulation across the tidal inlet cross-section. Positive discharge and transport indicate westward and northward flow, while negative values represent southward and eastward flow. 55
4.32 Comparison of bed level changes in Ameland inlet models with different grid resolutions: Top figure shows initial bathymetry differences interpolated from an unstructured to a structured grid, illustrating the variation in initial bed elevation due to grid resolution. Middle figure displays the bed level changes simulated with a higher grid resolution model. The bottom figure compares the bed level change of the baseline grid resolution model with that of the higher resolution model. Positive values indicate larger positive bed level changes in the baseline grid model simulation. 56
4.33 Transect analyses of bed level change for three distinct transects. Comparison of simulation results for two different grid resolution: base and high-resolution. Figures 1A, 2A and 3A show the initial bed level and bed level for the two simulations after 3 months. Figures 1B, 2B and 3B provide quantified sedimentation and erosion values. The transect numbering is consistent with those presented in Figure 4.7 57

5.1 Sketch of the Ameland inlet region including a quantitative description of average discharge and sediment transport per tidal cycle (12 hours and 25 minutes) for the simulation with Wadden Sea domain, base resolution grid and tide-only forcing. 59
5.2 Sketch of the Ameland inlet region including a quantitative description of average discharge and sediment transport per tidal cycle (12 hours and 25 minutes) for the simulation with Ameland domain, base resolution grid and tide-only forcing. 59
5.3 Sketch of the Ameland inlet region including a quantitative description of average discharge and sediment transport per tidal cycle (12 hours and 25 minutes) for the simulation with Wadden Sea domain, high resolution grid and tide-only forcing. 60
5.4 Schematic representation of the water and sediment transport dynamics at the Terschelling and Ameland barrier islands. Adapted from De Swart and Zimmerman (2009), see Figure 2.2. 63

A.1 Spatial representation of flow velocities (left column) and sediment transport (right column), zoomed-in version of figure 4.6. Top row: averaged values per tidal cycle (12 hrs, 25 mins) for maximum ebb velocity/transport over a 7-day simulation; middle row: corresponding data for flood velocity/transport; bottom row: the difference between the ebb and flood values. 68

B.1 Comparison of cumulative discharge (top figure) and sediment transport (lower figure) under tide-only forcing per tidal cycle (12 hrs, 25 mins) averaged over a 3-month simulation across the tidal inlet cross-section. Positive discharge and transport indicate westward and northward flow, while negative values represent southward and eastward flow. 70
B.2 Comparison of cumulative discharge (top figure) and sediment transport (lower figure) under tide-only forcing per tidal cycle (12 hrs, 25 mins) averaged over a 3-month simulation across the tidal inlet cross-section. Positive discharge and transport indicate westward and northward flow, while negative values represent southward and eastward flow. 71
B.3 Comparison of simulation results for the tidal inlet cross-section for two different model domains: Ameland and Wadden Sea. The figure showcases five subplots: the topmost plot shows the cumulative discharge for both domains, followed by a plot on cumulative sediment transport. The third and fourth plots illustrate average velocities during flood and ebb periods, respectively. The bottommost plot highlights the difference between the average flood and ebb velocities (ebb-flood). 72
B.4 Comparison of simulation results for the seaside Terschelling cross-section for two different model domains: Ameland and Wadden Sea. The figure showcases five subplots: the topmost plot shows the cumulative discharge for both domains, followed by a plot on cumulative sediment transport. The third and fourth plots illustrate average velocities during flood and ebb periods, respectively. The bottommost plot highlights the difference between the average flood and ebb velocities (ebb-flood). 73
B.5 Comparison of simulation results for the seaside Ameland cross-section for two different model domains: Ameland and Wadden Sea. The figure showcases five subplots: the topmost plot shows the cumulative discharge for both domains, followed by a plot on cumulative sediment transport. The third and fourth plots illustrate average velocities during flood and ebb periods, respectively. The bottommost plot highlights the difference between the average flood and ebb velocities (ebb-flood). 74
B.6 Comparison of simulation results for two different model domains: Ameland and Wadden Sea. The graph represents average water flow velocities across the tidal inlet cross-section over a 3-day period. 74
B.7 Top row: Ameland inlet initial bed level (left column) and bed level change (right column) after a 3-month simulation (Ameland domain, wind-inclusive forcing, baseline grid resolution). Bottom row: Zoomed-in version of top row focusing on the ebb-tidal delta. 75
B.8 Top row: Ameland inlet initial bed level (left column) and bed level change (right column) after a 3-month simulation (Wadden Sea domain, wind-inclusive forcing, baseline grid resolution). Bottom row: Zoomed-in version of top row focusing on the ebb-tidal delta. 76
B.9 Top row: Initial bed level of the Ameland inlet (left) and bed level change difference between the Ameland and Wadden Sea models after a 3-month simulation (right), under wind-inclusive forcing and baseline grid resolution. Positive values indicate larger positive bed level changes in the Ameland simulation. Bottom row: Zoomed-in version of the top row focusing on the ebb-tidal delta. 77
B.10 Transect analyses of bed level change for three distinct transects. Comparison of simulation results for two different model domains with wind-inclusive forcing. Figures 1A, 2A, and 3A show the initial bed level and bed level for the three simulations after 3 months. Figures 1B, 2B, and 3B provide quantified sedimentation and erosion values. The transect numbering is consistent with those presented in Figure 4.7. 78

C.1 Comparison of simulation results for the seaside Ameland cross-section for two different grid resolution: 30x30 m cells and 60x60 m cells. The figure showcases five subplots: the topmost plot shows the cumulative discharge for both domains, followed by a plot on cumulative sediment transport. The third and fourth plots illustrate average velocities during flood and ebb periods, respectively. The lower plot highlights the difference between the average flood and ebb velocities (ebb-flood). 80

C.2 Comparison of simulation results for the seaside Terschelling cross-section for two different grid resolution: 30x30 m cells and 60x60 m cells. The figure showcases five subplots: the topmost plot shows the cumulative discharge for both domains, followed by a plot on cumulative sediment transport. The third and fourth plots illustrate average velocities during flood and ebb periods, respectively. The lower plot highlights the difference between the average flood and ebb velocities (ebb-flood). 81
C.3 Comparison of cumulative discharge (top figure) and sediment transport (lower figure) for simulations with different grid resolution under tide-only forcing averaged per tidal cycle (12 hrs, 25 mins) over a 3-month simulation across the seaside AmelandC cross-section. Positive discharge and transport indicate westward and northward flow, while negative values represent southward and eastward flow. 82
C.4 Comparison of cumulative discharge (top figure) and sediment transport (lower figure) for simulations with different grid resolution under tide-only forcing averaged per tidal cycle (12 hrs, 25 mins) over a 3-month simulation across the seaside TerschellingE cross-section. Positive discharge and transport indicate westward and northward flow, while negative values represent southward and eastward flow. 83

D.1 Average wind flow from 22-6-2017 to 14-9-2017. 84
D.2 Average wind flow from 22-6-2017 to 4-7-2017. 85
D.3 Average wind flow from 4-7-2017 to 11-7-2017. 85
D.4 Average wind flow from 11-7-2017 to 18-7-2017. 86
D.5 Average wind flow from 18-7-2017 to 26-7-2017. 86
D.6 Average wind flow from 26-7-2017 to 4-8-2017. 87
D.7 Average wind flow from 4-8-2017 to 7-8-2017. 87
D.8 Average wind flow from 7-8-2017 to 9-8-2017. 88
D.9 Average wind flow from 9-8-2017 to 16-8-2017. 88
D.10 Average wind flow from 16-8-2017 to 23-8-2017. 89
D.11 Average wind flow from 23-8-2017 to 2-9-2017. 89
D.12 Average wind flow from 2-9-2017 to 8-9-2017. 90
D.13 Average wind flow from 8-9-2017 to 14-9-2017. 90

E.1 DelftBlue supercomputer at TU Delft 91

List of Tables

3.1 The 16 tidal constituents for northern boundary (location 3) with highest Signal-to-Noise Ratio (SNR). 23
3.2 Overview of all model simulation set-ups that are performed during the research. 24
3.3 Overview of model simulations which results are used per results section of Chapter 4. 24

4.1 Summary of wind conditions from 06-22-2017 to 09-14-2017 44

1

Introduction

This chapter begins by introducing the study area in Section 1.1, emphasizing its geographical importance and its value for both nature and humans. This is followed by a description of the characteristics of the area. Thereafter, the challenges that this area encounters, which are central to this research, are addressed. Section 1.2 discusses the relevance and provides context to the research topic. It describes three key components of model schematization: model domain, forcing components and grid resolution. Section 1.3 provides insights derived from prior studies and highlights the active interest in enhancing the understanding of the physical processes that are at play in this area. The main research question and sub-questions are formulated in Section 1.4. Section 1.5 serves as a guide for readers.

1.1. Study area

The Dutch Wadden Sea (Figure 1.1) is a tidal region located in the northern part of The Netherlands. It serves multiple purposes, including protection against severe wave conditions, providing a natural habitat for animals and plants and being an area for leisure activities. The Wadden Sea consists of barrier islands, tidal inlets, ebb-tidal deltas and basins.

Barrier islands are narrow strips of offshore deposited sediment that are parallel to the coast. Over time, these islands can change in size, shape and location, primarily due to the action of tides and waves. Tidal inlets are narrow waterways between barrier islands, allowing water to flow between the tidal basins and the ocean. Ebb-tidal deltas are sedimentary deposits located at the seaward side of a tidal inlet. They form as a result of sediment deposition occurring mainly during ebb tides. In contrast, flood-tidal deltas form on the landward side of the inlet and result from sediment deposition during the incoming tides. Tidal basins are areas that fill with water during high tides and drain during low tides, often exhibiting rich biodiversity.

The Wadden Sea tidal system is considered a sand-sharing system, as it exchanges sediment between its components to get to an equilibrium state regarding the distribution of available sediment (Elias, 2020). This process is described by conceptual models of e.g., Dean (1988); Stive and Wang (2003). Since 1935, approximately 650 million cubic meters of sediment have been imported into the Wadden Sea tidal basins (Elias, 2020; Elias et al., 2012). Much of this sediment comes from eroding ebb-tidal deltas, which are rapidly decreasing in volume (Elias et al., 2012). Although there has recently been a pilot sand nourishment (e.g., Elias, 2021), the Wadden Sea is still a relatively pristine tidal region (Elias, 2020). Only the size of the basins and barriers has been determined by coastal defense works, closure dams, dikes, seawalls and land reclamations (Elias, 2020). As a result, natural processes can freely happen within these established boundaries.

For effective and efficient coastal management, it is essential to understand the governing processes that shape and evolve this area over time. Focus is especially directed to the Ameland inlet (see Figure 1.1), as there are already a lot of ongoing endeavours to understand its physical processes and there is abundance of available field data. The relatively pristine nature, combined with the dynamic and ever-changing morphology, makes it an excellent research area.

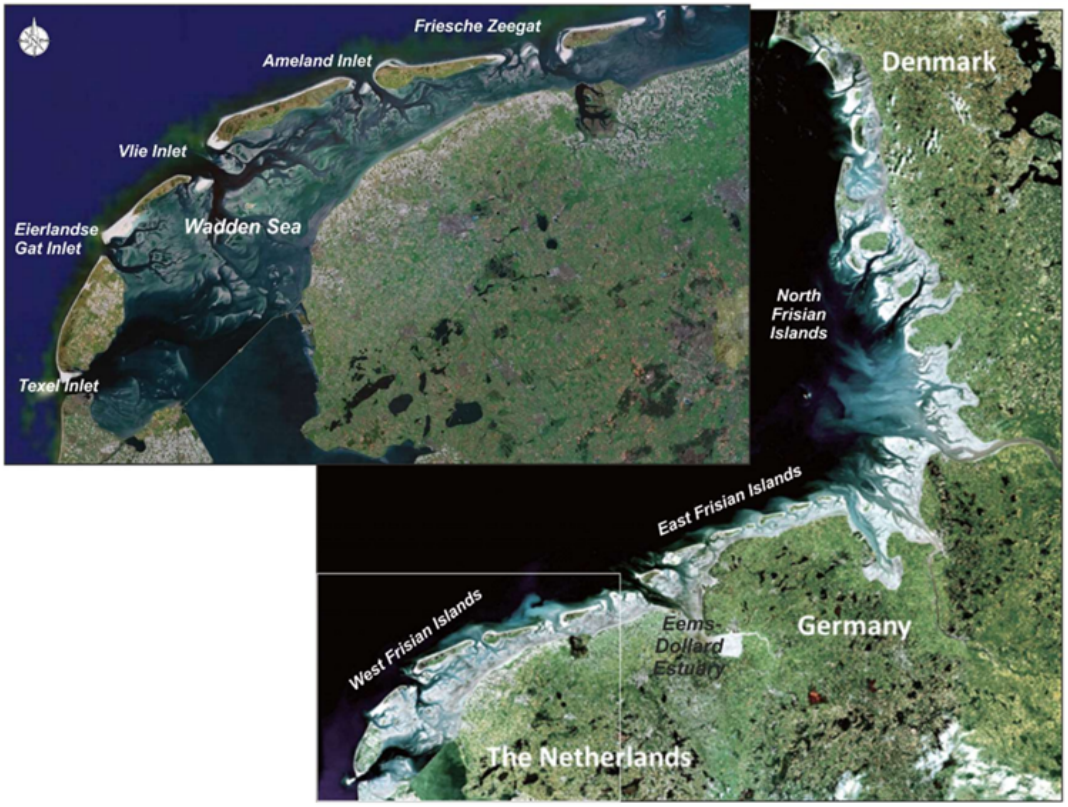

Figure 1.1: An overview of the islands and inlets that form the Wadden Sea (based on picture from www.waddensea-secretariat.org). Top panel shows the 5 most westerly inlets of the Dutch Wadden Sea (Elias, 2020).

1.2. Relevance and context

This research aims to improve the understanding of the key physical processes that influence the morphology the Ameland inlet by performing morphological forecasts with various model schematizations. When performing morphological forecasts, various forcing components are imposed upon a modelling grid with initial bathymetry and the resulting morphological changes can be analysed to determine the areas of erosion and sediment deposition. By varying the model schematization, alternative sedimentation and erosion patterns can be found. Comprehending the causes of these variations, by analysing hydrodynamic and morphodynamic processes, help identify the processes responsible for specific morphological changes. This can help improve future models of tidal inlets.

A process-based model is essential for this kind of research, as it represents the underlying processes in a system. One of the challenges in creating models that mimic the physical processes at the Ameland tidal inlet lies in schematizing the real-world complex processes and the interactions between them. Three important aspects of the schematization process are defining the model domain, selecting a grid resolution and imposing forcing components on the grid (boundaries). The schematizations should possess enough detail to ensure the model accurately portrays the physical processes of interest, while keeping computational requirements feasible.

Below each of these three important aspects of schematization process are discussed. This section ends by introducing the notion of residual transport.

Domain schematization
The model domain schematization determines the spatial extent of the modelling grid. The domain should be large enough to include all relevant processes and interactions that affect the system dynamics, but it should also be focused enough to ensure the specific area of interest is captured in sufficient detail. In the case of the Ameland tidal inlet, the domain might need to include regions upstream and downstream of the inlet, e.g., adjacent basins, inlets and ebb-tidal deltas. The water and

sediment transport dynamics between the Ameland basin and Terschelling basin (see Figure 2.3) could, for example, impact the morphological development of the Ameland ebb-tidal delta. Properly defining the domain ensures that boundary effects, which can significantly influence morphological change, are adequately addressed.

Grid schematization

The model grid schematization is important for determining the spatial resolution of the model. The resolution directly influences the level of detail at which the processes are resolved. A fine grid resolution can capture small-scale processes and features but comes at the cost of exponentially increasing computational requirements. In contrast, a coarser grid may overlook certain small-scale processes but the hydro- and morphodynamics will be faster to compute. For the intricate tidal interactions and sediment transport processes at the Ameland tidal inlet, it is crucial to strike a balance. Too coarse a grid might miss critical sediment transport dynamics, while a too fine grid can become computationally impractical.

To make understanding of the morphological development of the Ameland inlet easier, Elias et al. (2019) introduced a morphodynamic scale-cascade that encompasses four levels of aggregation: individual shoals, the ebb-tidal delta, the inlet system and the Wadden Sea as a whole (Figure 1.2). It was initially believed that small morphodynamic changes at the shoal level (level 1) would not significantly impact the ebb-tidal delta (level 2) or the dynamics of the inlet (level 3). Recently, Elias et al. (2019) demonstrated that interactions stemming from individual shoals can trigger complete channel and shoal relocation at the delta scale, potentially altering the configuration of the ebb-tidal delta. As a result, small-scale disturbances can have a substantial impact on the larger scales (Elias, 2021). Hence, if interested in the development of larger-scale morphological features, it is important to consider including smaller-scale morphological features and the dynamics around them. This underscores the importance of grid schematization, which includes having sufficient resolution for each grid cell and the associated bathymetric data.

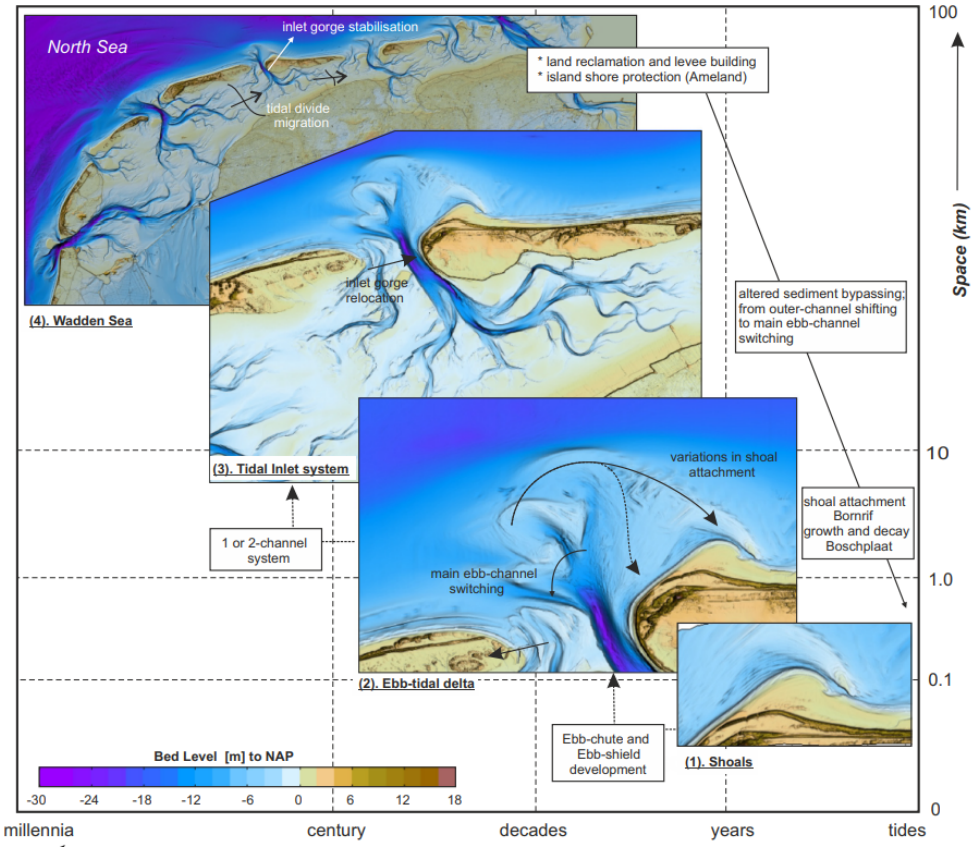

Figure 1.2: A cascade of scales and relevant processes to describe the chang in inlet dynamics over various time and spatial scales for Ameland Inlet (Elias et al., 2020).

Forcing components schematization
Forcing components, such as tidal constituents, imposed water level fluctuations on the model grid boundaries and wind, play a crucial role in driving morphological changes within a tidal system. While tidal constituents primarily represent the periodic rise and fall of sea levels due to the gravitational forces of the moon and the sun, the water level fluctuations incorporate other elements such as surge effects resulting from atmospheric pressures, river discharge and other dynamic processes. This research involves running models with various combinations of these forcing scenarios. Specifically, one model will focus on tide-only, another will impose water level fluctuations on the grid boundaries and another will integrate both the water level fluctuations and wind distribution over the model grid. While the detailed schematization of each individual forcing component is undeniably important, this study will not go into that aspect. This approach is chosen because the study uses a high-performance computing cluster, which is a relatively novel domain in morphodynamic modelling. This research serves as an initial exploration into utilizing high-performance computing (HPC) for tidal inlet morphological modelling. The ”brute-force” approach, i.e., using complete time series forcing components, is selected to optimize the utilization of available HPC resources. Analysing the effects of various scenarios of model forcing components is essential for a better understanding of how individual forcing components affect morphological change.

Residual transport
An effective method of analysing the differences in morphological changes between the model schematizations discussed above is looking at residual transport. Residual transport refers to the net transport over a certain period of time. Specifically, this analysis will focus on two aspects that are related to residual transport: the asymmetry in maximum and minimum spatial velocity and the asymmetry in maxima and minima spatial sediment transport. Asymmetry in maximum and minimum velocity can lead to uneven sediment transport, resulting in morphological change. These spatial maps are used to further enhance the understanding of morphological changes for the various model scenarios. This analysis can help identify areas that need improvement and ultimately lead to more accurate predictions of morphodynamic processes in tidal systems.

1.3. Previous studies

Studies performing morphological forecasts of the Ameland tidal inlet typically start by defining a modelling goal and then determining an appropriate model schematization. The challenge is to find a balance between computational requirements and a model schematization that is sufficiently detailed to be able to accurately model the morphological development of the Ameland tidal inlet. As computational resources are often limited and there is need to achieve research goals within specific timeframes, limitations exist within current state-of-the-art Ameland inlet models.

The model used by Harlequin (2021) tends to address the migration of individual morphological features, such as ebb-chute and -shield systems (first level of the cascade of scales, see Figure 1.2), rather than their development. A too schematized model might results in no or limited new morphological features to emerge from small-scale instabilities. These small-scale instabilities could, for example, emerge from extreme episodic storm events. Having to coarse forcing components schematization might result in limited generation of instabilities. Another schematization component to note in this study is the choice of domain schematization. The modelling domain only encompasses the Ameland ebb-tidal delta, inlet and basin and thus does not account for water and sediment transport between basins. Making the assumption that there is a theoretical tidal divide behind the barrier islands allows the model domain to be truncated at that tidal divide. Theoretically, no transport at this location would imply no impact on the morphological development of the Ameland ebb-tidal delta. However, it has been demonstrated that this theory does not always hold up, as there is for example exchange of water between the Terschelling and Ameland basins, particularly during strong south-western winds (Van Weerdenburg et al., 2021). This exchange does affect the morphological development of the Ameland ebb-tidal delta, but the extent of this impact is not yet fully understood.

State-of-the-art Ameland models being a too overly simplified representation of the real-world complex situation, could be the reason for recent modelling studies on the Ameland tidal inlet to have struggled to accurately predict morphological changes over longer simulation periods ($\mathcal{O}$ 4 years). While these

models perform reasonably well for shorter timescales ($\mathcal{O}$ 1 years), they tend to underestimate sediment transport in wave-dominated areas and fail to capture the dynamics of tide-dominated regions, such as ebb chutes and shield systems. This limitation becomes more pronounced as the simulation extends, resulting in greater discrepancies between the models predicted morphology and the actual measurements (Elias, 2021; Harlequin, 2021).

This research incorporates several recommendations made in recent literature for improving model schematization. First of all, the magnitude of sediment transport along the barrier islands is generally lower in models compared to measurement data. Thus, increasing the grid resolution along the coasts of the neighboring barrier islands is recommended to capture cross- and alongshore variations accurately, particularly in the surf zone (Harlequin, 2021). Secondly, current models for the Ameland ebb-tidal delta are considered medium-term (up to 5 years) and meso-scale (up to 10 km) models (Harlequin, 2020). These models capture the influence of larger-scale hydrodynamics and morphodynamics, as well as short-term morphological effects. However, to accurately simulate medium-term changes and allow for the interaction of small-scale features with larger morphological features, more advanced high-resolution morphodynamic models are needed. Therefore, entire time series are imposed on the models boundaries for the forcing components (”brute-force” forcing), limiting the level of schematization. This is also according to the recommendation by Harlequin (2021) that including storms in more detail could help more accurately predict morphological changes. Finally, the use of coarse grid resolutions in proportion to the size of the study area may hinder the accurate representation of minor local variations. This is particularly problematic given the latest findings suggesting that even small-scale disturbances can have effects on the entire tidal inlet system (Elias et al., 2020). Therefore, an advanced high-resolution morphodynamic model is recommended for the Ameland ebb-tidal delta to enable the interaction of small-scale features with larger morphological features.

Measurement data is widely available for the Wadden Sea and Ameland ebb-tidal delta, as several research programs have been and are conducted by the Dutch Directorate for Public Works and Water Management (Rijkswaterstaat) in collaboration with various companies, universities and research institutes. These programs aim to enhance our understanding of coastal morphology and develop effective strategies for coastal management. The most relevant program for this research project is Kustgenese2.0, a research project focused on studying the morphological development of the Dutch coastal zone. Research institutions such as Deltares, TU Delft and Utrecht University have contributed this project. It utilizes numerical models, field measurements and remote sensing techniques to analyse coastal morphological changes.

Other research programs focused on the Ameland tidal inlet include KPP B&O and SEAWAD. KPP B&O aimed to understand the role of sand nourishments through morphodynamic modeling and gain knowledge about the functioning of the Ameland tidal inlet. SEAWAD focused on bedforms, sediment transport and wave-current interactions on the outer delta. These research programs have generated valuable knowledge that contributes to the study of the Ameland ebb-tidal delta. Additionally, a recent government-funded research program called WadSED (Wadden Sea and Estuaries: System Dynamics and Sediment Management under Climate Change) was announced in December 2022. WadSED aims to innovate sediment management programs, tools and policies to protect the Dutch coast from rising sea levels, declining biodiversity and high dredging costs. These research efforts demonstrate the active nature of research into the Ameland tidal inlet region.

1.4. Aim and research questions

The primary aim of this thesis is to assess the added benefits of a morphodynamic forecast model with improved model schematization by critically examining and three important schematization components: the model domain, grid resolution and forcing components. The following main research questions has been formulated:

To what extent can improved model schematizations enhance short-term morphological forecasts of the Ameland tidal inlet?

Four sub-questions have been formulated to help answer the main research question:

Sub-question 1: What is the influence of single-inlet schematization?
This sub-question aims to analyse at the hydrodynamic interaction and sediment exchange between the Ameland tidal basin and adjacent basins. Furthermore, the influence of the interactions on morphological changes of the Ameland tidal inlet are discussed.

Sub-question 2: What is the influence of various forcing processes?
This sub-question has the aims to compare the effects of different combinations forcing components and analyse their effect on morphological changes.

Sub-question 3: What is the added value of increasing grid resolution?
This sub-questions aim to discuss the importance of capturing smaller-scale features and processes by comparing morphological changes between the base-resolution and the high-resolution model.

Sub-question 4: How does residual sediment transport vary across the various model schematizations?
This sub-question aims to asses the effects of model schematization on residual transport. The study specifically determines the maxima and minima spatial flow velocities and sediment transport.

1.5. Reader guide

In Chapter 1, the specific study area (1.1) being researched is introduced. This is followed by the relevance and context (1.2) of the study and the relevant information from previous studies (1.3). This chapter also sets out the aim and research questions (1.4) and provides this reader guide (1.5).

Chapter 2 focuses on the theoretical background. It starts with an overview of inlet classification (2.1) and moves on to morphological features (2.2), which includes detailing of the present-day morphological situation (2.2.1). The chapter ends by highlighting the general principles and definitions of relevant hydrodynamic processes (2.3).

Chapter 3 is all about the research methodology. The general research methodology (3.1) is discussed first, followed by introducing process-based modelling using Delft3D-FM (3.2) and stating the role of high-performance computing (3.3) in this study. More details on model setup are then provided (3.4), with subsections on model grid and initial bathymetry (3.4.1), grid resolution (3.4.2), forcing components (3.4.3) and map file data management (3.4.4). This chapter ends by presenting the different model scenarios (3.5) used in the study.

Chapter 4 contains the results and analysis. It begins with a comprehensive analysis of the baseline simulation: Wadden Sea domain with tide-only forcing (4.1). This foundational understanding is established to serve as a basis for analysing subsequent results of simulations with varying model schematizations. First variations in domain schematization (4.2) are explored, succeeded by an assessment of variations in forcing processes (4.3). The chapter then concludes with the impact of grid resolution (4.4). This report structure is visualized in Figure 1.3.

Chapter 5 contains the synthesis and discussion. This chapter provides an overview of transports (5.1.1) and synthesizes transport dynamics (5.1.2) and observed morphological change (5.1.3). Then a discussion follows, including reflecting on the use of high-performance computing (5.2.1) and making recommendations for future research (5.2.2).

Chapter 6 concludes the main body of the report. It answers the main research question (6.1) and sub-research questions (6.2).

Additional results for comparing models with different schematizations are provided in Appendices A, B and C. The temporal and spatial visualizations of wind flow are in Appendix D and Appendix E provides details about DelftBlue high-performance computing.

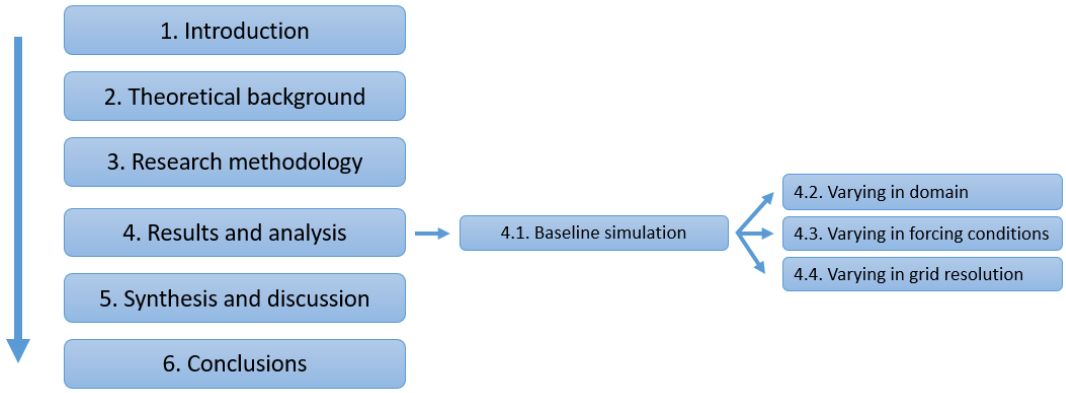

Figure 1.3: Flowchart illustrating the structure and progression of this report. The figure outlines the major sections of the report and highlights the subdivisions within the ”Results and analysis” chapter.

2

Theoretical background

The objective of this chapter is to classify the Ameland tidal inlet (2.1), to discuss the morphological characteristics (2.2) and to provide a general understanding of the primary physical processes shaping the area (2.3).

2.1. Inlet classification

The Wadden Sea has a tidal range ranging from eastern to western direction from 1.4 meters to 4.4 meters. The significant wave height averages 1.4 meters (Elias et al., 2020). The Ameland inlet specifically has a tidal range of 2.0 meter. Based on the characterization of tidal inlets, the Ameland inlet can be categorized as a mixed-energy inlet (Figure 2.1). In mixed-energy inlets, both wave and tidal forces influence its dynamics. Generally, the barrier islands in these conditions have a ”drumstick” shape (wide and short) with stable tidal inlets in between them (Davis and Hayes, 1984).

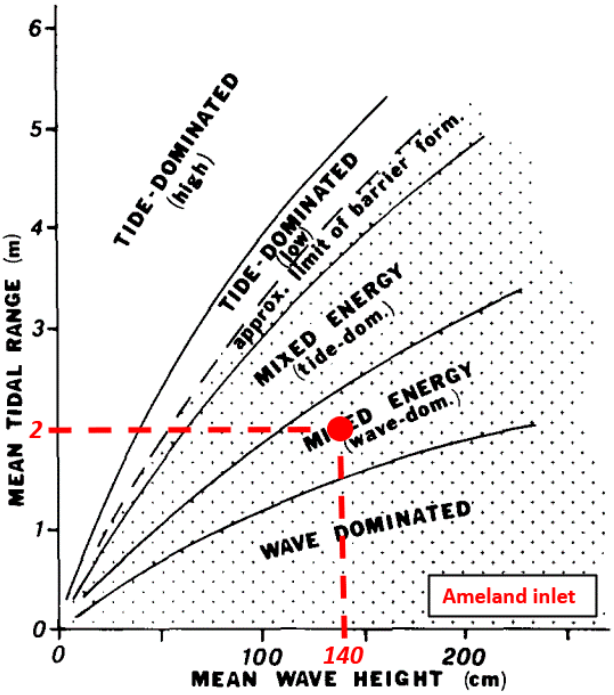

Figure 2.1: Graphical representation of tidal influence versus wave height, defining the regions of tide-dominated, mixed-energy and wave-dominated conditions. The position of Ameland Inlet is highlighted and falls into the mixed energy domain (Davis and Hayes, 1984).

2.2. Morphological features

A sketch of a schematized tidal inlet can be seen in Figure 2.2. This Figure illustrates the dynamic interactions between various morphological features and processes. At the largest scale, the tidal region is characterized by the presence of barrier islands, which are elongated islands parallel to the coast. Adjacent to the barrier islands, salt marshes or tidal flats can be found. The marshes are coastal wetlands that are flooded and drained by salt water brought in by the tides. The tidal inlet is the waterway between the barrier islands, which transports water and sediment from the ocean to the basin and visa versa. This process is dependent on tidal fluctuations. At the mouth of the tidal inlet, where the tidal currents meet the ocean waves, an ebb-tidal delta is formed. This is an area where sediment is deposited by the ebb tide when flow velocities drop below a certain threshold value (Elias et al., 2020). On the landward side of the inlet, a flood delta is created by the deposition of sediment carried by the flood tide. Note that when comparing the schematic illustration in Figure 2.2 to the detailed map of the Ameland tidal inlet in Figure 2.3, a notable difference emerges regarding the flood delta. The sketch illustrates the flood delta as a relatively confined area on the landward side of the inlet. In contrast, the Ameland tidal inlet map shows an expansive flood delta extending to the boundaries of the tidal basin. This implies that the morphological processes during flood tides in the Ameland tidal inlet is stronger than tidal inlets with less pronounced flood deltas.

Littoral drift is the transport of sediment along the coast caused by the action of waves and currents. Sand bypassing occurs when sand from the littoral drift is transported across the ebb-tidal delta. Tidal flats are extensive, flat areas where sediment is deposited that are exposed at low tide and submerged at high tide. Lastly, the tidal watershed is a theoretical boundary that separates the tidal basins. In theory, the tidal watershed is located where there is no hydrodynamic and morphodynamic interaction between adjacent basins.

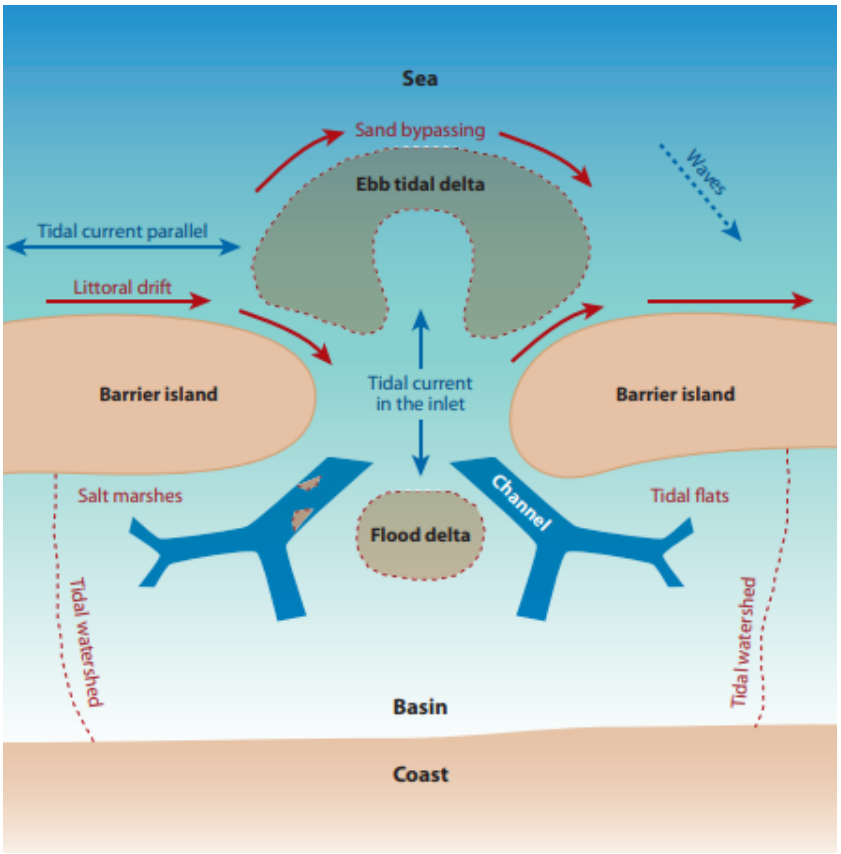

Figure 2.2: Sketch of the most important features and processes of a tidal inlet system (De Swart and Zimmerman, 2009).

2.2.1. Present-day situation

An overview of the Ameland tidal inlet with naming of the individual morphological features of the present-day Ameland tidal inlet can be seen in Figure 2.3. The most relevant morphological features are discussed below, based on the description of Elias (2021).

The inlet gorge features a deep main ebb-channel, the Borndiep [1], along the west coast of Ameland. The deepest parts of this channel exceed 25 meters in depth. In the basin, Borndiep connects to the Dantziggat [2], which curves eastward into the basin towards the tidal divide of Ameland (Pinkewad). To the west, separated by the shoal Zeehondenplaat [16], a smaller channel system formed by Oosterom [3] and Boschgat [4], both curving southward towards the tidal divide of Terschelling (Terschellinger Wad), is present. Currently, Boschgat does not directly connect to the Westgat [6] flood channel. A shallow platform segmented by a series of smaller, dynamic channels and shoals lies between the eastern island tip of Terschelling (Boschplaat [15]) and Borndiep.

The main channel on the ebb-tidal delta is the Akkepollegat [7]. Although Akkepollegat had a pronounced seaward outflow in the past, recently, two ebb-chutes [9, 10] have formed along its western margin. The most seaward, oldest ebb-chute and its associated ebb-shield, now called Kofmansplaat, cover most of the shoal area known as Kofmansbult [11]. North of this, the ebb-delta nourishment is visible as a shallow platform just seaward of the Kofmansplaat. The eastward migration of Kofmansplaat has distorted the outflow of Akkepollegat and rotated the channel eastwards. Extensive sedimentation has occurred in the channel resulting in the almost disappearance of the channel in the 2019 bathymetry. The deepest part of Borndiep, the main inlet channel, is now curved towards the younger, southern ebb-chute channel. The latter channel may have already taken over as the main ebb channel on the ebb-tidal delta.

The main ebb-tidal delta shoal area, known as Bornrif [12], lies east of Akkepollegat, which is downdrift in relation to the littoral drift. Along its eastern margin, now connected to the coast of Ameland, remnants of the shoal Bornrif Bankje [13] are still visible. This shoal formed and migrated as a narrow swash bar along the seaward margin of the ebb-tidal delta shoal and attached to the Ameland coast just east of the Bornrif Strandhaak [14]. The Bornrif Strandhaak was a large ebb-delta shoal that attached to the coastline around 1985. This natural mega-nourishment resembles the ”Zandmotor” (Stive et al., 2013) both in dimension and layout and has supplied the downdrift coastline of Ameland with sand over the past decades. Just west of this location, at the northwest tip of Ameland island, repeated sand nourishments [20] and extensive shore-protection works are needed [19] to maintain the coastline. In the 2019 bathymetry, a recent (2019) large nourishment is still visible along the coastline. While shoal attachments built out the coastline of Ameland, the opposite was observed along the coastline of Terschelling. The eastern tip of this island, Boschplaat [15], has receded over 1.5 km since 1975.

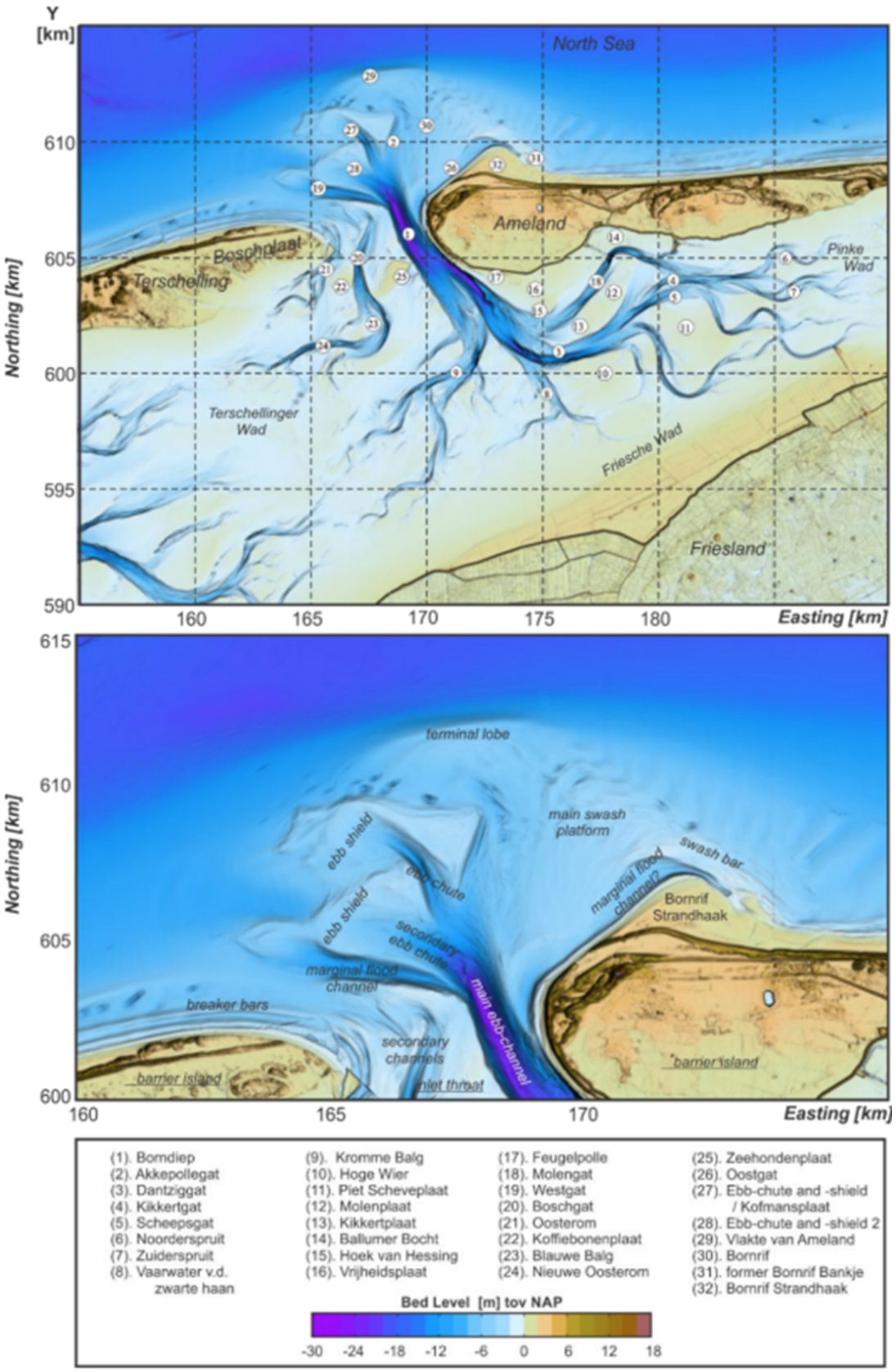

Figure 2.3: Topographic maps of the Ameland tidal inlet region showing in the top figure the broader geographical context and in the bottom figure a detailed overview of the ebb-tidal delta (Elias, 2020).

Zooming in on the ebb-tidal delta region, a few distinct morphological features can be observed. The terminal lobe of the ebb-tidal delta is the furthest point where sediment carried by ebb currents is deposited. Submerged or partially submerged sandbars, known as breaker bars, form due to the action of breaking waves and are crucial for reducing the force of waves before they reach the shoreline. A recent intervention in this dynamic environment is ebb delta nourishment from 2017 (e.g., Elias, 2021). This pilot nourishment of 5 million cubic meters did not significantly impact the autonomous behavior of the outer delta, likely due to the relatively small volume compared to the dynamic volume present on the ebb-tidal delta (Lambregts, 2021). The ebb shield prevents wave action and littoral drift at the ebb channel. Adjacent to the ebb shield are ebb chutes that facilitate water outflow during ebb tide. On the margins of the ebb-tidal delta, marginal flood channels enable water inflow into the inlet during flood tide. Secondary channels, smaller tributaries branching off from the main channels, assist in distributing water and sediment across the inlet system. The main ebb channel, a narrow and deep segment of the inlet, is where tidal currents are most powerful. These strong velocities through the inlet gorge enforce the self-sustaining nature of the inlet (Escoffier, 1940). Adjacent to the main ebb channel is the main swash platform, a large, shallow sandbank where waves break and sediment is deposited. Here, swash bars are formed that over time migrate towards the shore and eventually attach to the Ameland coast. The ebb-tidal delta has a sand buffering function, influences local dynamics of physical processes, affects the tidal basins and is a conduit for coastal sediment transport (Elias et al., 2020). It is desirable to maintain the ebb-tidal deltas at a size, because that allows them to preserve their functions. Without an outer delta, the neighbouring barrier islands would probably be subject to much more variation in coastline position (Elias, 2021). Insufficient sediment in the ebb-tidal deltas can, for example, lead to the erosion of nearby barrier islands, resulting in reduced coastal safety and the loss of valuable ecological areas.

The ebb-tidal delta can be consequently divided into six zones where the behaviour and underlying processes differ (Elias, 2021). The six distinct zones of the ebb-tidal delta are described by summarizing parts of Elias (2021). See Figure 2.4 a visual representation.

Zone I - Upstream Island Coast (Terschelling)
Situated to the west of the island of Terschelling, this zone is where the coast is subjected to erosion, serving as a sediment source for the following zones. Here, both tidal currents and waves impact the coastal processes. The wave-driven transports, especially those directed towards the east, have a particularly influential role.

Zone II - Shallow Platform of Boschgat
Positioned between the tail of Terschelling and the main channel, this region hosts a variety of small channels and banks and is relatively stable. The sand present here is primarily moved around by ebb and flood currents, with a structural loss of sand channeling towards the deeper regions of Borndiep. While the western part is still dominated by waves, the dominant process shifts towards tidal action when moving closer to the middle of the inlet gorge.

Zone III - Ebb-chutes and -shields
This zone is located on the western side of the outer delta. Driven by the outflowing tidal currents from the main ebb channel, this zone has witnessed the formation of ebb-chutes and -shields, especially in the years after 2005. These formations significantly impact the morphodynamics, giving this zone its characteristic features.

Zone IV - Edge of the Outer Delta
Though not differentiated as a distinct morphological area, this zone its dynamics are primarily dominated by (storm) waves. Sediments are deposited on its seaward side, facilitated by the ebb currents and wave action. However, during storm events, erosion becomes a dominating process. Incoming waves from the North Sea approach the shore, they increase in height and then partially break on this ebb-delta margin.

Zone V - Outer Delta Platform (Bornrif)
This zone is a sediment reservoir, holding the dominant volume of sand downstream of the main ebb channel. There is accumulation of sediment at the northern part of the outer delta, caused from the outflows of the main ebb channel. The platform itself is relatively stable and this platform is wave-dominated.

Zone VI - Bank Landing Area
This is where the outer delta banks attach to the shore. The growth is not continuous but rather in stages. As banks approach this area, the formation of channels leads to erosion, specifically before the actual landing of a bank. Once a bank erodes, the sediment is redistributed, leading to local extension of the coastline.

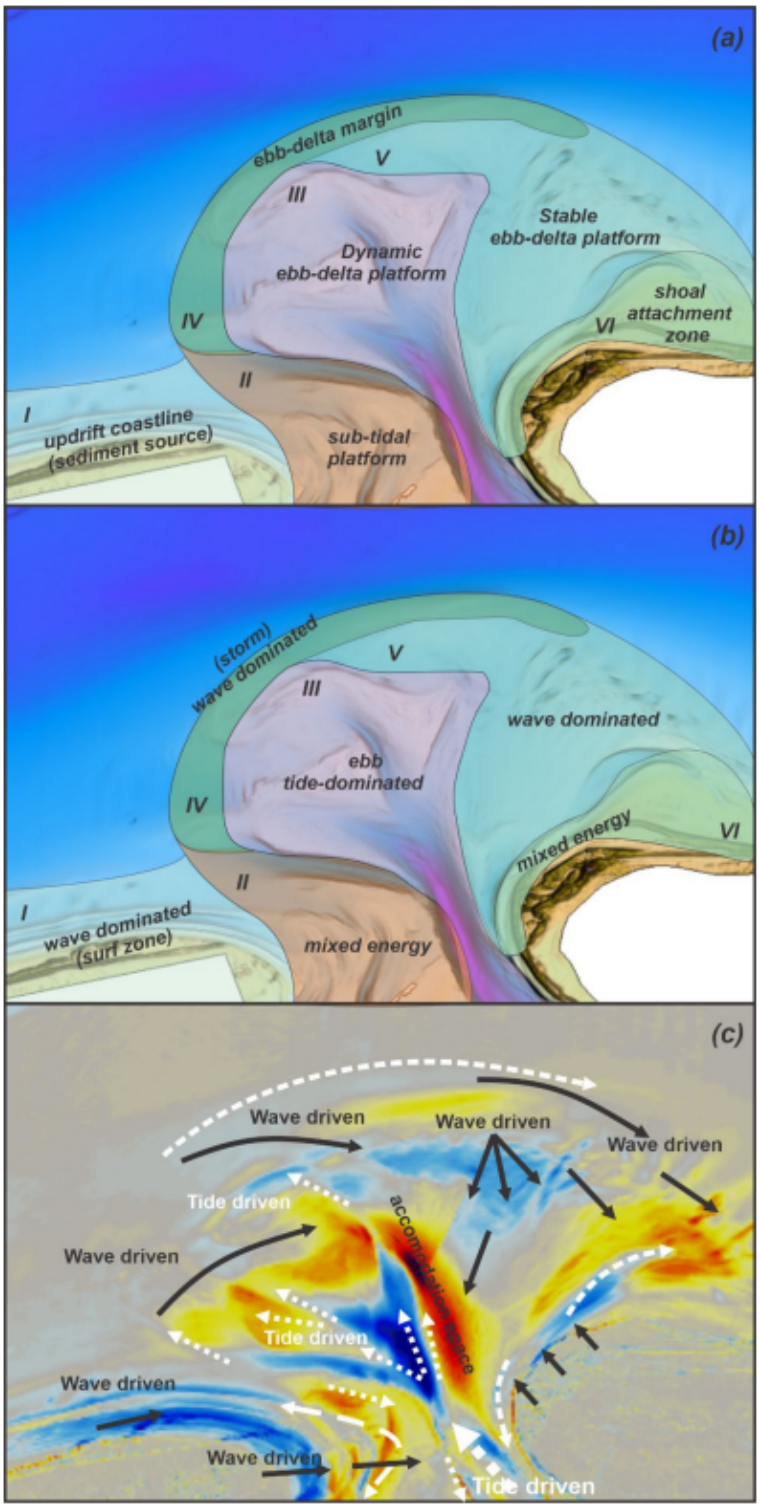

Figure 2.4: Overview of ebb-tidal delta dynamics where (a) specifies the six distinct morphological zones; (b) determines the energy characteristics of the six zones; and (c) visualizes the interplay of wave-driven and tide-driven forces on sediment transport (Elias, 2021).

2.3. General principles and definitions of relevant hydrodynamic processes

This section describes the relevant hydrodynamic principles and concepts that govern the morphological development of the Wadden Sea. It particularly emphasizes those essential for evaluating the influence of model schematization on morphological forecasts of the Ameland tidal inlet. First the astronomical tide is covered, then the non-astronomical factors wind and waves and finally several other key hydrodynamic and morphodynamic concepts are introduced.

Astronomical tide
Tidal processes play a fundamental role in shaping the morphodynamics of tidal inlet systems. The astronomical tide arises from the gravitational attraction of the sun and moon on the water masses. These tidal components are essential in determining the overall water level variations and currents within the system. The Wadden Sea has a semi-diurnal tidal signal, which means having a tidal pattern where each tidal day (24 hours and 50 minutes) has two high tides and two low tides. Consequently, high and low tides reach the Wadden Sea approximately every 6 hours and 12.5 minutes. The two primary currents that emerge from this tidal movement are the flood current (i.e., incoming tide) and the ebb current (i.e., outgoing tide).

Non-astronomical factors
In parallel to the previously discussed tidal forces, non-astronomical factors also play a significant role in determining the morphodynamics of coastal regions. Most notable for the Wadden Sea region are wind-generated surface gravity waves and storm surges. Originating from the forces of the atmosphere rather than the gravitational attraction of the sun and moon. These components bring additional variations in water levels and currents affecting sediment transport.

Storm surges arise during intense weather conditions, primarily driven by strong winds and atmospheric pressure changes. Such events push-up water against the coast, resulting in elevated water levels. This surge consequently enables incoming waves to travel further and breaking closer to the shore. Wind speed, duration and fetch determine the magnitude, frequency and energy of these waves. Due to North Sea's shallow basin there is minimal contributions from distant ocean swells.

Interactions between these non-astronomical components and tidal dynamics are complex. For instance, in situations where wind-generated waves re-suspend sediment,tidal currents subsequently can transport this sediment. This illustrates the intricate interplay between the forces that shape this morphologically active area.

Beyond tidal and non-astronomical components, several other key principles drive the morphological evolution of tidal inlet systems. These principles include the tidal divide, ebb and flood dominance, velocity asymmetry and residual transport. Analysing these can offer insights into the behavior and character of coastal regions like the Wadden Sea.

Tidal divide
Figure 2.5 shows a simplistic sketch of barrier islands, tidal basins and tidal divides. Conceptually, a tidal basin can be seen as the spatial domain influenced by a single tidal inlet. The tidal divide is the theoretical line separating two tidal basins. Essentially, it is the watershed of tidal basins, where water on either side of the divide flows toward different inlets. The position of a tidal divide can change location due to various factors like human interventions or variations in sea level. One of these human interventions that has had significant impact on the locations of the Wadden Sea tidal divides is the closing of of the Zuiderzee (see Figure 2.6).

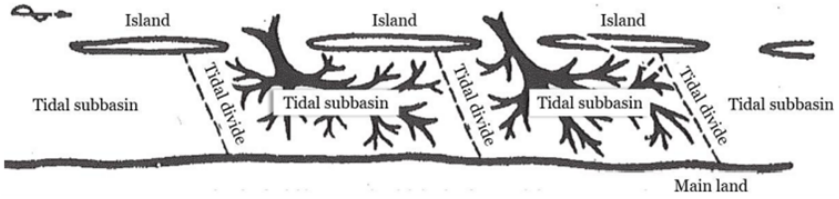

Figure 2.5: Sketch of the various components of a tidal system (Stive and Wang, 2003).

There are two types of tidal divides, namely hydraulic tidal divides and morphological tidal divides (Vroom and Wang, 2012). The hydraulic tidal divide represents the line separating two tidal sub-basins based on flow dynamics. On the other hand, the morphological tidal divide appears as a raised, spine-like formation on the seabed between two neighboring tidal basins. These two types of tidal divides do not necessarily align at the same location. This is mainly because of the different time scales that hydrodynamic and morphodynamic processes act on. Figure 2.6 shows the approximate positions of both the hydrodynamic (top figure) and morphodynamic (bottom figure) tidal divides of the Wadden Sea region.

Van Weerdenburg et al. (2021) shows that there is wind-driven exchange flows over these theoretical tidal divides in the Wadden Sea, especially during strong during storm events. These wind-generated currents can lead to residual flows through the tidal inlet, potentially altering the morphological development of the ebb-tidal delta. This ”theoretical” tidal divide theory does thus not always hold up for each tidal divide, underlining the importance of addressing the water and sediment transport dynamics at these tidal divides for morphological modelling.

Ebb and flood dominance
Another concept that is used throughout this report is ebb and flood dominance. Ebb and flood dynamics play a vital role in shaping the ebb and flood delta of a tidal inlet system. When a region is considered as ebb dominant, the ebb currents (seaward flowing) are stronger than the flood currents (landward flowing). The opposite applies to flood-dominated areas. Within any tidal environment, whether it’s a tidal inlet system or another coastal setting, the area can spatially vary in its ebb or flood dominance due to the highly variable bathymetry.

Velocity asymmetry and residual transport
In tidal environments, flow asymmetry refers to the variations in velocity or duration between flood and ebb-tidal currents. While the tidal signal might initially appear symmetrical, subtle differences can result in significant influence on sediment transport dynamics. This research primarily focuses on velocity asymmetry, which means the difference in flow velocities between the incoming flood and outgoing ebb currents. This asymmetry in velocity is one of the factors leading to residual sediment transport. Residual sediment transport in itself is the net sediment movement after accounting for both flood and ebb phases.

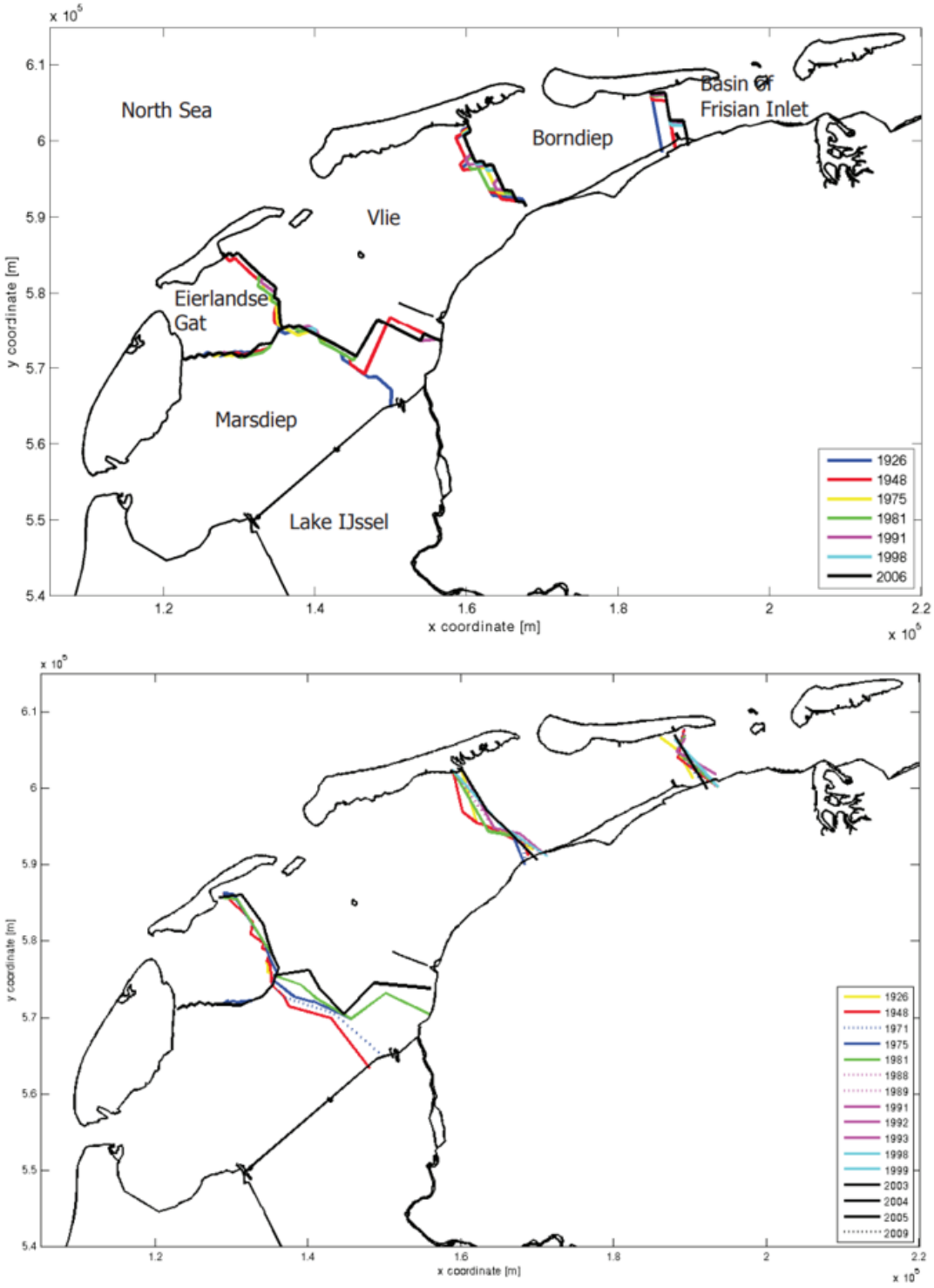

Figure 2.6: Approximate location of the tidal divides in the Wadden Sea over various years, based on the data from Vroom and Wang (2012).

3

Research methodology

This chapter on the research methodology starts with a general description in Section 3.1. Thereafter process-based modeling using Delft3D-FM is introduced in Section 3.2. The subsequent sections provide context on the incorporation of high-performance computing (3.3) and details the model setup (3.4). The chapter ends with presenting the model schematization scenarios in Section 3.5.

3.1. General research methodology

The overarching methodology for this research is executing a process-based model to compute both hydrodynamics and morphodynamics of the Wadden Sea to assess morphological changes of the Ameland tidal inlet. Using a systematic and sequential approach, different domain, grid and forcing schematizations are applied to the model. The simulation results are then both quantitatively and qualitatively analysed to gain a comprehensive understanding of the differences in morphological changes and the underlying processes that drive them at the Ameland tidal inlet for the various model schematizations.

Two modelling domains are considered:

- A single-inlet schematization, focusing on the Ameland tidal inlet, basin and ebb- and flood-tidal delta.
- A broader multi-inlet schematization, capturing the entirety of the Wadden Sea area.

Three combinations of forcing conditions are applied to to the models boundaries and grid. The primary factors driving morphological change in tidal regions that are considered are: tidal fluctuations, water levels fluctuations and wind.

To address the influence of grid resolution there are two grid schematizations:

- A base resolution featuring grid sizes of 60x60m within the inlet.
- A high-resolution grid featuring grid sizes of 30x30m within the inlet.

The models are all used to simulate hydrodynamics and morphodynamics for for a baseline period of three months. This duration offers an initial insight into the differences among the scenarios, while still keeping manageable computational demands. Notably, the chosen three-month simulation period aligns with a time frame that has extensive data availability due to the Kustgenese2.0 measurement campaign. While this research primarily focuses on model-to-model comparisons and does not directly compare model results with measurement data, the selected period ensures consistency and a strong connection with prior research.

The analysis of the differences in model output is multi-faceted, as this research uses both qualitative and quantitative analytical techniques. The qualitative analysis is based on interpretative assessments of the morphological changes. This involves evaluation of patterns of morphological changes observed. On the other hand, the quantitative analysis is based on numerical evaluations. Metrics derived from

the simulations are quantitatively analysed to determine their significance and relevance to the research objectives. Key processes include:

- Water and sediment exchange between basins.
- Water and sediment interchange through the Ameland tidal inlet.
- Residual sediment transport and spatial tidal velocity asymmetry.

With this approach, the study not only achieves its objectives of evaluating the benefits of enhanced model schematizations for morphological forecasts but also adds to the understanding of the hydrodynamic and sedimentary interactions occurring within the Ameland tidal inlet and between the Ameland basin and adjacent basins. By utilizing high-performance computing resources, this research aims to improve the accuracy of morphodynamic predictions. The advantages of this research approach include the ability to conduct what-if scenarios regarding model schematization, is a direct extension of recent modeling studies on the Ameland ebb-tidal delta and has the ability to produce visually appealing figures with quantitative results comparing the different scenarios. Thereby, this research can serve as one of the first utilizing Delft3D-FM on the DelftBlue supercomputer and can create a path for other research with this combination.

3.2. Process-based modelling using Delft3D-FM

Delft3D is one of the primary modelling software tools used in hydraulic engineering. Morphological forecasts in Delft3D are performed using a process-based modeling approach, which relies on the theoretical knowledge of relevant physical processes and their interplay. The computation is following a sequence of processes, as illustrated in Figure 3.1. The model starts with an initial bathymetry and boundary conditions. Forcing, combined with the initial conditions, result in sediment transport. Based on the sediment transport, the bed level change is calculated and this change is then fed back to the bathymetry for the next time step. There are, however, various acceleration techniques (e.g., Roelvink, 2006; Harlequin, 2020), which compute the morphological changes in different ways. For this research, the brute force technique is specifically chosen so that focus is on the influence of the forcing components themselves and do not have to worry about how the acceleration technique influences the results. This method of using ”brute-force” forcing components is also chosen to maximize the usage of the available high-performance computing resources and serve as one of the pioneering studies of using high-performance computing on Delft3D tidal inlet modelling. More on the incorporation of high-performance computing in the following section (3.3).

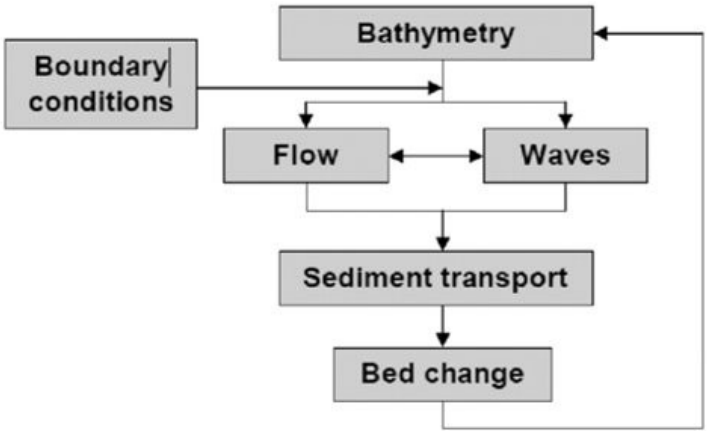

Figure 3.1: Flow diagram for Delft3D-FM, sourced from Hillen et al. (2009) and originally adapted from Roelvink (2006).

The FLOW module of Delft3D is used for performing the simulations. FLOW computes water motion and sediment transport caused by various driving forces. The model assumes a density of sediment particles of 2650 kg/m^3. Although waves play a significant role in influencing currents and water levels, and vice versa, this study utilizes only the flow module without incorporating wave forcing.

3.3. Incorporation of high-performance computing

High-performance computing (HPC) plays a crucial role in enhancing the accuracy of coastal morphological predictions by enabling simulations with unprecedented detail in physical processes. With recent advancements in high-performance computing, notably the opening of Snellius in 2021 and DelftBlue in 2022, there has evolved a substantial potential for improving morphodynamic forecasts. This research aims to incorporate HPC to not only make computational times feasible for the various model runs that are needed to answers the research questions, but also to provide a preliminary exploration into the practicalities of employing HPC on coastal engineering problems. The DelftBlue supercomputer from TU Delft was utilized for this purpose. More details about DelftBlue can be found in Appendix E.

3.4. Model setup

This section details the model configuration. This is essential background information for understanding the model results and ensure future replicability of similar research. First the model grid and initial bathymetry are given in Section 3.4.1. Then the grid resolution at the inlet throat is presented to give the reader a feel for the resolution on which the morpho- and hydrodynamics are solved. Section 3.4.3 gives context to the model its forcing components and Section 3.4.4 gives insight on data management.

3.4.1. Grid and initial bathymetry

The CGII-FM model is the baseline model used for the simulations in this research. The CGII-TM model, based on Delft3D-FM software, calculates waves, flow and sediment transport.

CGII-FM has a flexible mesh grid, which gives the model more versatility and computational efficiency compared to a structured grid approach. The FLOW grid for the CGII-FM model is based on the Wadden Sea model developed by Laan et al. (2019). On the side facing the sea, the models boundaries go far beyond the direct influence of the inlet. The conditions along the open-sea side are determined by water level boundaries from a larger-scale model, DCSM.

The model has a single vertical layer, making it a 2D model. The model domain extends from IJmuiden at the Holland Coast all the way to the German Wadden Sea, encompassing the Ems-Dollard Estuary (see Figure 3.2). The grid orientation is aligned with the North-Sea coast and the grid involves one step in grid refinement using triangular grid cells. The bathymetry of the model is based on the Vaklodingen data from 2014 to 2018 (see Figure 3.3).

No calibration and validation is performed for this research, as the model was assumed to be sufficiently accurate for the objectives of this research.

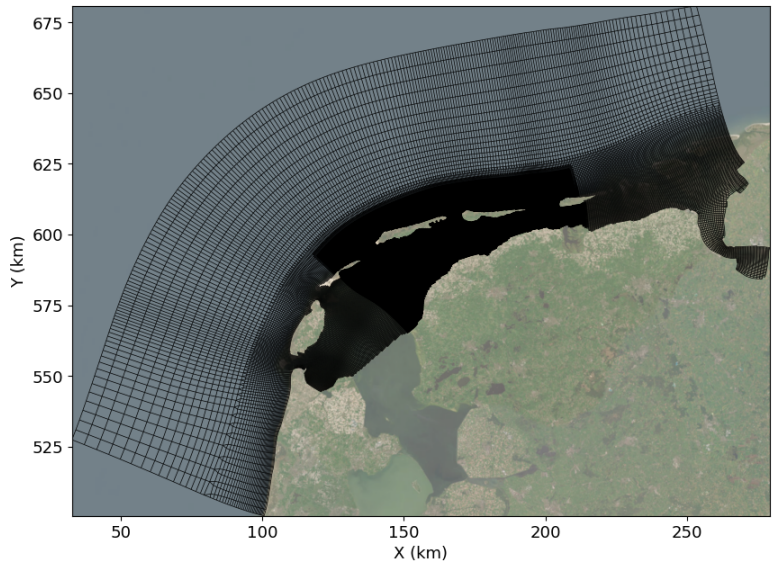

Figure 3.2: Wadden Sea grid (base resolution).

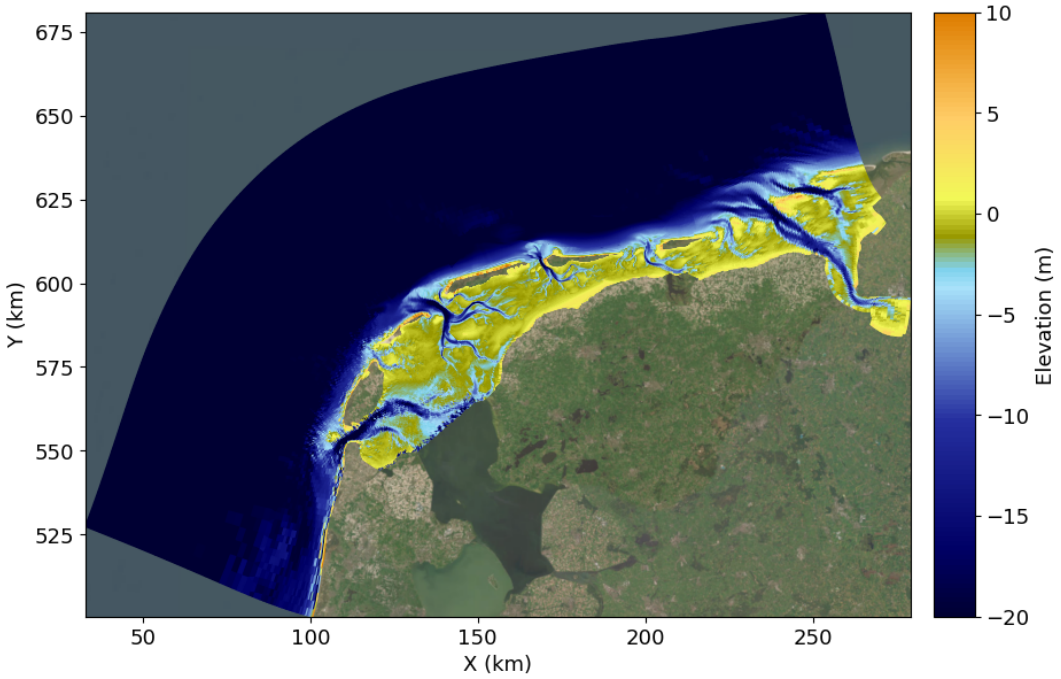

Figure 3.3: Visualization of the initial bathymetry (generated with Vaklodingen data from 2014 to 2018).

Figure 3.4 shows the locations of the so-called thin dams. These are implemented in the model when simulation with a single-inlet domain, as these prevent water and sediment transport between adjacent tidal basins. The reason for still using the entire grid for the Wadden Sea is to not influence any other dynamic processes and solely assess the differences between simulations with a single-inlet schematization versus simulations with a multi-inlet schematization.

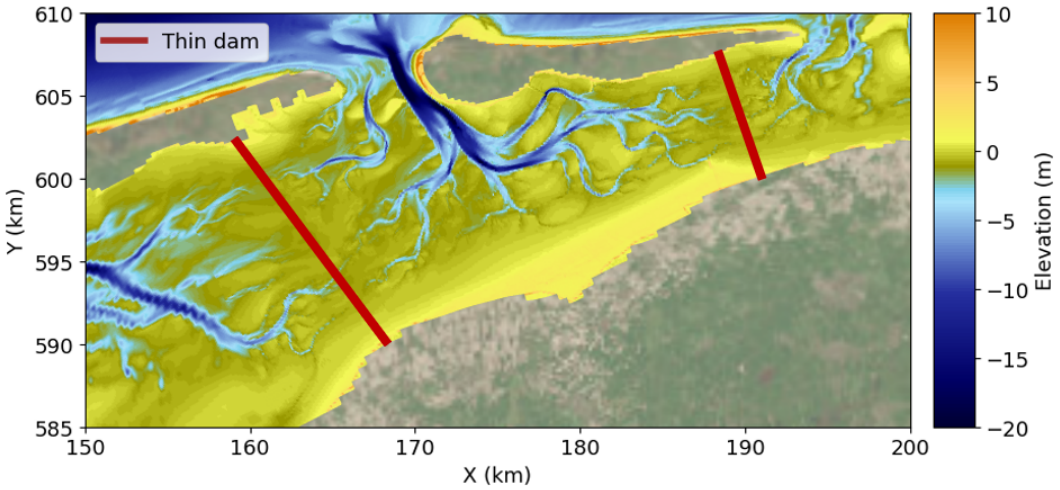

Figure 3.4: Location of thin dams on initial bathymetry to schematize multi-inlet Wadden Sea model as a single-inlet Ameland model.

To analyse water and sediment interaction between basins and the water and sediment transport dynamics through the inlet gorge, multiple cross-sections are defined in Figure 3.5. While the naming convention for these sections is adapted from the baseline model, this report often clarifies the location by adding descriptors such as ”seaside” or ”landside” for cross-sections parallel to the barrier islands. Instead of referencing the ”Ameland-Terschelling” cross-section, the cross-section at the inlet throat is defined as ”tidal inlet cross-section”. Transport to the east and north is regarded as positive, while transport to the west and south is considered negative.

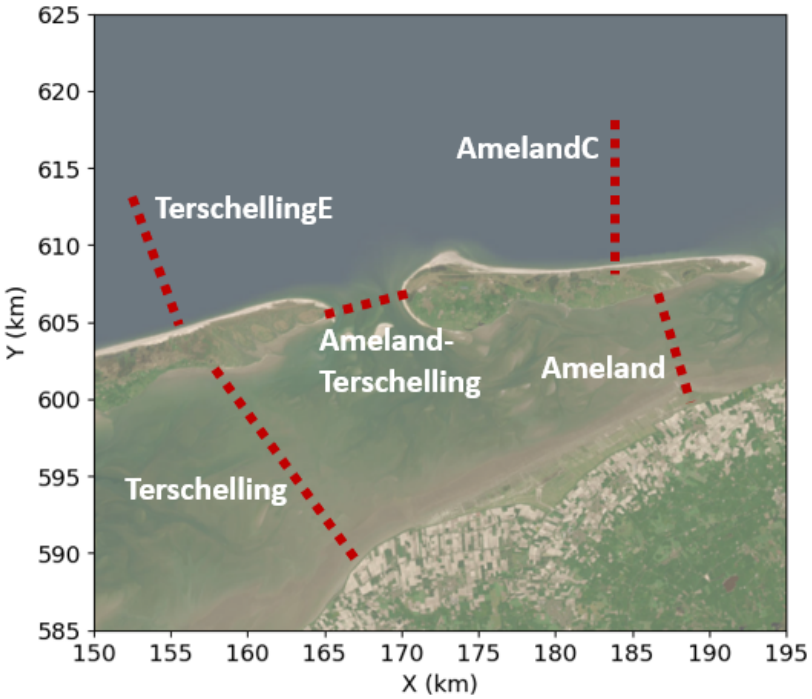

Figure 3.5: Naming and locations of cross-sections that are used for the cross-sectional hydrodynamic analysis.

3.4.2. Grid resolution

Figure 3.6 and 3.7 show the grid and initial bathymetry at the inlet gorge, which is located between the barrier island Terschelling and Ameland. Figure 3.6 shows the baseline grid with cells of approximately 60 by 60 meter. Figure 3.7 show the high-resolution grid with grid cells of approximately 30 by 30 meter.

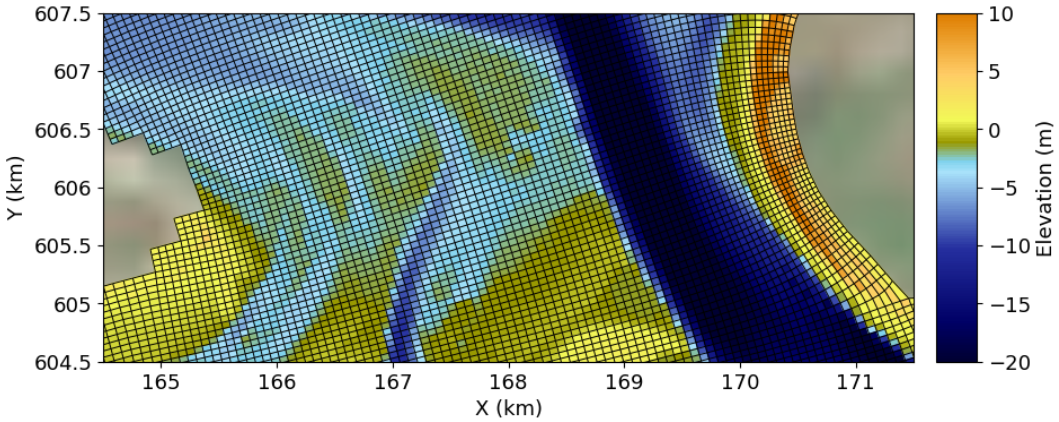

Figure 3.6: Base resolution grid and initial bathymetry at the inlet throat (grid cells are approximately 60 by 60 meters).

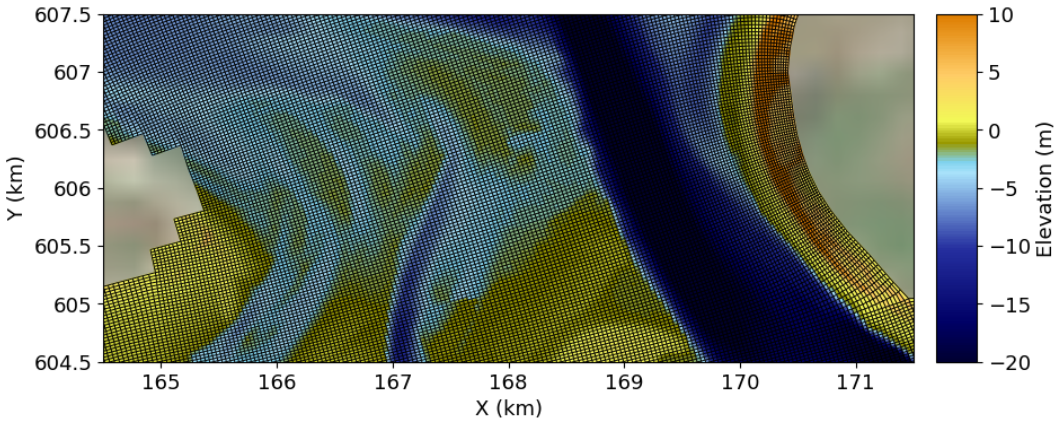

Figure 3.7: High resolution grid and initial bathymetry at the inlet throat (grid cells are approximately 30 by 30 meters).

3.4.3. Forcing components

Water level time series are prescribed at open model boundaries. These water level boundary conditions are derived from the DCSMv6-ZUNOv4 model (Zijl et al., 2013). Using TTIDE.py software, the tidal constituents have been derived and a new time series for a tide-only simulations has been generated (Table 3.1). Meteorological forcing (atmospheric pressure and wind) is based on the ERA5 atmospheric reanalysis (Hersbach, 2019). Lastly, there are three locations where inland water flows into the Wadden Sea basin. These locations are the Stevin, Lorentz and R.J. Clevering sluices (Figure 3.8).

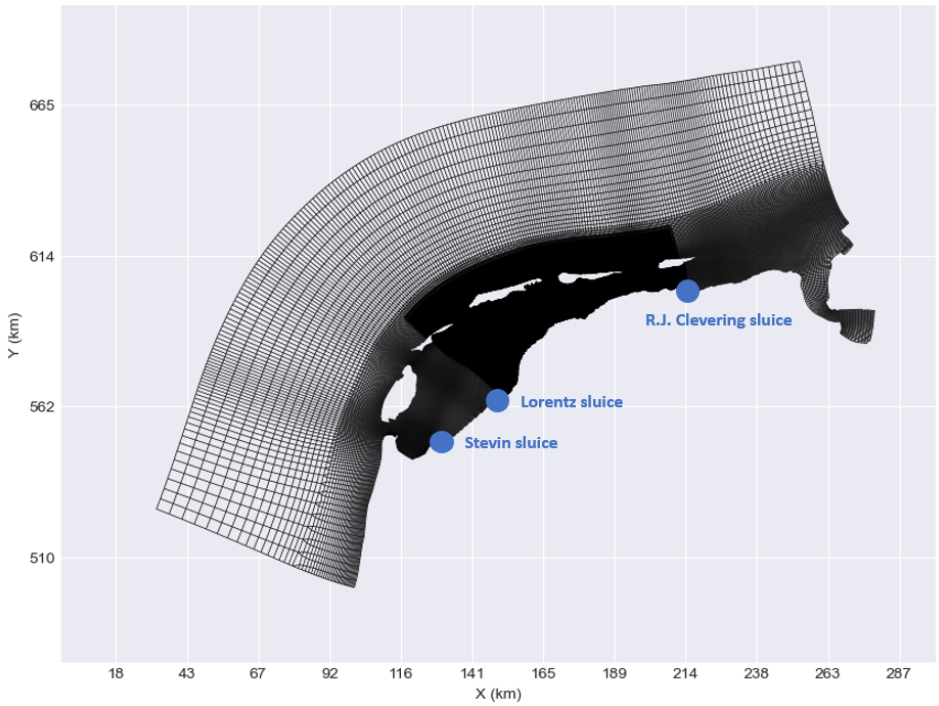

Figure 3.8: Locations of the three sluices where inland water flows into the Wadden Sea basin.

Table 3.1: The 16 tidal constituents for northern boundary (location 3) with highest Signal-to-Noise Ratio (SNR).

Tide	Freq (cph)	Amp (m)	Pha (°)	SNR
M2	0.081	0.88	125.6	1.7e+04
N2	0.079	0.14	228.1	3.6e+02
O1	0.039	0.07	63.3	2.5e+02
K1	0.042	0.06	3.8	1.7e+02
M4	0.161	0.03	103.1	1.8e+02
S2	0.083	0.22	347.3	1.2e+03
L2	0.082	0.07	191.8	1.4e+02
Q1	0.037	0.03	130.5	38
P1	0.042	0.03	23.6	64
2N2	0.077	0.03	297.9	25
MU2	0.078	0.07	57.3	1.3e+02
All other constituents are used in the tidal signal generation but are not presented in this table.				

3.4.4. Map file data management

The model is split into 48 partitions to enable parallel computing on multiple CPUs. As the chosen model domain and simulation settings resulted in huge data output, not all data partitions are kept. The grid domain that consists of the saved partitions can be seen in Figure 3.9.

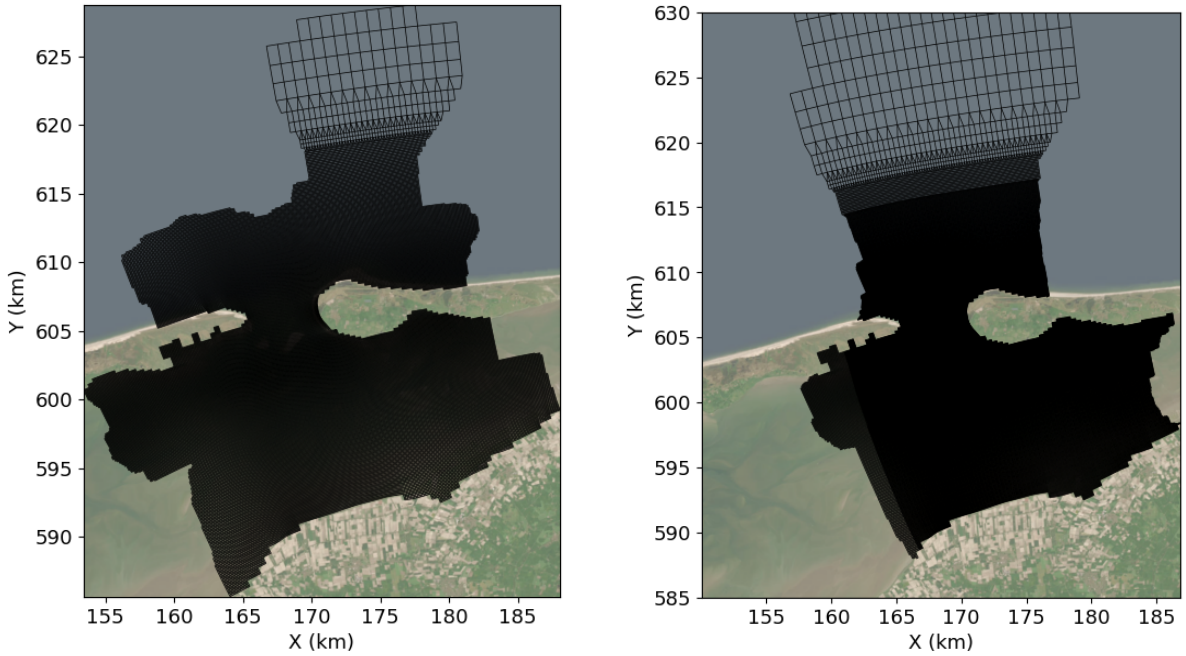

Figure 3.9: Selected partitions for base (left figure) and high (right figure) resolution grid to reduce data storage.

3.5. Model scenarios

Based on the previously discussed model schematizations a overview of all model scenarios is given in table 3.2.

Table 3.2: Overview of all model simulation set-ups that are performed during the research.

Simulation	Domain	Resolution	Forcing	Duration	Map Output
1	Ameland	Base	Tide	3 months	1 hour
2	Ameland	Base	Water level	3 months	1 hour
3	Ameland	Base	Water level, Wind	3 months	1 hour
4	Ameland	High	Tide	3 months	1 hour
5	Ameland	High	Water level	3 months	1 hour
6	Ameland	High	Water level, Wind	3 months	1 hour
7	WadSea	Base	Tide	3 months	1 hour
8	WadSea	Base	Water level	3 months	1 hour
9	WadSea	Base	Water level, Wind	3 months	1 hour
10	WadSea	High	Tide	3 months	1 hour
11	WadSea	High	Water level	3 months	1 hour
12	WadSea	High	Water level, Wind	3 months	1 hour
13	Ameland	Base	Tide	7 days	10 minutes
14	WadSea	Base	Tide	7 days	10 minutes
15	Ameland	High	Tide	7 days	10 minutes
16	WadSea	High	Tide	7 days	10 minutes

In the main body of this report, only the data from simulations with highest added value for answering the research questions are included. Figures with results for several other simulations can be found in the Appendix. A table of which simulation is used in Chapter 4 can be found in Table 3.3.

Table 3.3: Overview of model simulations which results are used per results section of Chapter 4.

Domain (RQ1)	Forcing (RQ2)	Grid (RQ3)	Residual Transport (RQ4)	Model set-up
x				1 - Ameland Base Tide
x	x	x		7 - WadSea Base Tide
	x			8 - WadSea Base Water level
	x			9 - WadSea Base Water level, Wind
		x		10 - WadSea High Tide
			x	13 - Ameland Base Tide
			x	14 - WadSea Base Tide

4

Results and analysis

This chapter starts by presenting the results from the baseline simulation in Section 4.1. This baseline simulation has a model grid domain of the entire Wadden Sea, tide-only forcing and a grid resolution of 60 by 60 meter grid cells near the Ameland inlet. Focus is first on describing the water and sediment interchange through the Ameland inlet, the exchange of water and sediment between the Ameland basin and adjacent basin and presenting the spatial asymmetry for flow velocity and sediment transport. Thereafter the spatial distribution of sediment and erosion and accompanying transect analysis of bed level change is presented.

The subsequent four sections present results from simulations using various model schematizations, where each is compared to the baseline simulation. Section 4.2 focuses on variations in domain schematization when having tide-only forcing, Section 4.3 varies in forcing processes and Section 4.4 varies in grid resolution.

The results for an intermediate step between Section 4.2 and 4.3 are included in Appendix B. This chapter describes variation in model domain, similar to 4.2, but then for simulations where wind forcing is included.

4.1. Baseline simulation: Wadden Sea with tide-only forcing

The results of the baseline simulation are presented in four parts: Section 4.1.1 includes a cross-sectional hydrodynamic analysis, Section 4.1.2 presents spatial asymmetry maps comparing ebb and flood velocities and sediment transport and Section 4.1.3 shows the spatial distribution of sedimentation and erosion and contains the transect analysis of the bed level change.

4.1.1. Cross-sectional hydrodynamic analysis

This cross-sectional analysis is used to present water and sediment transport dynamics for the Ameland tidal inlet region. One observation that stand out the most is that, even if transportation patterns are solely driven by tidal fluctuations, there is not to be neglected residual discharge over the cross-section that are placed at the ”theoretical” tidal divides (middle element of Figure 4.1).

Furthermore, the baseline simulation has a slight import of water into the Ameland basin, due to the negatively developing cumulative discharge shown in the top element of Figure 4.1 (as positive values indicate an northward flow direction). Residual discharge for the other four cross-sections, defined perpendicular to the barrier island Terschelling and Ameland, are in eastward direction (as positive values also indicate an eastward flow direction). The seaward cross-section (TerschellingE and AmelandC) have respectively approximately a 5x and 10x greater magnitude compared to their landward cross-section (Terschelling and Ameland).

The oscillation patterns among the cross-sections highlight the tidal effects at different locations in the study area. Observing the top element of Figure 4.1, which represents the residual discharge through the tidal inlet, both the daily and biweekly oscillations are prominent, indicating the influence of the daily

high and low tides and the spring-neap tidal cycle. The daily oscillations are much less prominently visible for the other cross-sections due to the cumulative values being order of magnitudes larger. The spring-neap tidal pattern is visible for the Terschelling cross-section and very subtle for the seaside AmelandC and TerschellingE cross-sections.

The observed differences in visibility of the tidal oscillation patterns across various cross-sections can be attributed to, among others, the tidal oscillation pattern itself, a combination of the physical geometry of the area, location of the cross-section, bathymetry and the nature of the residual discharge data being analyzed. When considering the nature of the data, visibility is influenced by the magnitude of residual transport in relation to the magnitudes of the flood and ebb transport over the same cross-section. For example, if the magnitude of the residual discharge is relatively large compared to the flood and ebb discharge, it is more difficult to discern the tidal oscillation patterns in the data (lower elements of Figure 4.1). Conversely, if the magnitude of the residual discharge is relatively small compared to the magnitudes of flood and ebb discharge, the tidal oscillation patterns are better visible (top element of Figure 4.1).

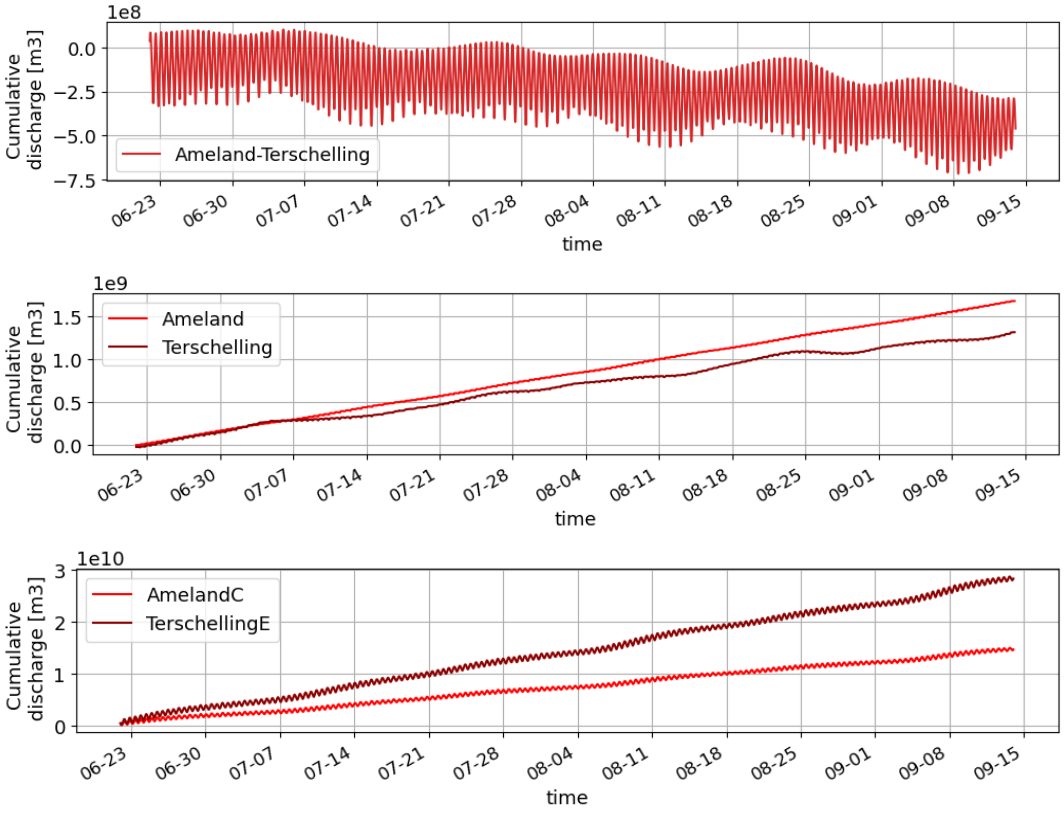

Figure 4.1: Cumulative residual discharge for a 3-month simulation for five different cross-sections. The top Figure contains data for the tidal inlet, the middle for two cross-sections defined at the landside of the barrier island Terschelling and Ameland and the lower Figure for two cross-sections defined at the seaside of the barrier islands.

The top element of Figure 4.2 shows the residual sediment transport for the tidal inlet, the middle element for the landside cross-sections Ameland and Terschelling and the lower element for the seaside cross-sections AmelandC and TerschellingE. While for the residual discharge in Figure 4.1 the tidal inlet cross-section showed lower levels of discharge compared to the other cross-sections, the residual sediment transport is significantly larger (two and three orders of magnitude). The residual cumulative transport trends indicates that the tidal inlet does have significant sediment transport, indicating that it is highly morphodynamic compared to the locations of the other cross-sections. This is important when interpreting the direction of residual transport. For example, the Ameland and Terschelling cross-section have opposite directions for residual transport, however the magnitude of this transport is negligible in

the bigger picture. Essentially, the residual sediment transport over the landside cross-sections could be approximated as being zero compared to the residual sediment transport through the tidal inlet.

The trend lines in Figure 4.2 show different levels of dependency on the spring-neap tidal cycle. Especially the difference in dependency for the seaside cross-sections AmelandC and TerschellingE is noteworthy. TerschellingE is clearly located where there is more influence of tidal dynamics compared to the AmelandC. This could be due to having stronger tidal currents, affected by the local bathymetry and the geophysical shape and orientation of the barrier island themselves.

For the TerschellingE cross-section, there is not equal residual sediment transport during each spring-tide. During one spring-tide there is pronounced residual sediment transport, followed by a spring-tide with relatively no residual sediment transport. This is consequently more a four-weekly pattern than a biweekly spring-neap tidal pattern.

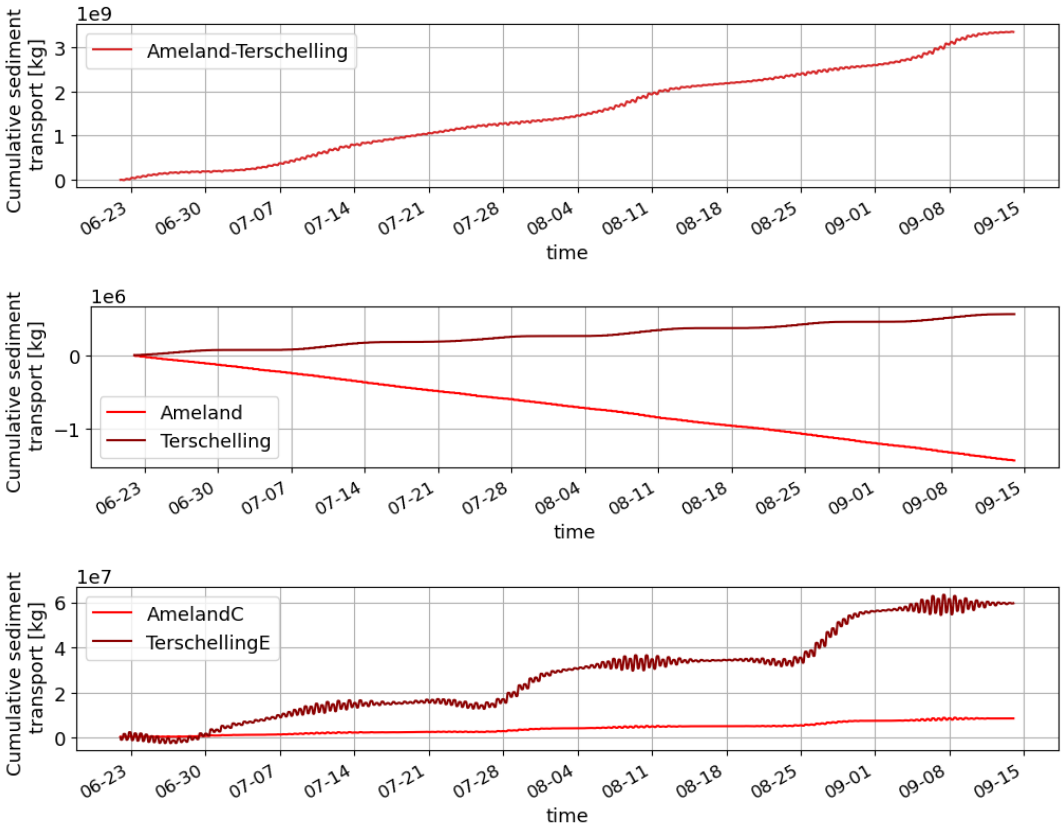

Figure 4.2: Cumulative sediment transport for a 3-month simulation for five different cross-sections. The top figure contains data for the tidal inlet, the middle for two cross-sections defined at the landside of the barrier island Terschelling and Ameland and the lower figure for two cross-sections defined at the seaside of the barrier islands.

To help interpret the trends observed in Figures 4.1 and 4.2, Figures 4.3 to 4.5 show the average ebb and flood velocities and the difference between them for the tidal inlet and two seaside cross-sections. The average velocities for the landside cross-sections were too low and inconsistent to be meaningful. These figures were generated by first identifying the instances when the flow direction at the inlet alternates from flood to ebb and vice versa. Then the average velocities were then determined by taking the mean of the flow velocities during each phase of flood and ebb, resulting in two data points for each tidal cycle of approximately 12 hours and 25 minutes. The oscillations observed on the daily interval show the occurrence of the less intense spring and neap tide followed by a more pronounced spring-neap tide. This is the reason for the four-weekly pattern observed in the residual sediment transport trend for the seaside TerschellingE cross-section (lower element of figure 4.2. During this milder spring-tide, flow velocities are below the critical shear stress resulting in limited sediment transport.

Figure 4.3 shows that there are for the entire 3-month period higher average ebb than flood velocities through the tidal inlet. The difference between average ebb and flood velocities are less defined for the seaside TerschellingE and AmelandC cross-sections, while being more often higher for the flood velocities than ebb velocities.

The top element of Figure 4.1 indicated a slight import of water into the Ameland basin. This, however, did not result in an import of sediment into the Ameland basin. By contrast, there was a significant export of sediment through the tidal inlet. This is related to the higher average ebb velocities (Figure 4.3).

The eastward directed residual discharge for all other cross-sections are accompanied by eastward directed sediment transport for all cross-section except the landside Ameland cross-section. This relation is, however, very sensitive as the sediment transport for the landside cross-sections are essentially zero compared to the magnitude of sediment transport of the tidal inlet. This is accompanied by the fact that there is small difference between the average ebb and flood velocities for the seaside TerschellingE and AmelandC cross-sections.

Average velocities for the seaside TerschellingE cross-section (Figure 4.4) are generally higher than the average velocities over the AmelandC cross-section (Figure 4.5). This is accompanied by the fact that TerschellingE showed more residual discharge and sediment transport in figures 4.1 and 4.2. This is another reason for cross-section TerschellingE to show significantly more dependency in sediment transport on the spring-neap tidal cycle for than AmelandC cross-section, as sediment transport is to a higher order dependent on flow velocities.

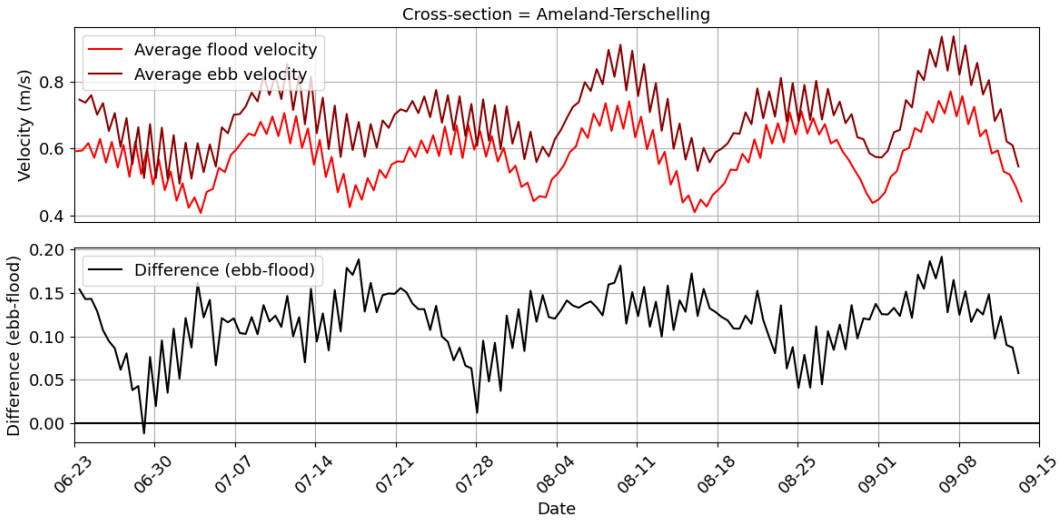

Figure 4.3: Comparison of average flood and ebb velocities over time (top) for the tidal inlet cross-section and their difference (bottom) during the 3-month simulation period (positive difference meaning higher ebb velocity).

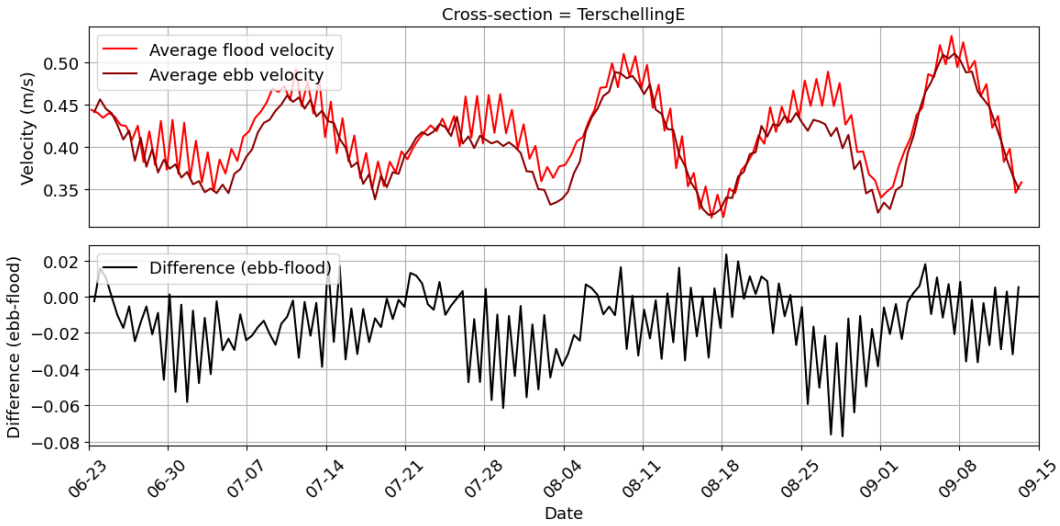

Figure 4.4: Comparison of average flood and ebb velocities over time (top) for the seaside Terschelling cross-section and their difference (bottom) during the 3-month simulation period (positive difference meaning higher ebb velocity).

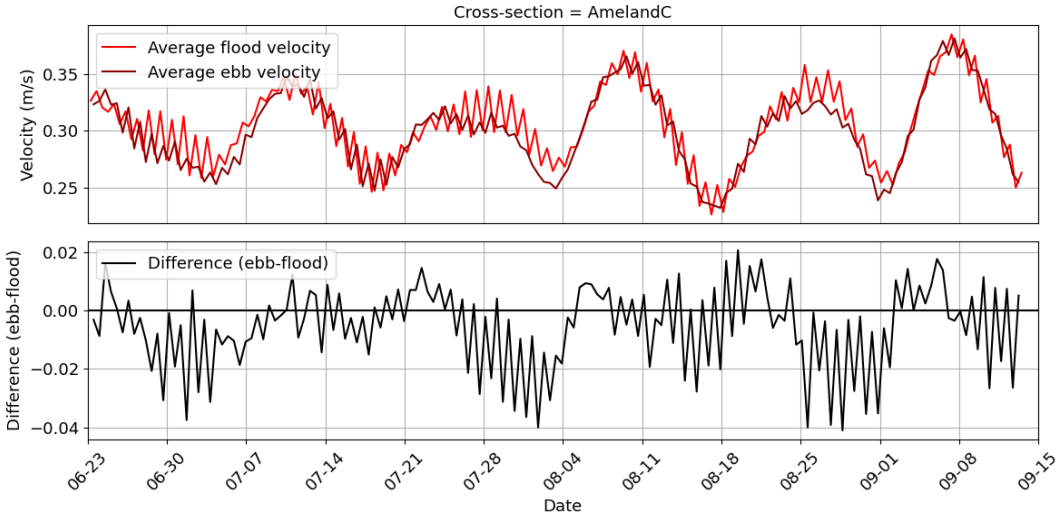

Figure 4.5: Comparison of average flood and ebb velocities over time (top) for the seaside Ameland cross-section and their difference (bottom) during the 3-month simulation period (positive difference meaning higher ebb velocity).

The cross-sectional analysis presented above provides comprehensive overview of water and sediment transport dynamics in the Ameland tidal inlet region, with the key takeaways being:

1. Despite transportation patterns being primarily driven by tidal fluctuations, there is a significant residual discharge over the cross-sections at the ”theoretical” tidal divides.
2. The baseline simulation suggests a slight import of water into the Ameland basin.
3. The residual discharge for all cross-sections perpendicular to the barrier islands of Terschelling and Ameland are eastward, with the magnitude being significantly greater for the seaward cross-sections (AmelandC and TerschellingE) compared to the landward ones.
4. The tidal effects, including both daily and biweekly oscillations, are evident at different locations, with varying visibility across cross-sections depending on their positioning, physical geometry, bathymetry and the magnitude of residual transport. This is particularly the case between the

seaside cross-sections (AmelandC and TerschellingE), with TerschellingE showing a more pronounced influence. The higher general velocities at TerschellingE, compared to AmelandC, explain the greater dependency of sediment transport on the spring-neap tidal cycle observed for TerschellingE.

5. For TerschellingE, the residual sediment transport is not consistently biweekly but shows a four-weekly pattern, influenced by the strength of the spring tides and corresponding flow velocities.
6. The tidal inlet shows high morphodynamic activity with significant sediment transport, whereas sediment transport over the landside cross-sections is negligible when compared to that of the tidal inlet.
7. There are consistently higher average ebb velocities through the tidal inlet over the 3-month period. The average ebb and flood velocities for the seaside cross-sections show lower levels of variation in magnitudes.
8. Although there is an import of water into the Ameland basin, there is a significant export of sediment through the tidal inlet, correlating with higher ebb velocities.
9. The relationship between directionally consistent residual discharge and sediment transport is sensitive, especially for landside cross-sections where sediment transport is relatively minimal.

4.1.2. Spatial maxima of ebb and flood transport

In previous Section 4.1.1 transport through the tidal inlet and interactions between the Ameland and neighbouring basins were determined by analysing hydrodynamics on cross-sections. This section build further on that by showing spatial maps of flow velocities and sediment transport in order to determine the areas of flood and ebb dominance over the entire Ameland inlet domain. It is important to also look at spatial maps instead of only cross-sections, as average ebb of flood dominance of a cross-section is dependent on the location and length of the cross-section. The figures provided in this section give a good overview of where in the domain transports are high and where there are no or negligible small transports.

Figure 4.6 is organized into three rows and two columns. The left column, across all three rows, represents flow velocities, while the right column represents sediment transport. Each row visualizes a different kind of parameter. The first row presents averaged values per tidal cycle (12 hrs, 25 mins) for maximum ebb transport over a 7-day simulation. The middle row shows the corresponding data for flood transport. The bottom row contains the difference between the ebb and flood values, with positive values indicating higher ebb velocities.

The flow velocity maps (left column) and sediment transport maps (right column) show channelized patterns, especially for the main tidal inlet where the strongest transports are observed. Darker shades in these channels highlight the main pathways of water and sediment transport. There is an asymmetric behavior in flow velocities and sediment transport across the domain, as indicated by regions showing higher or lower values during ebb or flood conditions.

Sediment transport is closely linked to flow velocity, which is reflected in the complementary nature of the right column maps to the left column. However, the sediment transport maps show fewer areas with non-zero values compared to the flow velocity maps. This is attributed to the presence of regions where flow velocities do not exceed the critical shear stress threshold necessary to mobilize sediment.

Notably, there is a significant aggregation of sediment transport within the main channel, signifying the movement of material away from the basin or the ebb-tidal delta, depending on the direction of flow. This transport does not directly suggest erosion within the main channel, as it could also be a result of mild erosion over a large area, with the sediment converging in the narrower inlet channels. Areas having minimal transport are typically situated outside the main tidal channels and the ebb-tidal delta, serving as zones of sediment deposition.

The differential map, shown in the bottom row, indicate areas of ebb and flood dominance by quantifying the relative strength of transport during each tidal phase. The positive values indicate ebb dominance in the main channel, highlighting sediment export of the Ameland basin.

Ebb-dominated flow velocities and sediment transport are characteristic of the entire domain, with the exception of flow velocities in the marginal flood channel at the ebb-tidal delta and at the seaward side of the outermost ebb shield. The flood dominance of the marginal flood channel is attributed to its role in directing water into the main channel during flood tides, whereas during ebb tides, the water predominantly exits the basin through the ebb chutes. Bathymetry exerts a significant influence on the water and sediment transport patterns and the process of bypassing is suggested as a possible cause for higher flood velocities at the outer delta locations.

Figure A.1 provides a zoomed-in version of Figure 4.6, focusing on the Ameland ebb-tidal delta.

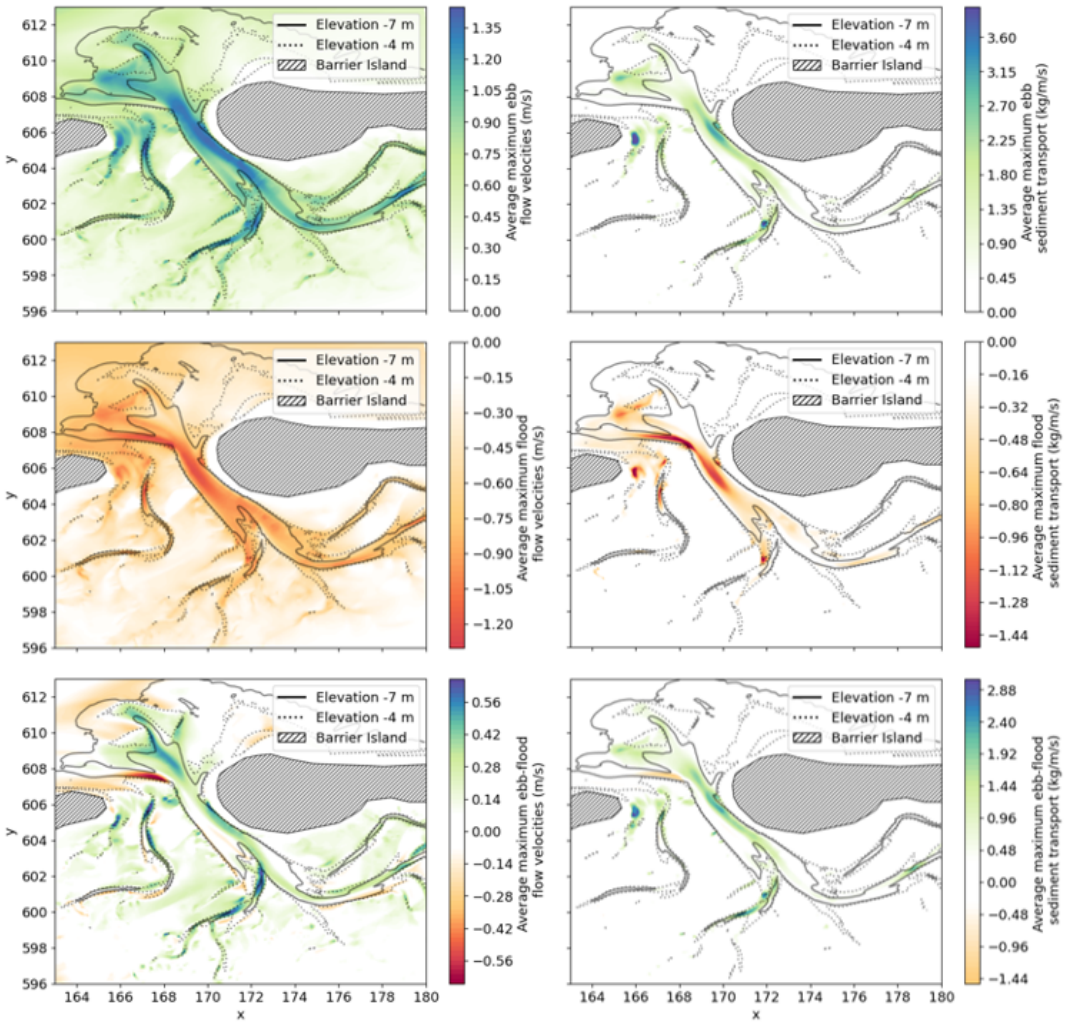

Figure 4.6: Spatial representation of flow velocities (left column) and sediment transport (right column). Top row: averaged values per tidal cycle (12 hrs, 25 mins) for maximum ebb velocity/transport over a 7-day simulation; middle row: corresponding data for flood velocity/transport; bottom row: the difference between the ebb and flood values.

4.1.3. Spatial distribution and transect analysis of bed level change

Figure 4.7 contains four elements. The left column represents the initial bed level and the right column contains data of sedimentation and erosion after a 3-month simulation. The lower row is a zoomed-in version of the top row, only focusing on the Ameland ebb-tidal delta. The transects used in this section are also highlighted in the lower elements.

The sedimentation and erosion pattern indicates a seaward expansion of the two ebb shields at the ebb-tidal delta. Additionally, notable sedimentation and erosion occur at the secondary inlet channels, located west of the Borndiep main channel. In contrast, minimal to no sedimentation or erosion is observed at the ebb-delta margin and the Bornrif platform. Bed level change is less apparent in the flood basin.

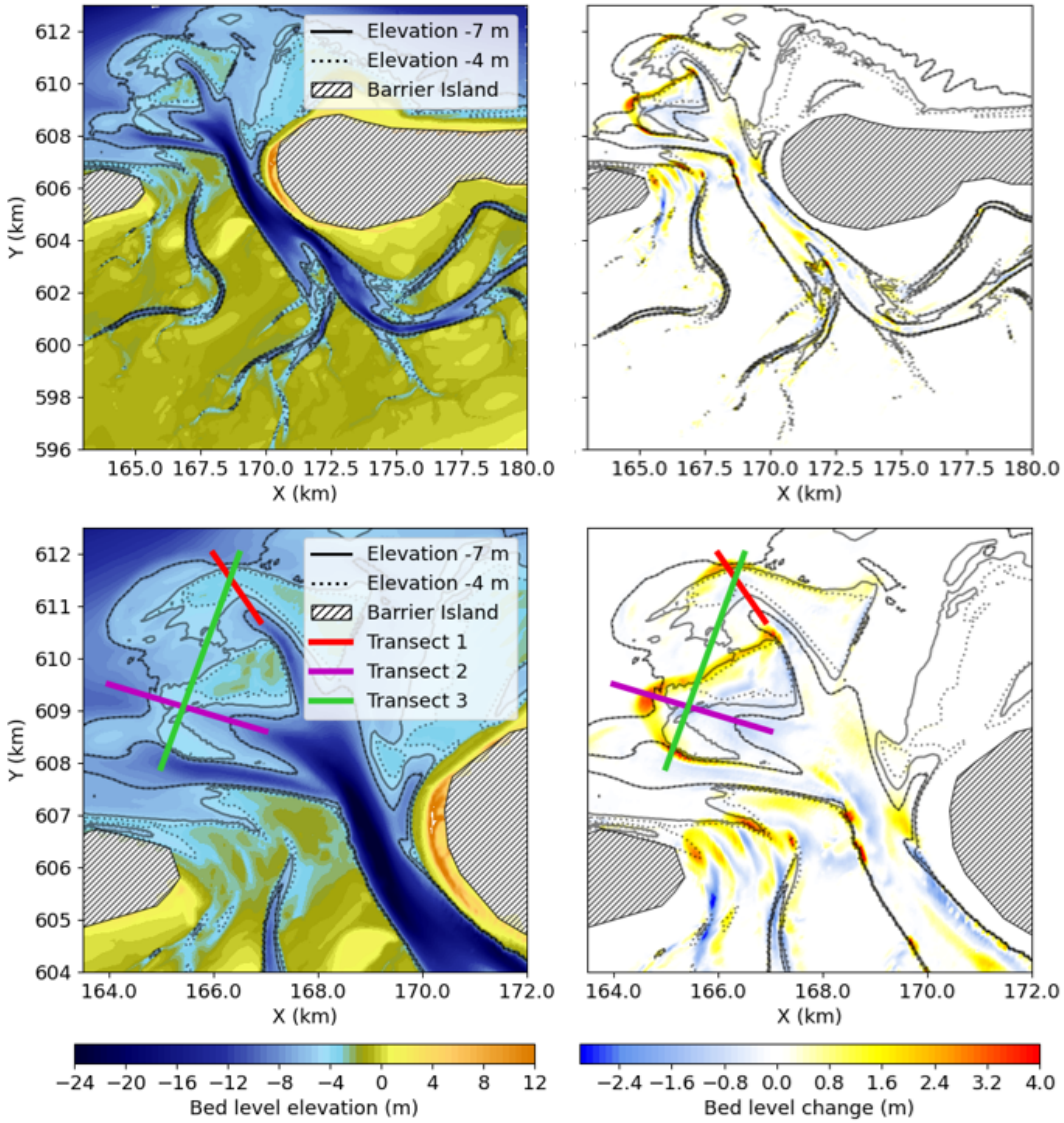

Figure 4.7: Top row: Ameland inlet initial bed level (left column) and bed level change (right column) after a 3-month simulation (Wadden Sea domain, water levels forcing, baseline grid resolution). Bottom row: Zoomed-in version of top row focusing on the ebb-tidal delta and highlighting the locations of Transect 1, Transect 2 and Transect 3.

Figure 4.8 provides a transect analysis of bed level changes across three distinct transects. Each transect is divided into two figures: one showing the initial bed level and indicates areas of sedimentation and erosion (A series) and the other quantifies the sedimentation and erosion (B series).

The figures for transect 1 and 2 show the seaward expansion of the two ebb shields. The bed level is steeper at both sides of the ebb shield for transect 1 compared to transect 2. Both show smoothing of the landward side and a steepening of the seaside of the ebb shield.

The figure for transect 3 shows the bed level change pattern across the ebb-tidal delta. This transect is provided to give context to the nature of sedimentation and erosion. On the one hand, there can be sedimentation visible when there is a expansion of an ebb shield, however there can also be sedimentation observed in other areas where the bed level increases. Both indicate sedimentation, but the underlying mechanism is different.

For element 2A, there is erosion across a much wider domain than for the area where there is sedimentation. While the spatial sedimentation and erosion distribution (Figure 4.7) draws attention to this area of high sedimentation, the total volume of erosion might be more significant although spread-out over a larger area. This is one important consideration to bear in mind when interpreting spatial sedimentation and erosion distributions.

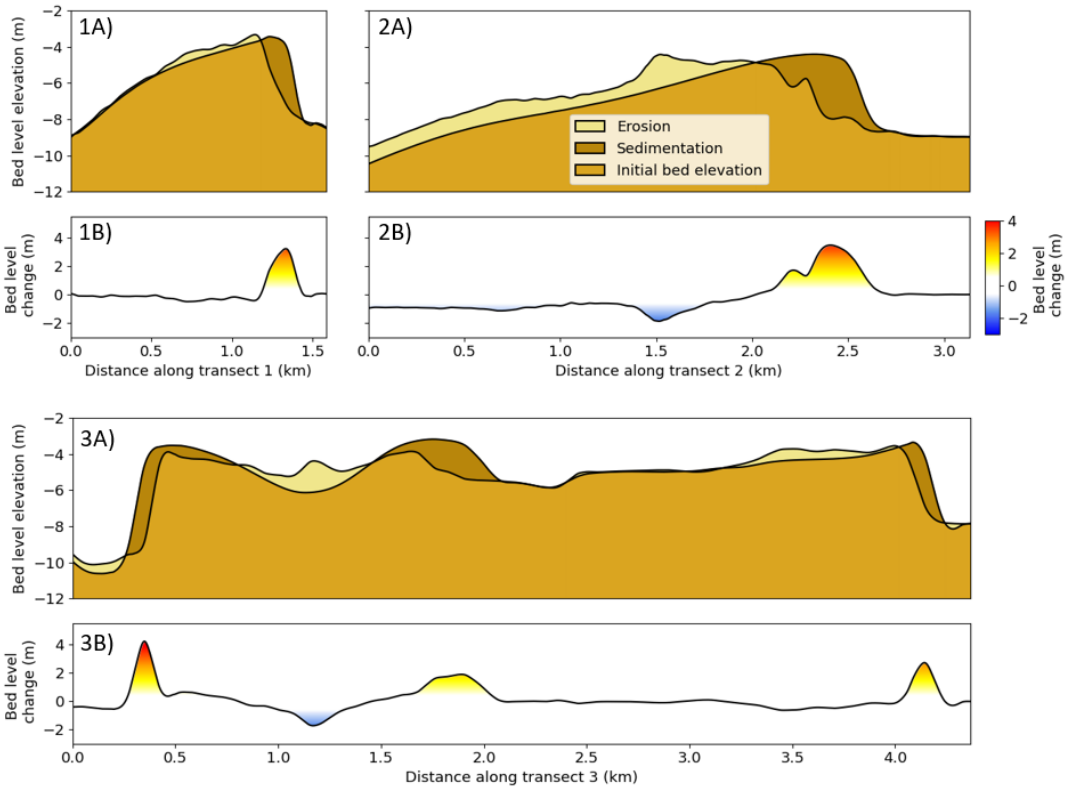

Figure 4.8: Transect analyses of bed level change for three distinct transects. Figures 1A, 2A and 3A show the initial bed level with highlighted areas of sedimentation and erosion. Figures 1B, 2B and 3B provide quantified sedimentation and erosion values. The transect numbering is consistent with those presented in Figure 4.7.

4.2. Variation in model domain (tide-only forcing)

This section builds further upon the previous section by comparing the simulation of the baseline model with Wadden Sea domain to a simulation with a smaller domain of the Ameland tidal inlet and basin. The Wadden Sea domain can be interpreted as a multi-inlet schematization, while the Ameland domain is a single-inlet schematization as it only includes the Ameland tidal inlet.

This section specifically focuses on differences between the two simulations. First the water and sediment interchange through the Ameland inlet, the exchange of water and sediment between the Ameland basin and adjacent basin are compared in Section 4.2.1. Then Section 4.2.2 analyse the differences in spatial maxima and minima of ebb and flood transport. This is followed by a section on spatial distribution of bed level change and transect analysis (4.2.3).

4.2.1. Cross-sectional hydrodynamic analysis

Line charts show during which periods in time the transports diverges between different simulations and when the transports stay the same (i.e., parallel to each other). Figures 4.9 and 4.10 show transport dynamics for the two seaward cross-sections AmelandC and TerschellingE. The minimal difference in residual discharge translates to a meaningful difference in residual sediment transport, despite the variations in average flow velocities being barely noticeable.

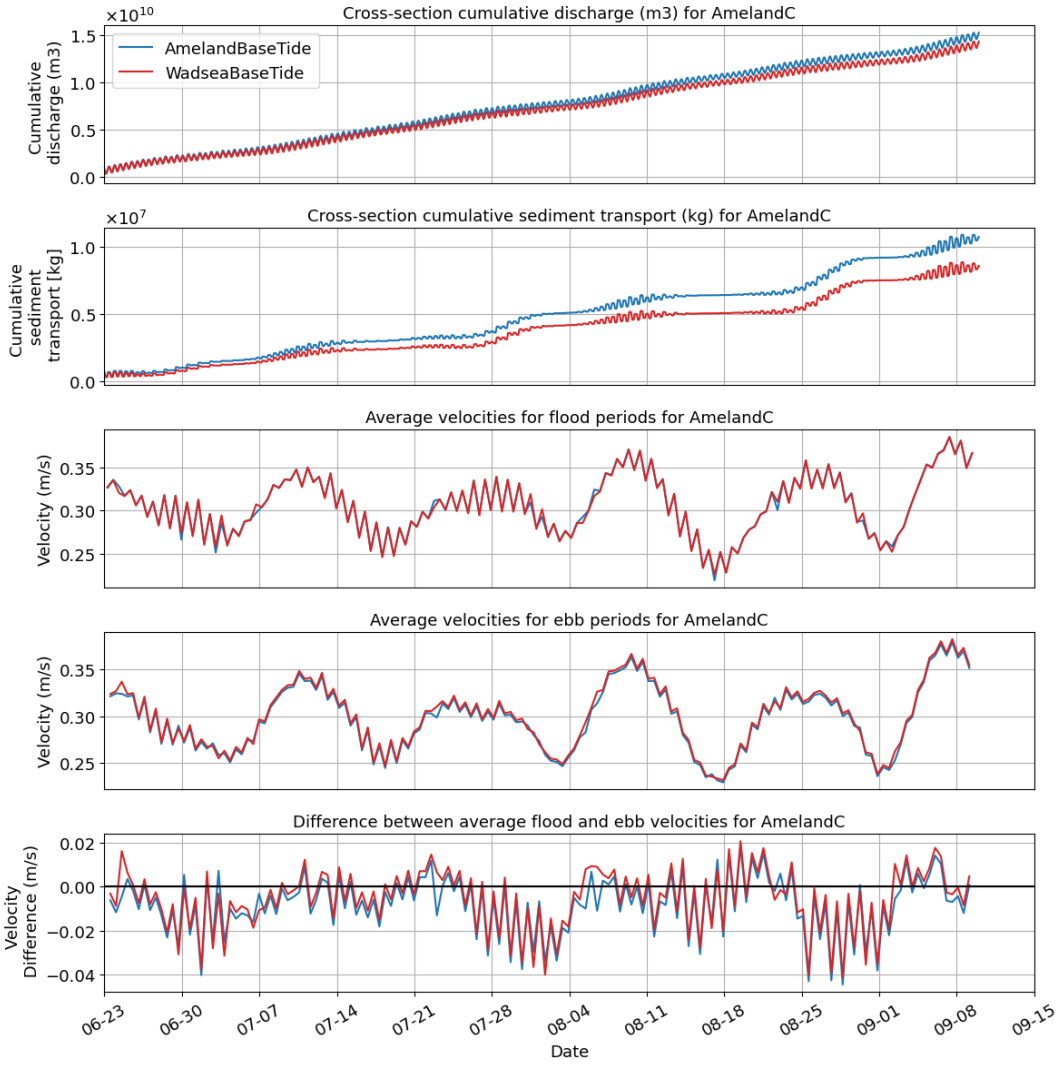

Figure 4.9: Comparison of simulation results for the seaside Ameland cross-section for two different model domains: Ameland and Wadden Sea. The figure showcases five subplots: the topmost plot shows the cumulative discharge for both domains, followed by a plot on cumulative sediment transport. The third and fourth plots illustrate average velocities during flood and ebb periods, respectively. The lower plot highlights the difference between the average flood and ebb velocities (ebb-flood).

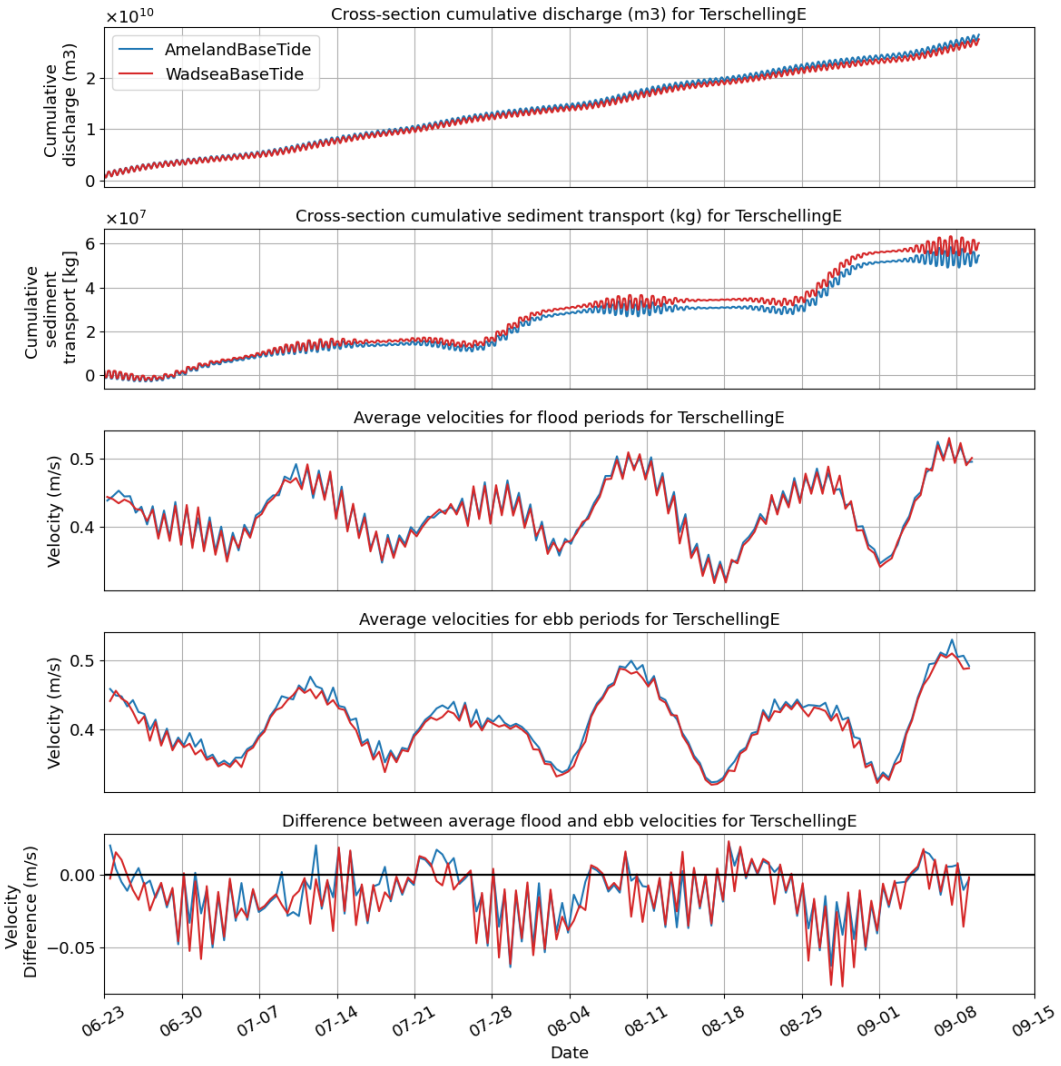

Figure 4.10: Comparison of simulation results for the seaside Terschelling cross-section for two different model domains: Ameland and Wadden Sea. The figure showcases five subplots: the topmost plot shows the cumulative discharge for both domains, followed by a plot on cumulative sediment transport. The third and fourth plots illustrate average velocities during flood and ebb periods, respectively. The lower plot highlights the difference between the average flood and ebb velocities (ebb-flood).

Figure 4.11 shows that the multi-inlet schematization (Wadden Sea model) shows a slight net import of water in the Ameland basin. The net import of the single-inlet schematization (Ameland model) shows relatively no import or export of water. This is as expected, as this single-basin schematization cannot store significantly more or less water due to fixed boundaries.

The model with Ameland domain shows about twice as much export of sediment through the tidal inlet compared to the baseline model. This can be related to the fact that, while the Ameland model shows higher ebb and flood velocities compared to the Wadden Sea model (third and fourth element of Figure 4.11, the difference between ebb and flood velocities is larger for the Ameland model (fifth element of Figure 4.11).

Another difference to note between this multi-line chart for the tidal inlet cross-section compared to the multi-line charts for the AmelandC and TerschellingE cross-sections (figures 4.9 and 4.10) is in the periods of significant residual sediment transport. The analysis of seaside cross-sections AmelandC and TerschellingE showed that significant residual sediment transport occurred during periods characterized by a moderate spring-tide, however this figure for the tidal inlet cross-section (Figure 4.11), shows that fastest development of the net sediment transport occurs during periods with a more pronounced spring-tide.

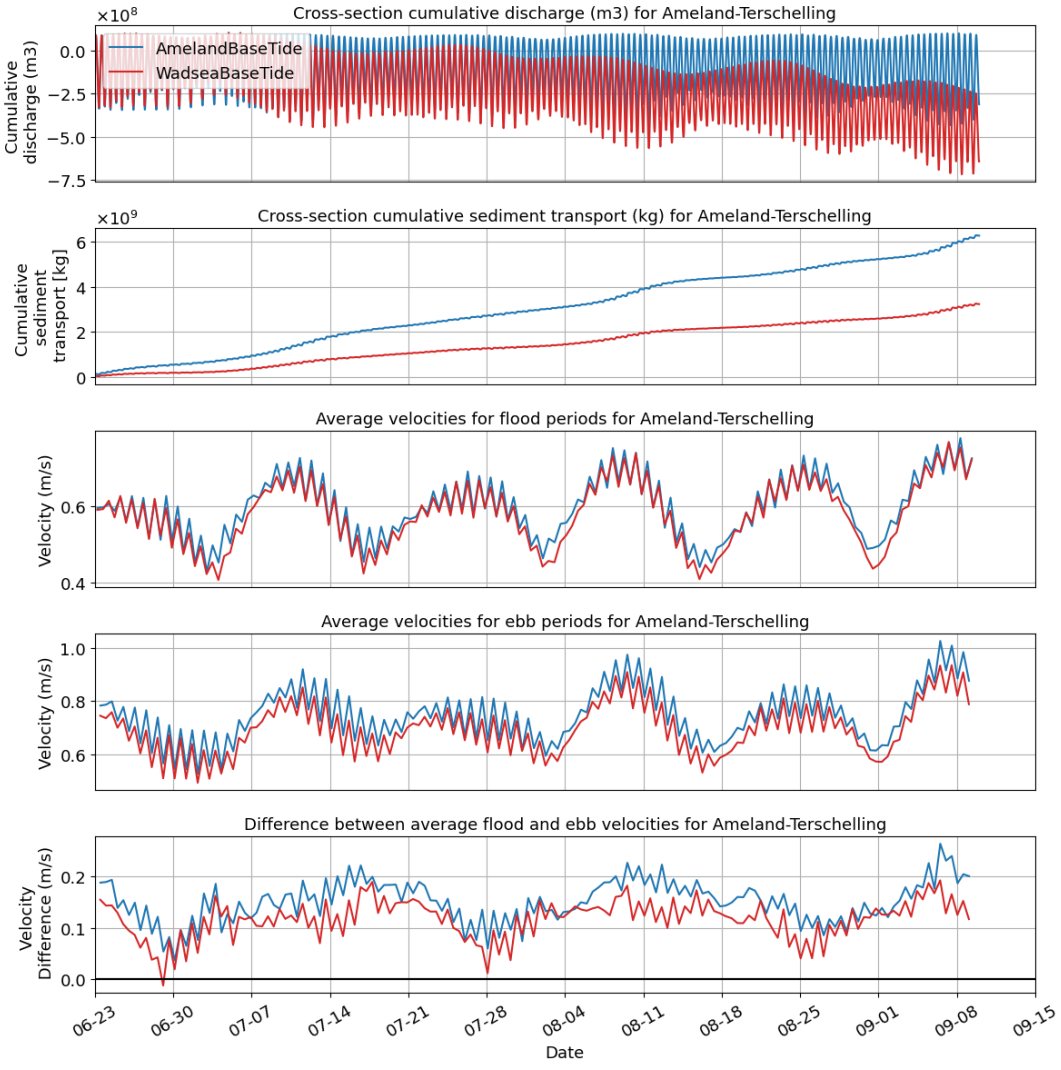

Figure 4.11: Comparison of simulation results for the tidal inlet cross-section for two different model domains: Ameland and Wadden Sea. The figure showcases five subplots: the topmost plot shows the cumulative discharge for both domains, followed by a plot on cumulative sediment transport. The third and fourth plots illustrate average velocities during flood and ebb periods, respectively. The bottom plot highlights the difference between the average flood and ebb velocities (ebb-flood).

Following is a series of bar charts, showing positive, negative and residual discharge and sediment transport for various cross-sections for different model schematizations. East- and northward directed transport is determined as the positive direction. The bars in the bar charts are defined as the average cumulative discharge or sediment transport per tidal cycle of 12 hours and 25 minutes. As the data is obtained from 3-month simulations, the average represents data for 180 consecutive tidal cycles. Bar charts are used to highlight differences between model scenarios, not only in residual transport but also in the magnitudes of ebb and flood transport per tidal cycle.

Figure 4.12 shows the bar chart for the tidal inlet cross-section. While the relative size of residual discharge is very small (top element), the relative size of residual sediment transport is significant (lower element). On average, both simulations have a flood dominant discharge and ebb dominant sediment transport. This is due to the previously discussed difference in ebb and flood flow velocities. The single-inlet schematization (Ameland model) shows more extreme ebb-dominance than the multi-inlet schematization (Wadden Sea model). This extremer ebb-dominance does mainly result from the single-inlet simulation having a larger export of sediment, as the two models have approximately the same magnitudes of sediment transport during flooding. Note that sediment transport is measured in kilograms (*kg*). To calculate this, the volume of sediment transported (measured in cubic meters, m^3) is multiplied by the sediment density, which is 2650 *kg*/m^3.

Bar charts for the seaside cross-sections TerschellingE and AmelandC are provided in Appendix B.

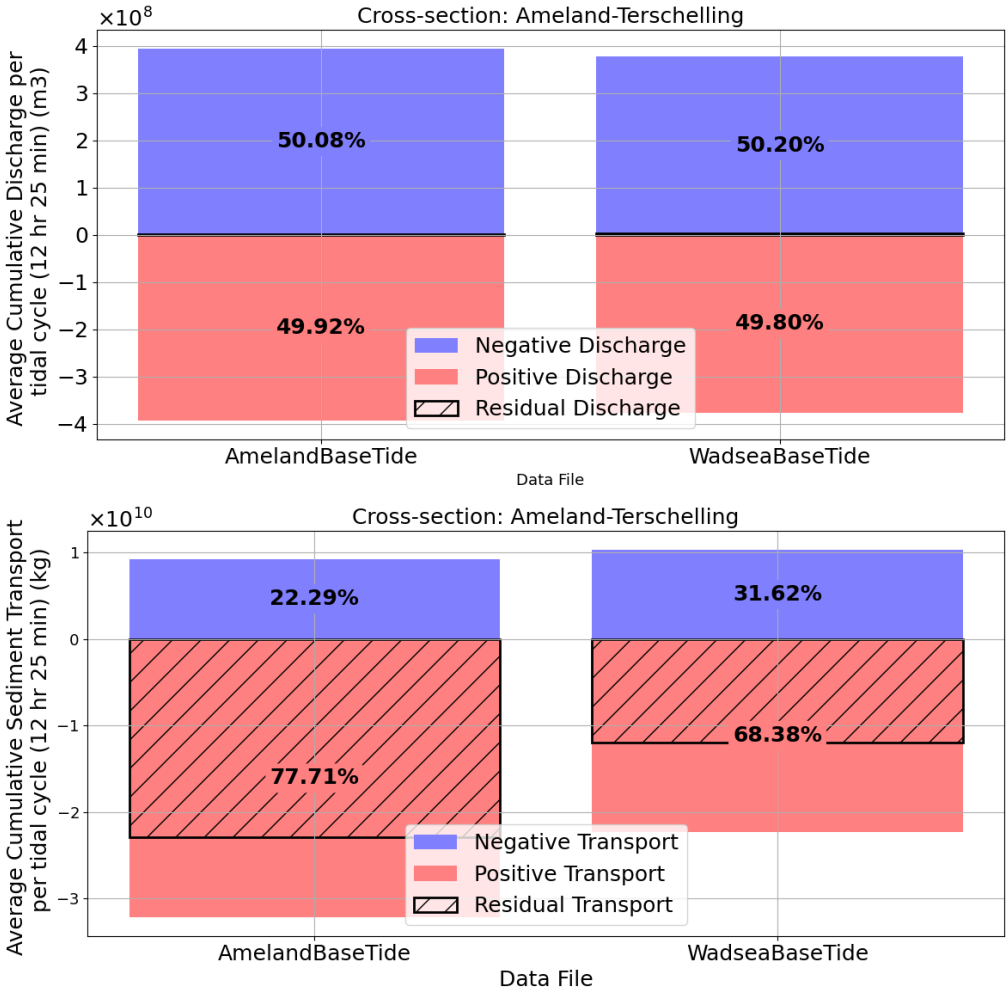

Figure 4.12: Comparison of cumulative discharge (top figure) and sediment transport (lower figure) under tide-only forcing per tidal cycle (12 hrs, 25 mins) averaged over a 3-month simulation across the tidal inlet cross-section. Positive discharge and transport indicate westward and northward flow, while negative values represent southward and eastward flow.

Asymmetry in velocity signal is one aspect influencing residual sediment transport. Asymmetric behavior impacts the direction and magnitude of net sediment movement. Additionally, phase difference between velocity signals also affect residual transport dynamics. Phase variations can result from diverse external forcing or interactions within the system.

Figure 4.13 shows the average flow velocity across the tidal inlet cross-section for the Ameland and Wadden Sea schematizations. The average velocity signal for the Wadden Sea schematization slightly lags behind that of the Wadden Sea schematization. Additionally, the peaks and troughs of both signals have subtle variances in their patterns.

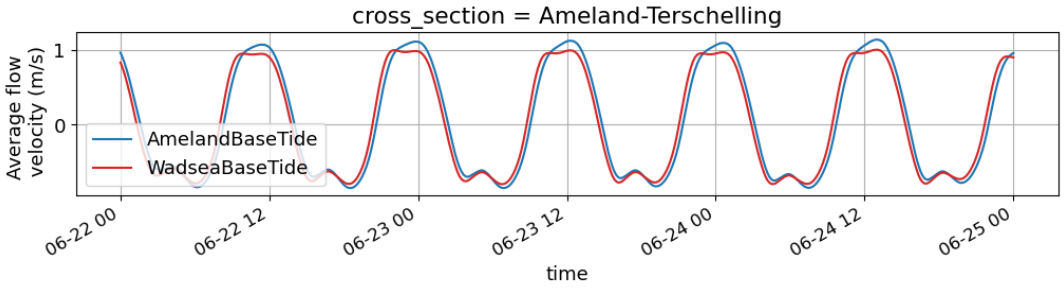

Figure 4.13: Comparison of simulation results for two different model domains: Ameland and Wadden Sea. The graph represents average water flow velocities across the tidal inlet cross-section over a 3-day period.

4.2.2. Spatial maxima of ebb and flood transport

Section 4.1.2 describes the spatial distribution of ebb and flood flow velocity and sediment transport for the baseline simulation. Figures 4.14 and 4.15 adds on that analysis by presenting in the left columns the data obtained from the single-inlet Ameland schematization and in the right columns the difference between the multi-inlet and single-inlet simulations (where positive values indicate the single-inlet simulations having higher velocities and transports).

Darker shades in the right column of Figure 4.14 indicates that the Ameland simulation has higher ebb flow velocities across the ebb-tidal delta, main inlet channel and western side of the Ameland basin. The Ameland simulations also has higher flood velocities at the western side of the Ameland basin. This translates to mixed differences at the western side of the basin and in higher ebb velocities in the main inlet channel and ebb-tidal delta for the Ameland model. This signifies that more sediment is moved out of the basin for the Ameland model.

Figure 4.14 reveals that the Ameland simulation has higher ebb sediment transport in the main tidal channel and at the inlet throat. It also shows that the Ameland model has higher flood transports in tidal channels in the basin that extent from the main inlet channel in western direction. These flood sediment transport magnitudes are, however, only a small fraction of the ebb sediment transport magnitudes. Consequently, the Ameland model shows more extreme ebb-dominance over the entire tidal inlet region regarding sediment transport.

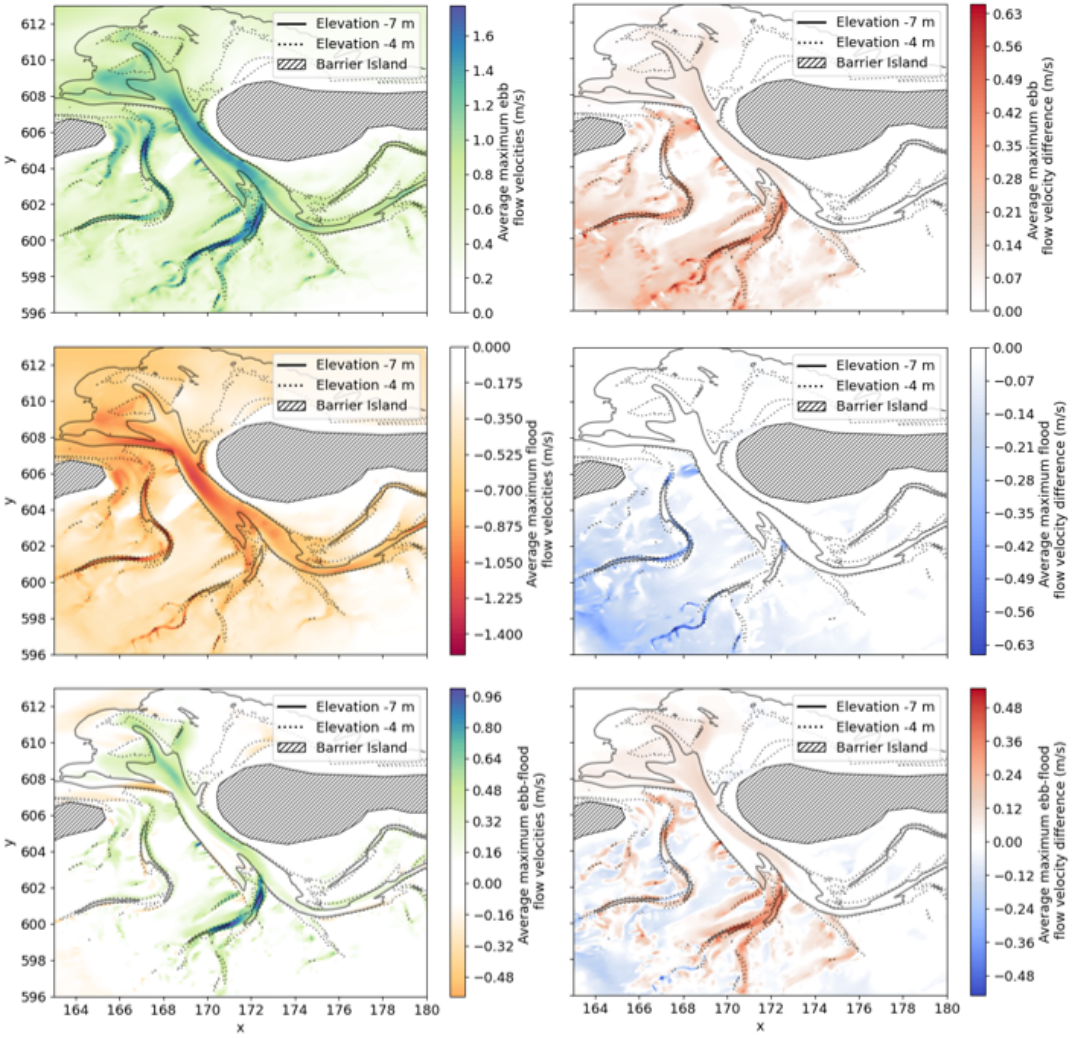

Figure 4.14: Spatial representation of flow velocities comparing two different model domains: Ameland and Wadden Sea over the ebb-tidal delta. The left column (a) represents data from the Ameland simulation, while the right column (b) shows the difference in velocities between the Ameland and Wadden Sea simulations (Ameland-Wadden Sea). Top row: averaged values per tidal cycle (12 hrs, 25 mins) for maximum ebb flow velocity over a 7-day simulation; middle row: corresponding data for flood flow velocity; bottom row: the difference between the ebb and flood values.

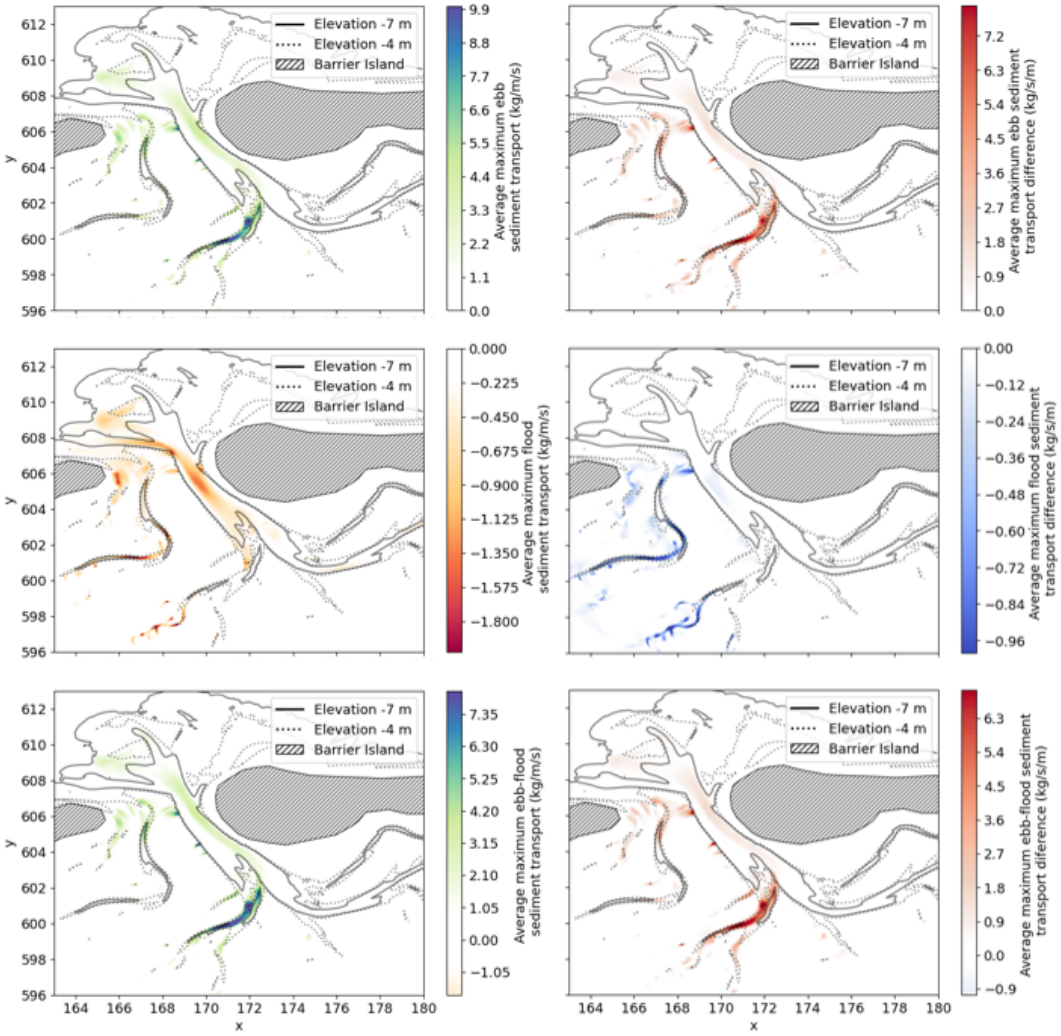

Figure 4.15: Spatial representation of sediment transport comparing two different model domains: Ameland and Wadden Sea over the ebb-tidal delta. The left column (a) represents data from the Ameland simulation, while the right column (b) shows the difference in sediment transport between the Ameland and Wadden Sea simulations (Ameland-Wadden Sea). Top row: averaged values per tidal cycle (12 hrs, 25 mins) for maximum ebb sediment transport over a 7-day simulation; middle row: corresponding data for flood sediment transport; bottom row: the difference between the ebb and flood values.

4.2.3. Spatial distribution and transect analysis of bed level change

The sedimentation and erosion pattern indicates a seaward expansion of the two ebb shields at the ebb-tidal delta. Additionally, notable sedimentation and erosion occur at the secondary inlet channels, located west of the Borndiep main channel. In contrast, minimal to no sedimentation or erosion is observed at the ebb-delta margin and the Bornrif platform.

While no bed level change was apparent in the flood basin for the baseline simulation, there is significant sedimentation and erosion for the Ameland inlet model (4.16). Additionally, severe change is observed in the main inlet channel and the Boschgat is connecting to the main inlet channel.

Figure 4.17 indicates that the Ameland simulation has more severe bed level change compared to the Wadden Sea model. Generally, the areas of erosion are deeper and areas of sedimentation have a higher elevation in the Ameland model. This means that patterns of sedimentation and erosion align, but the magnitudes differ considerably.

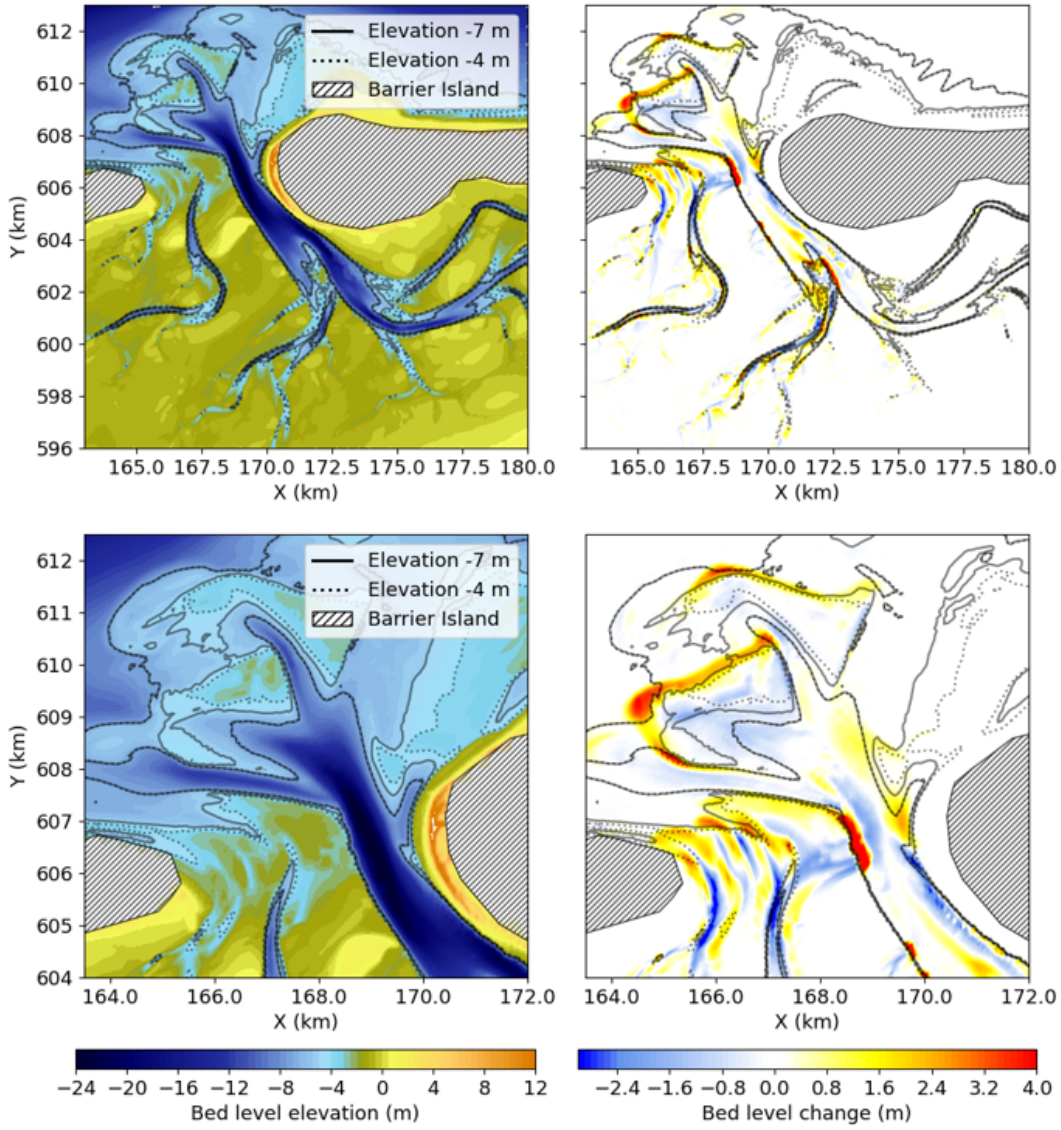

Figure 4.16: Top row: Ameland inlet initial bed level (left column) and bed level change (right column) after a 3-month simulation (Ameland domain, tide-only forcing, baseline grid resolution). Bottom row: Zoomed-in version of top row focusing on the ebb-tidal delta.

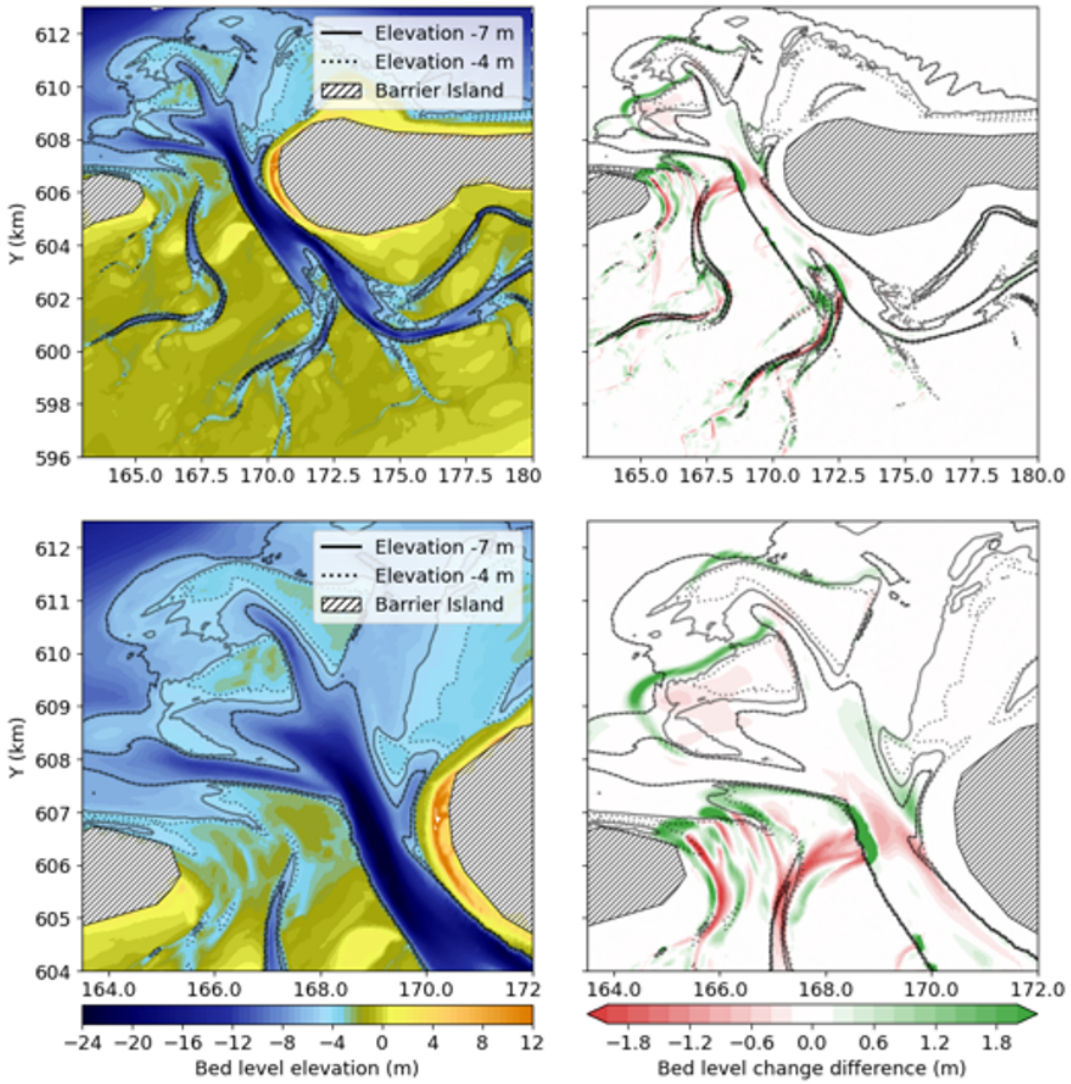

Figure 4.17: Top row: Initial bed level of the Ameland inlet (left) and bed level change difference between the Ameland and Wadden Sea models after a 3-month simulation (right), under tide-only forcing and baseline grid resolution. Positive values indicate larger positive bed level changes in the Ameland simulation. Bottom row: Zoomed-in version of the top row focusing on the ebb-tidal delta.

The results from the transect analysis indicate that both simulations result is comparable transects, with the Ameland simulation having a more extreme seaward expansion of the ebb-shields (1A and 2A from Figure 4.18). This can be related to the Ameland simulation showing much more export of sediment (4.2.1). The Ameland has a slightly milder slope for the outer side of the ebb-shield closest to shore (1A), but similar slopes are observed at the most seaward ebb shield (2A).

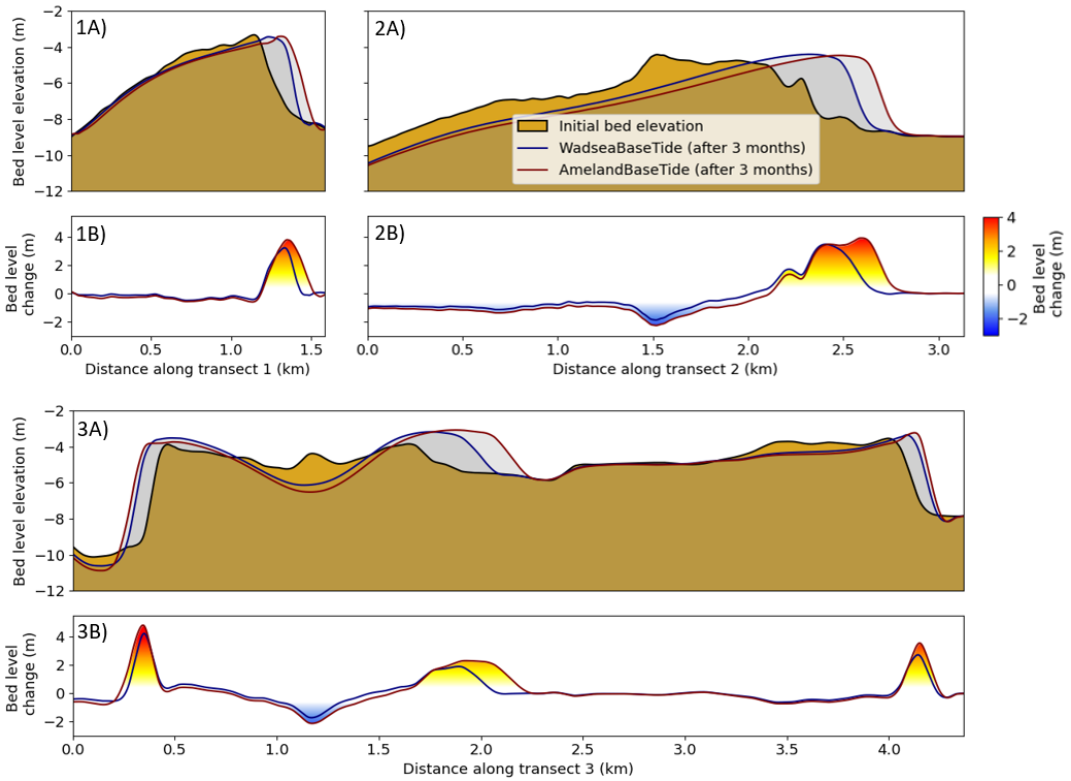

Figure 4.18: Transect analyses of bed level change for three distinct transects. Comparison of simulation results for two different model domains: Ameland and Wadden Sea. Figures 1A, 2A and 3A show the initial bed level and bed level for the two simulations after 3 months. Figures 1B, 2B and 3B provide quantified sedimentation and erosion values. The transect numbering is consistent with those presented in Figure 4.7.

4.3. Variation in forcing processes (Wadden Sea domain)

The analysis of Section 4.2 indicated that a single-inlet Ameland domain schematization showed different water and sediment transport dynamics compared to a more inclusive multi-inlet Wadden Sea schematization. This section details simulations with the Wadden Sea domain further, analysing the effects of varying forcing actors.

To help interpret differences between models with or without the wind forcing component, distinct periods of wind flow have been analysed in Appendix D. This analysis resulted in the information presented in Table 4.1.

Table 4.1: Summary of wind conditions from 06-22-2017 to 09-14-2017

Start Date	End Date	Wind Condition
06-22-2017	07-04-2017	Weak western wind
07-04-2017	07-11-2017	Almost no wind
07-11-2017	07-18-2017	Weak western wind
07-18-2017	07-26-2017	Almost no wind
07-26-2017	08-04-2017	Mild south-western wind
08-04-2017	08-07-2017	Mild western wind
08-07-2017	08-09-2017	Almost no wind
08-09-2017	08-16-2017	Almost no wind
08-16-2017	08-23-2017	Weak south-western wind
08-23-2017	09-02-2017	Almost no wind
09-02-2017	09-08-2017	Mild south-western wind
09-08-2017	09-14-2017	Strong south-western wind

Periods of virtually no wind, weak wind and mild wind alternate with each other, ending with a period with strong wind. The wind generally comes from (south-)western direction.

4.3.1. Cross-sectional hydrodynamic analysis

Comparing model results for simulation that include wind forcing is more comprehensive because the wind forcing actor is very time-dependent. Figure 4.20 shows this time-dependency for the cumulative water and sediment transport through the Ameland tidal inlet. During periods in time with moderate to strong southwesterly wind, there is significant divergence between the trends in cumulative discharge between model simulations that include or exclude wind forcing. The cumulative sediment transport is, however, not much affected by wind severity.

Simulations without wind have a slight import of water into the Ameland basin, whereas simulations that include the wind forcing actor show a net export of water for the Ameland inlet cross-section. While the simulation with wind showed slightly more export of sediment, the change is not of similar magnitude compared to the change in residual discharge dynamics.

The simulation incorporating wind forcing reveals a substantial increase in residual discharge at the landside Terschelling cross-section, along with a more modest elevation in outflow at the landside Ameland cross-section (Figure 4.19), which aligns with the net water export observed at the Ameland inlet.

The significant divergence in residual discharge, while having limited divergence for residual sediment transport could, be attributed to the divergence in residual discharge happens during a period of neap-tide. This indicates that the flow velocities are too low to mobilize sediment. Finally, there is net export of sediment for the Ameland inlet for all variations, caused by average ebb velocities which are most often 0.05 to 0.2 m/s higher.

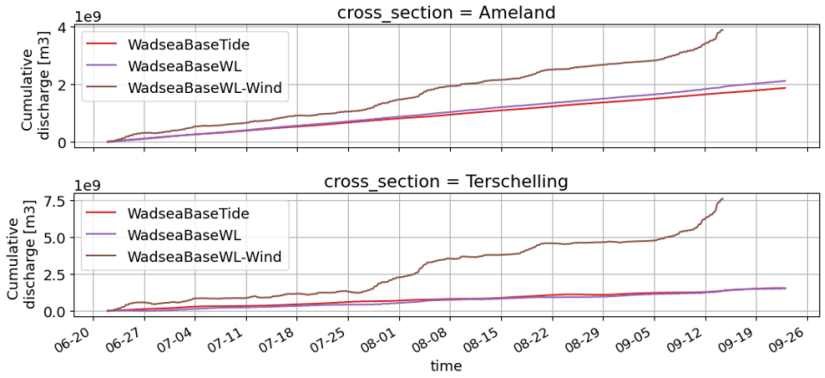

Figure 4.19: Temporal progression of cumulative water discharge for three different forcing scenarios at the landside Ameland (top figure) and Terschelling (bottom figure) cross-sections.

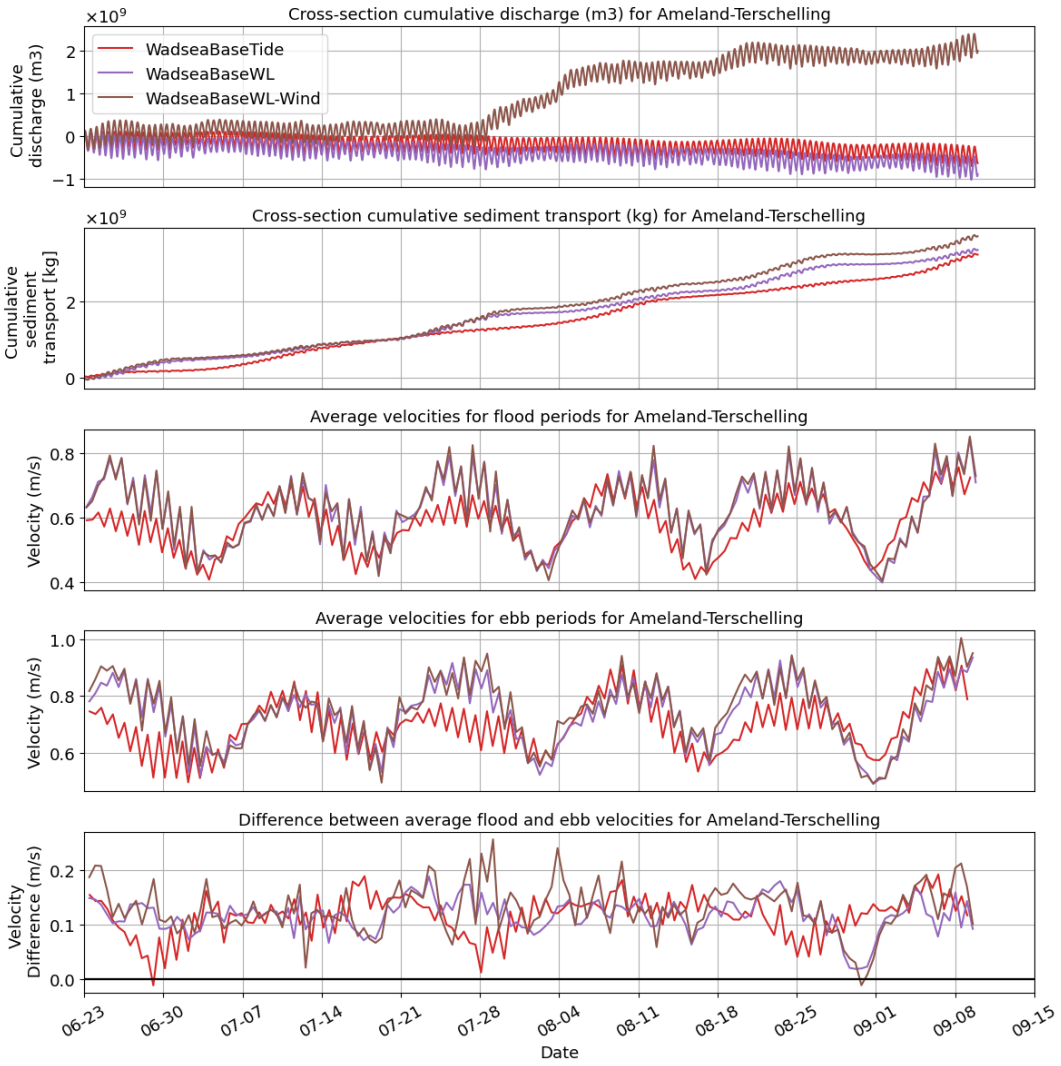

Figure 4.20: Comparison of simulation results for the tidal inlet cross-section for three different forcing processes: tide-only, water levels, wind. The figure showcases five subplots: the topmost plot shows the cumulative discharge for both domains, followed by a plot on cumulative sediment transport. The third and fourth plots illustrate average velocities during flood and ebb periods, respectively. The lowest plot highlights the difference between the average flood and ebb velocities (ebb-flood).

Figures 4.21 and 4.22 show the cumulative water and sediment transport for the cross-sections defined at the seaward side of the barrier islands. The cumulative discharge (top elements of these two figures) show a similar trends as the tidal inlet cross-section, as the wind forcing causes more extreme cumulative discharge. Where the wind forcing actor did not provide a clear distinction in cumulative sediment transport over the tidal inlet cross-section between the three simulations, it does provide it for the seaward AmelandC and TerschellingE cross-sections.

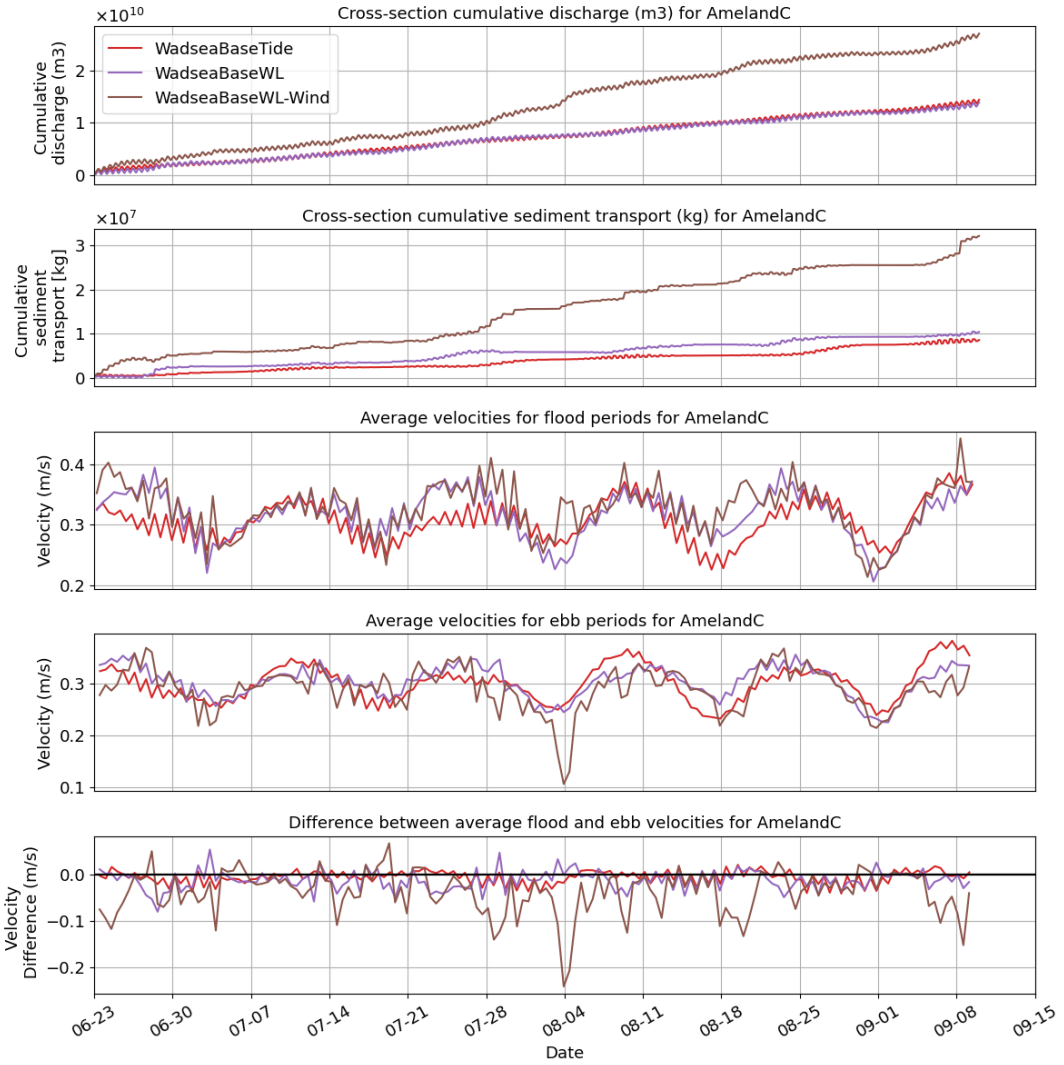

Figure 4.21: Comparison of simulation results for the seaside Ameland cross-section for three different forcing processes: tide-only, water levels, wind. The figure showcases five subplots: the topmost plot shows the cumulative discharge for both domains, followed by a plot on cumulative sediment transport. The third and fourth plots illustrate average velocities during flood and ebb periods, respectively. The lowest plot highlights the difference between the average flood and ebb velocities (ebb-flood).

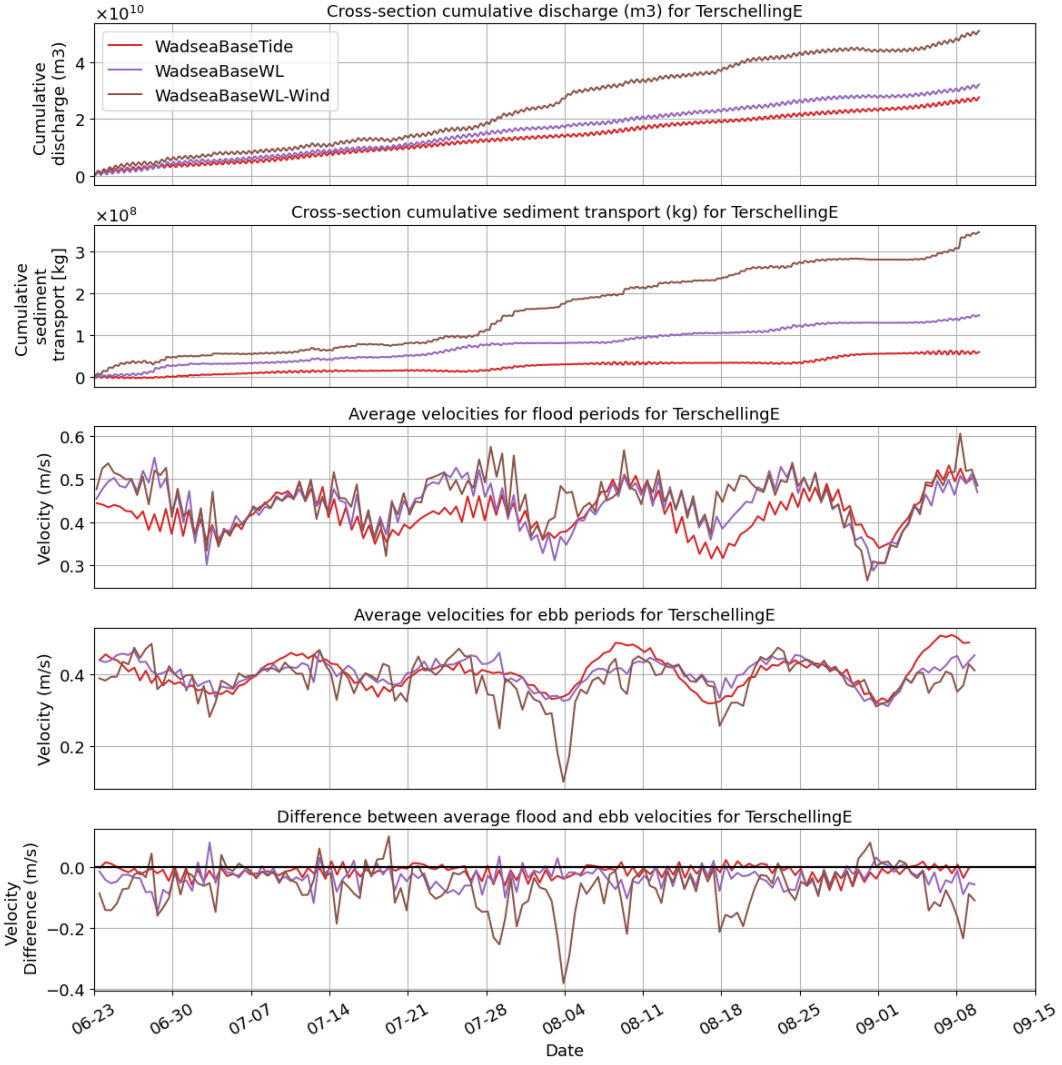

Figure 4.22: Comparison of simulation results for the seaside Terschelling cross-section for three different forcing processes: tide-only, water levels, wind. The figure showcases five subplots: the topmost plot shows the cumulative discharge for both domains, followed by a plot on cumulative sediment transport. The third and fourth plots illustrate average velocities during flood and ebb periods, respectively. The lowest plot highlights the difference between the average flood and ebb velocities (ebb-flood).

Presenting bar charts of the ebb and flood cumulative transport averaged over the tidal cycles does not give a representative image for the entire simulation period. This is because the effects of the very time-dependent wind forcing are averaged across all tidal cycles. Especially when only having simulated for 3-months, severe episodic wind events can influence the model outcomes significantly. Therefore only the bar chart for sediment transport the tidal inlet cross-section is presented here, as the trend in that data seems little to be affected by the wind forcing actor. Figure 4.23 shows that the tide-only simulation results in reduced ebb and flood sediment transport magnitudes when compared with simulations that incorporate additional forcing actors such as water level fluctuations and wind. Although these factors increase overall sediment transport during flood and ebb tides, the sediment pathways can lead to comparable levels of residual transport across a tidal cycle.

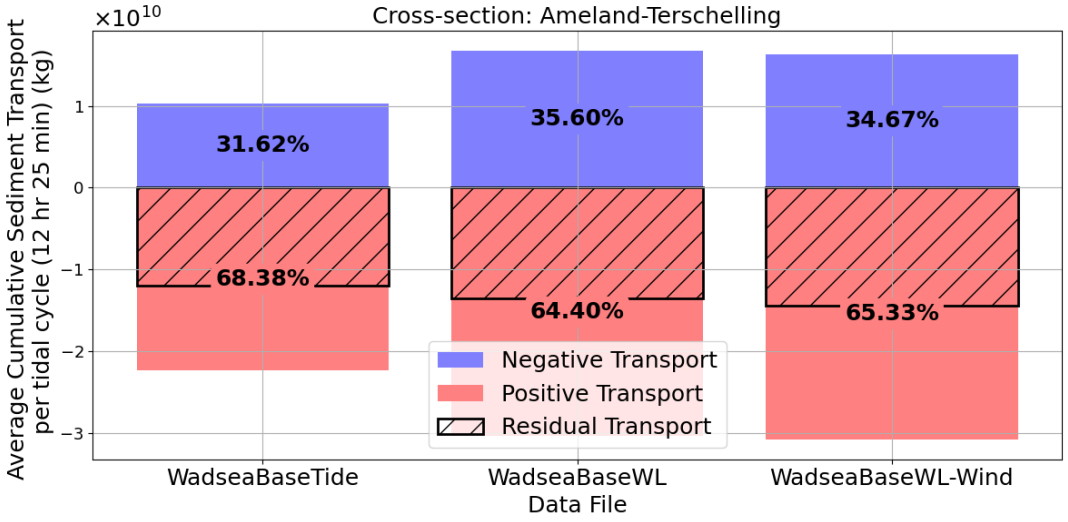

Figure 4.23: Comparison of cumulative sediment transport for three forcing variations per tidal cycle (12 hrs, 25 mins) averaged over a 3-month simulation across the tidal inlet cross-section. Positive discharge and transport indicate westward and northward flow, while negative values represent southward and eastward flow.

Figure 4.24 shows the average flow velocity over the Ameland tidal inlet cross-section for a 3-day period. In this period there was a relatively mild wind condition. The peaks and troughs of the signals have subtle variances in their patterns. This can be one of the reasons for divergent sediment transport behaviors between the model schematizations, leading to diverging morphological changes over time.

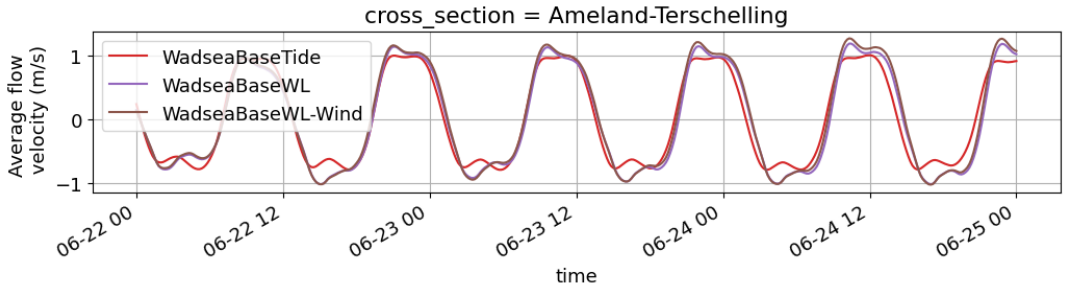

Figure 4.24: Comparison of simulation results for three different forcing processes: tide-only, water levels, wind. The graph represents average water flow velocities across the tidal inlet cross-section over a 3-day period.

4.3.2. Spatial distribution and transect analysis of bed level change

Similar to previous simulation results shown, the sedimentation and erosion pattern indicates a seaward expansion of the two ebb shields at the ebb-tidal delta. Additionally, notable sedimentation and erosion occur at the secondary inlet channels, located west of the Borndiep main channel. In contrast, minimal to no sedimentation or erosion is observed at the ebb-delta margin and the Bornrif platform. Differences between the two simulations having tide-only and water level fluctuation forcing predominantly arise mainly at the secondary inlet channels, which is a highly morphodynamic area.

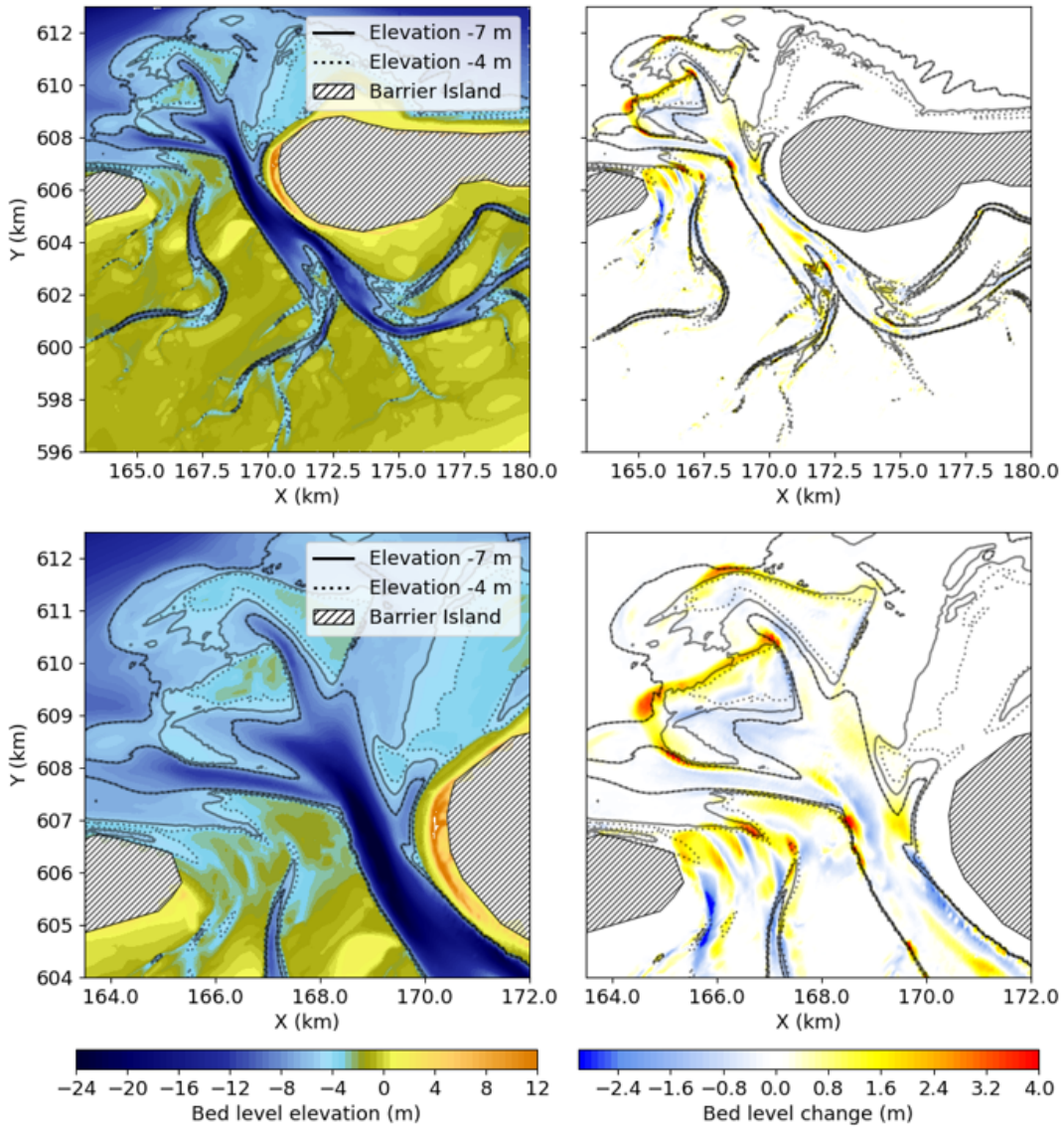

Figure 4.25: Top row: Ameland inlet initial bed level (left column) and bed level change (right column) after a 3-month simulation (Wadden Sea domain, water levels forcing, baseline grid resolution). Bottom row: Zoomed-in version of top row focusing on the ebb-tidal delta.

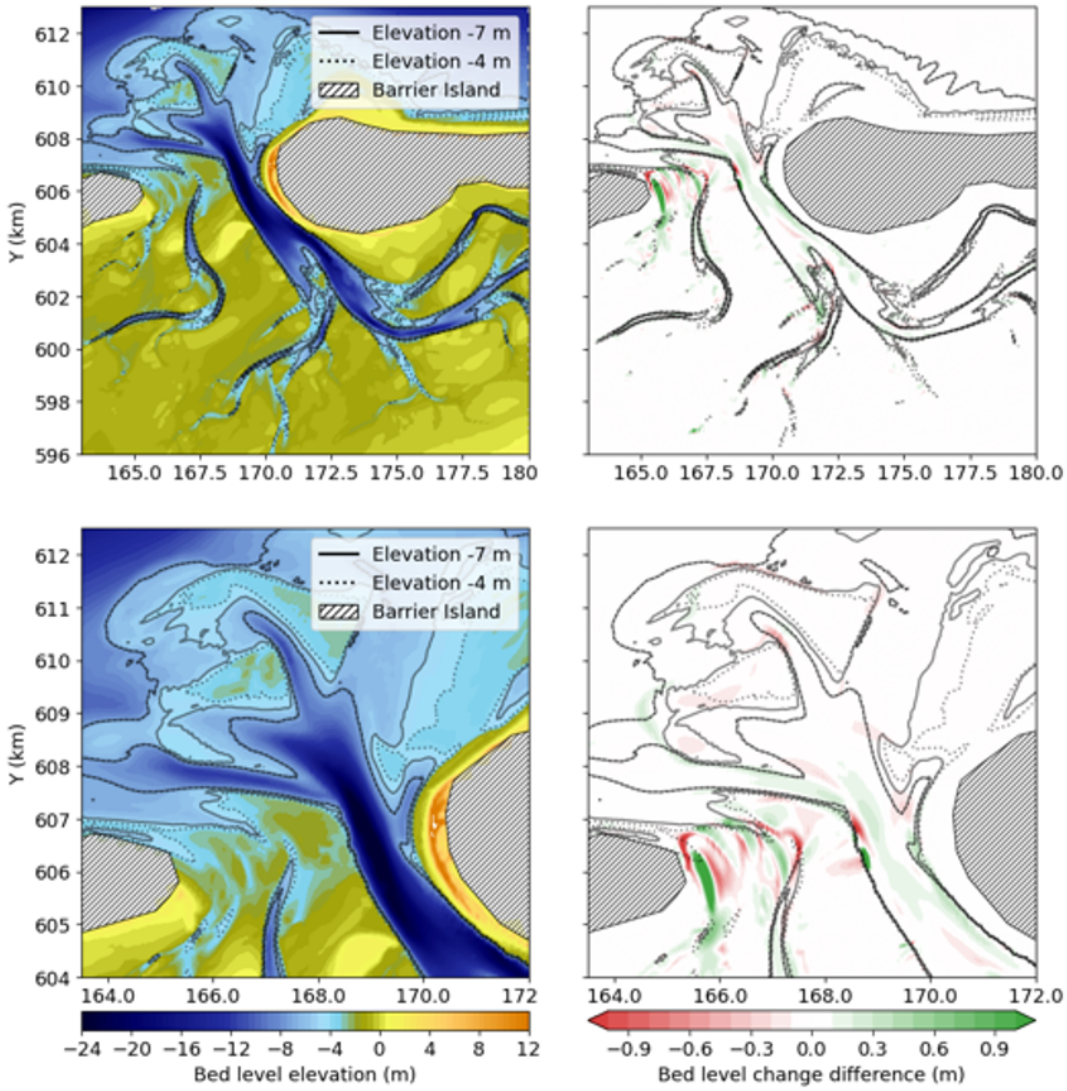

Figure 4.26: Top row: Initial bed level of the Ameland inlet (left) and bed level change difference between the tide-only and water levels forcing models after a 3-month simulation (right), with Wadden Sea domain and baseline grid resolution. Positive values indicate larger positive bed level changes in the tide-only simulation. Bottom row: Zoomed-in version of the top row focusing on the ebb-tidal delta.

Again, similar to previous simulation results shown, the sedimentation and erosion pattern indicates a seaward expansion of the two ebb shields at the ebb-tidal delta. Additionally, notable sedimentation and erosion occur at the secondary inlet channels, located west of the Borndiep main channel. In contrast, minimal to no sedimentation or erosion is observed at the ebb-delta margin and the Bornrif platform. Differences between the two simulations having tide-only and wind-inclusive forcing arise mainly at the secondary inlet channels and ebb-tidal delta.

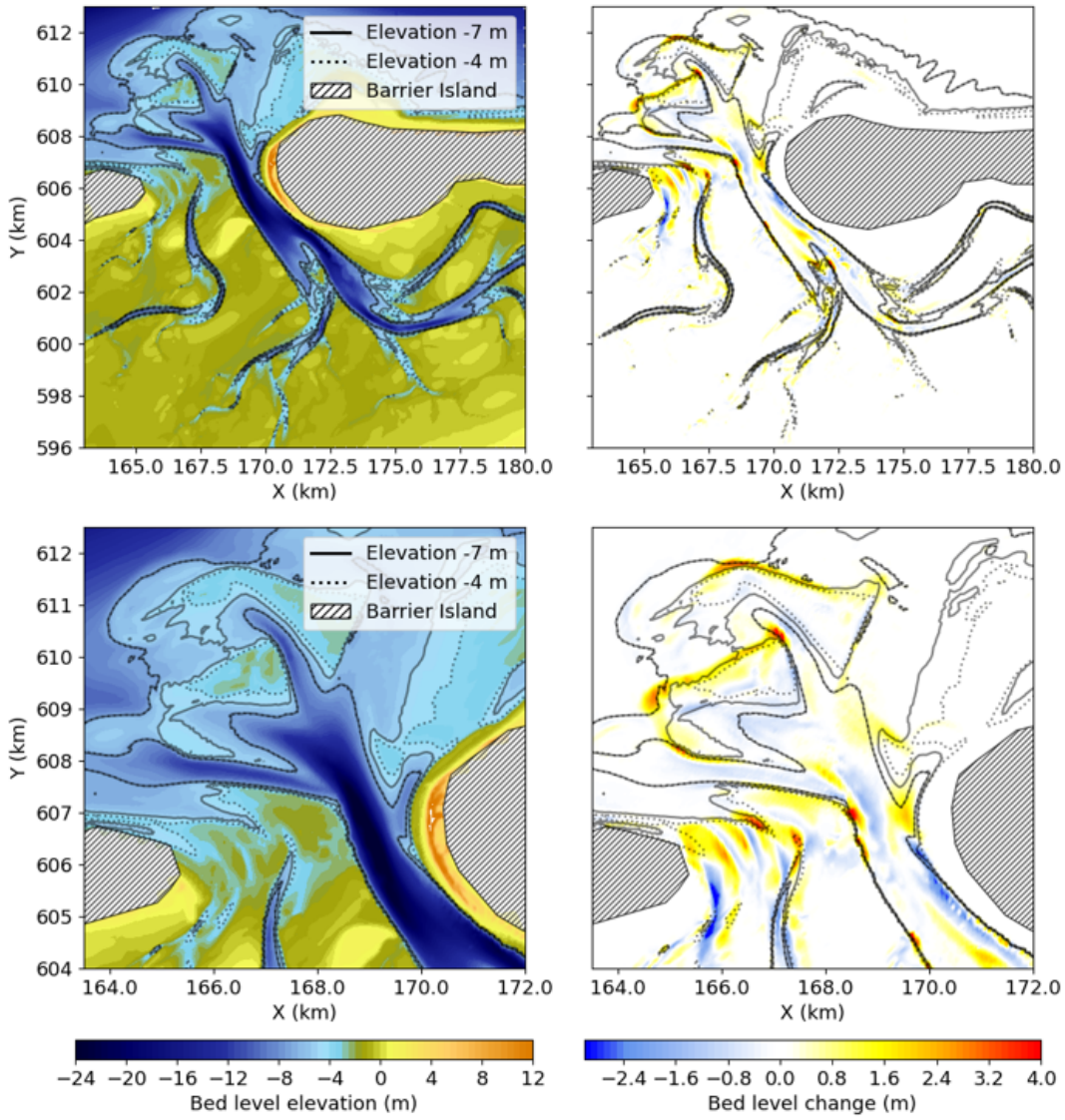

Figure 4.27: Top row: Ameland inlet initial bed level (left column) and bed level change (right column) after a 3-month simulation (Wadden Sea domain, wind-inclusive forcing, baseline grid resolution). Bottom row: Zoomed-in version of top row focusing on the ebb-tidal delta.

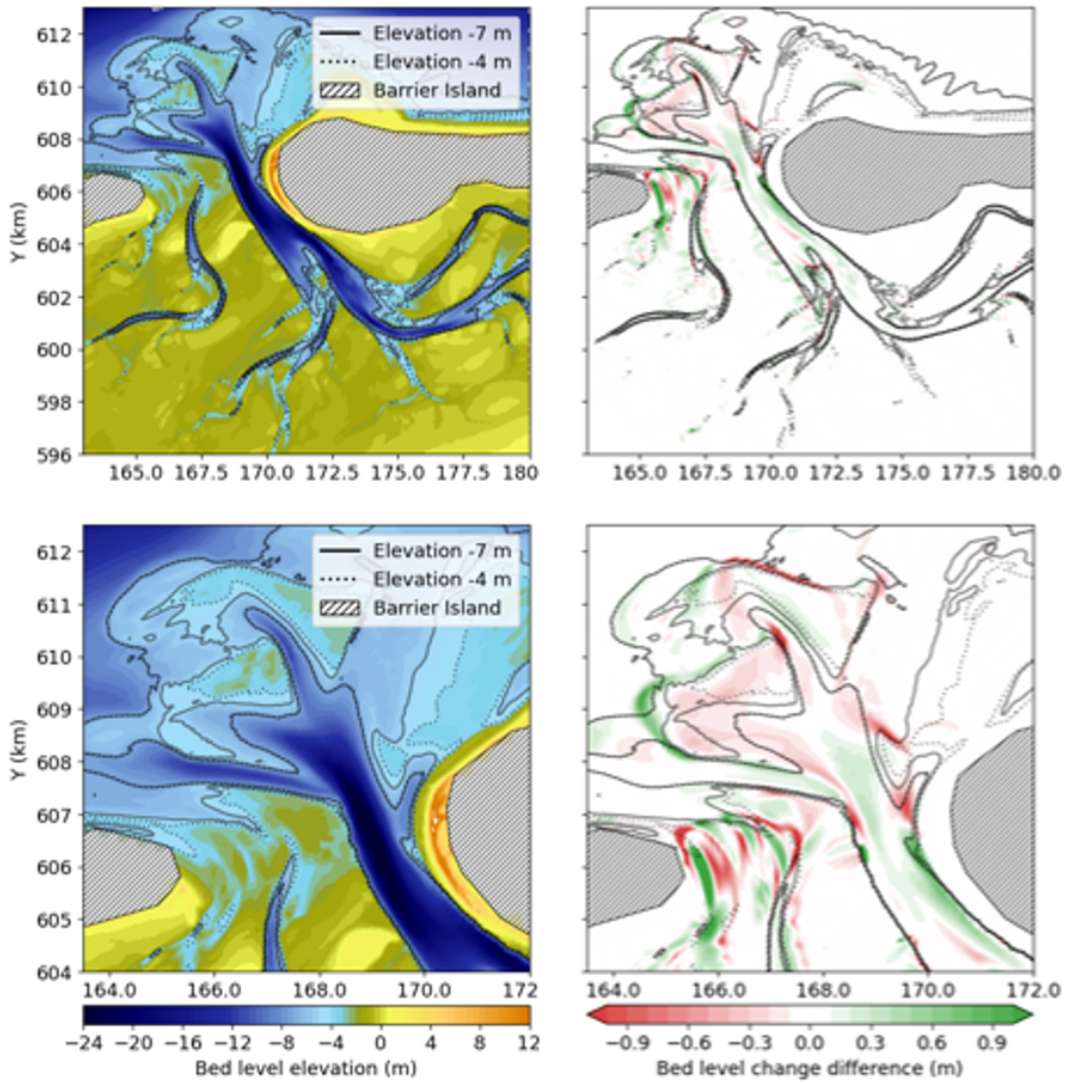

Figure 4.28: Top row: Initial bed level of the Ameland inlet (left) and bed level change difference between the tide-only and wind-inclusive forcing models after a 3-month simulation (right), with Wadden Sea domain and baseline grid resolution. Positive values indicate larger positive bed level changes in the tide-only simulation. Bottom row: Zoomed-in version of the top row focusing on the ebb-tidal delta.

The transect analysis shows that varying forcing conditions does not result in significant bed level change differences. Especially when comparing the changes in Figure 4.29 with the larger differences in bed level change observed for the two simulations with varying model domain schematization (Figure 4.18).

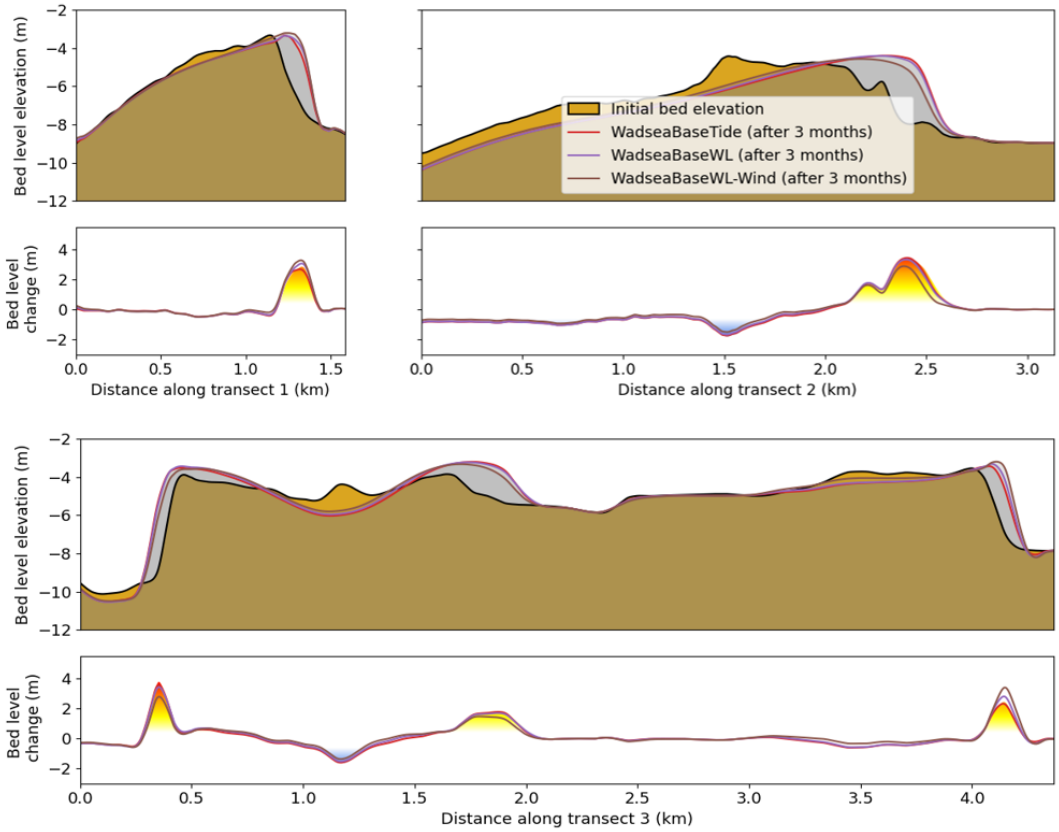

Figure 4.29: Transect analyses of bed level change for three distinct transects. Comparison of simulation results for three different forcing variations. Figures 1A, 2A and 3A show the initial bed level and bed level for the three simulations after 3 months. Figures 1B, 2B and 3B provide quantified sedimentation and erosion values. The transect numbering is consistent with those presented in Figure 4.7.

4.4. Variation in grid resolution (Wadden Sea domain, tide-only forcing)

This section compares model results for simulations with different grid resolutions. The baseline resolution has grid cells of approximately 30 by 30 meter near the Ameland inlet and the high-resolution grid 60 by 60 meter. First results from a cross-sectional hydrodynamic analysis are given in Section 4.4.1 and then the spatial distribution and transect analysis of bed level change is presented in Section 4.4.2.

4.4.1. Cross-sectional hydrodynamic analysis

Figure 4.30 shows slight divergence in cumulative discharge and sediment transport between the two simulations with different grid resolution. The model with higher resolution grid has slightly larger import of water and export of sediment. An increase in grid resolution causes a more refined representation of small-scale morphological features and flow patterns. This results in slightly different average velocity values with the overall trends being identical.

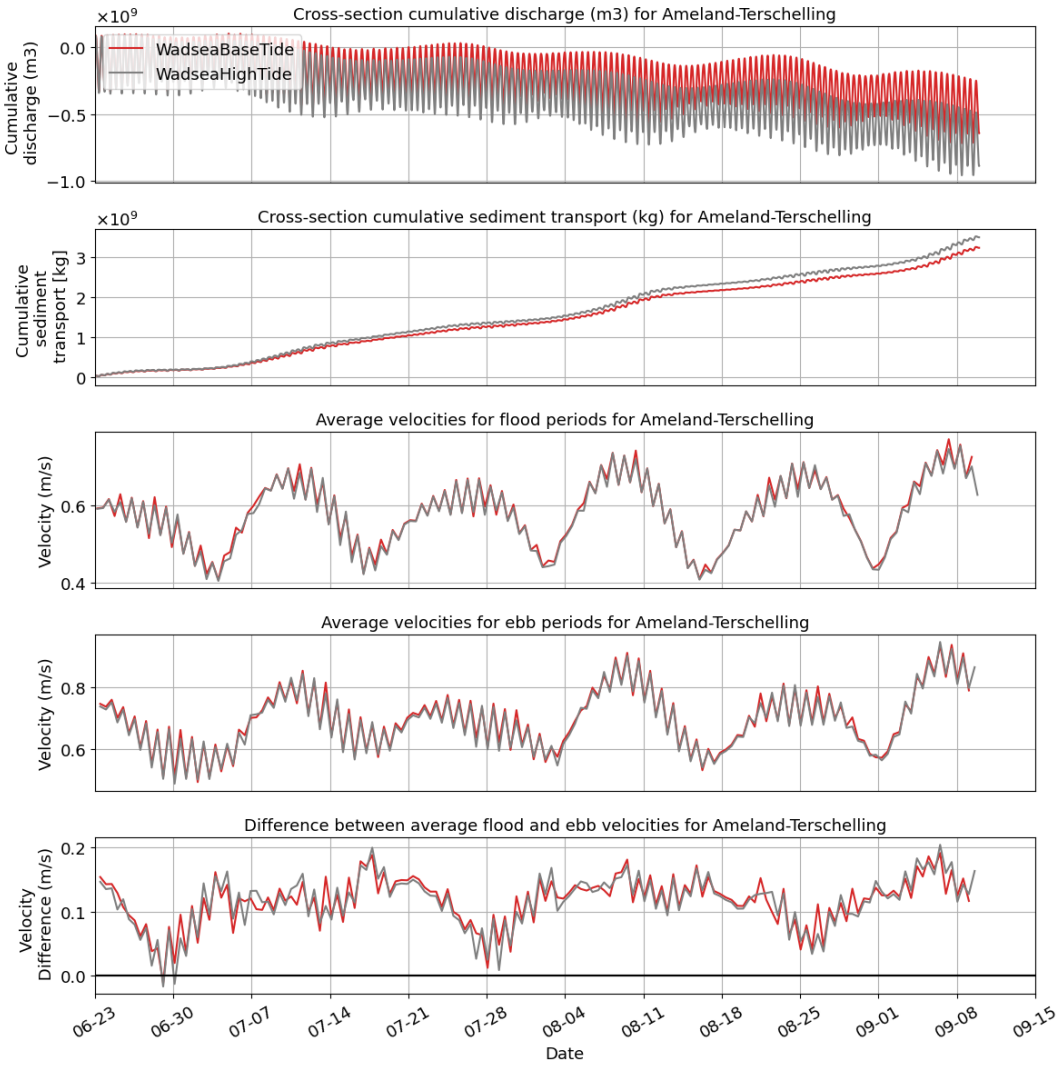

Figure 4.30: Comparison of simulation results for the tidal inlet cross-section for two different grid resolution: 30x30 m cells and 60x60 m cells. The figure showcases five subplots: the topmost plot shows the cumulative discharge for both domains, followed by a plot on cumulative sediment transport. The third and fourth plots illustrate average velocities during flood and ebb periods, respectively. The lower plot highlights the difference between the average flood and ebb velocities (ebb-flood).

The bar chart for cumulative transport over the tidal inlet cross-section shows that the magnitudes of ebb and flood transport for the two model grid resolutions are also very similar, with the higher resolution model having slightly increased sediment transport magnitudes.

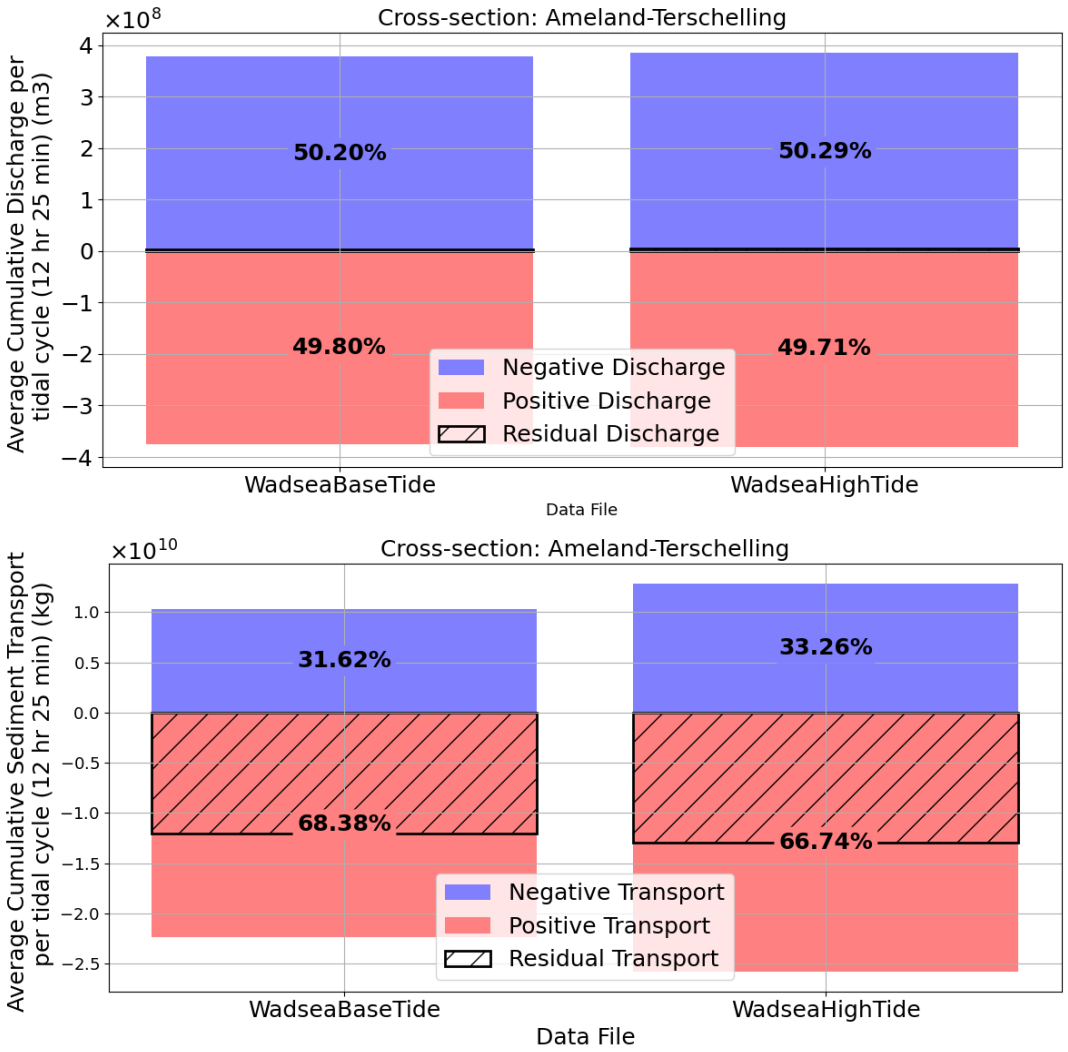

Figure 4.31: Comparison of cumulative discharge (top figure) and sediment transport (lower figure) for simulations with different grid resolution under tide-only forcing averaged per tidal cycle (12 hrs, 25 mins) over a 3-month simulation across the tidal inlet cross-section. Positive discharge and transport indicate westward and northward flow, while negative values represent southward and eastward flow.

4.4.2. Spatial distribution and transect analysis of bed level change

Making comparisons in bed level change for models with unstructured grids of different grid resolutions requires careful interpolation. This is because direct subtraction of data from different unstructured grids can lead to inaccuracies due to the differences in how data points are distributed. Both unstructured grids were interpolated onto the same structured grid. The interpolation method plays a crucial role in determining the differences observed between the initial bed levels and subsequent bed level changes. For this analysis, the ”cubic” interpolation method was chosen, which uses polynomial interpolation and considers the nearest 16 cells.

Two areas of interest emerged from analysing the resulting interpolated data: the Dantziggat, the main channel at the flood delta, and, the Koffiebonenplaat (shoal situated to the west of the main channel and located at the secondary inlet channels). In these areas, the initial bathymetry between the baseline and high-resolution simulations already shows differences of up to approximately 2.5 meters. Such significant differences should be taken into account when comparing bed level change. This variation

may be in part due to variations in initial bathymetries of the unstructured grids, but as well due to the method of interpolation used.

Comparing the bed level change for the simulation with high-resolution grid (middle element of Figure 4.32) to the change for the baseline simulation, results in differences up to approximately 1 meter (bottom element of Figure 4.32). The largest differences arise at the locations where the initial bed already displayed varying bed level elevation. The other regions, for example the ebb-tidal delta, show minor differences in bed level change between the two simulations.

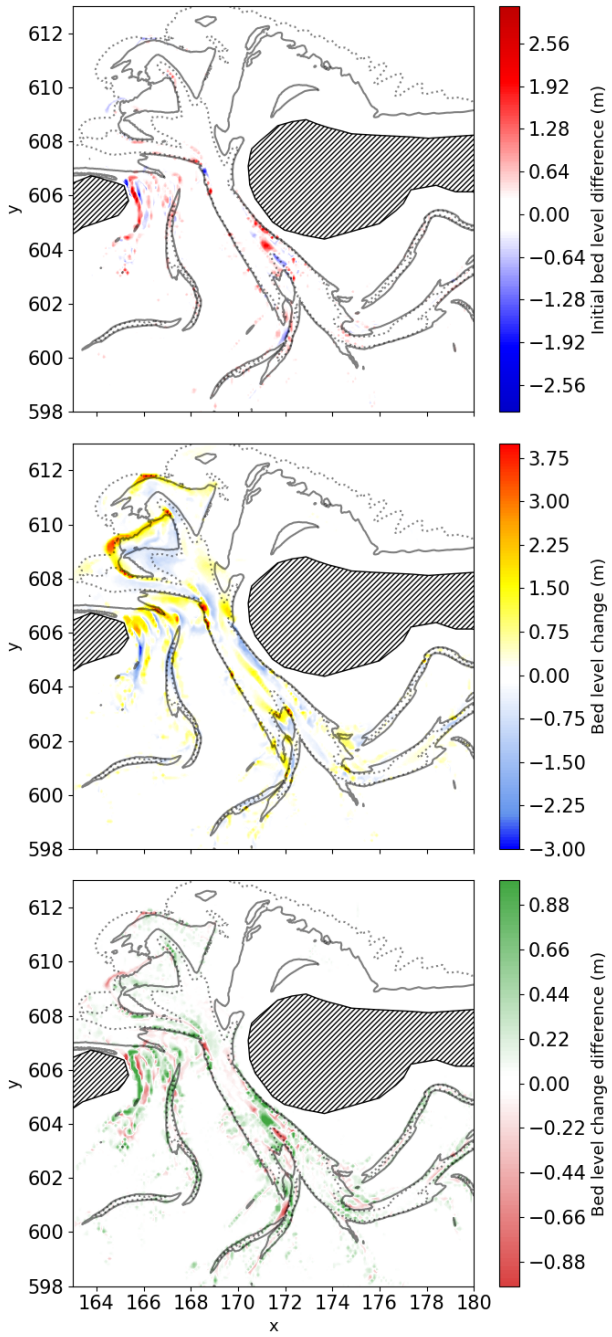

Figure 4.32: Comparison of bed level changes in Ameland inlet models with different grid resolutions: Top figure shows initial bathymetry differences interpolated from an unstructured to a structured grid, illustrating the variation in initial bed elevation due to grid resolution. Middle figure displays the bed level changes simulated with a higher grid resolution model. The bottom figure compares the bed level change of the baseline grid resolution model with that of the higher resolution model. Positive values indicate larger positive bed level changes in the baseline grid model simulation.

The transect analysis shows that varying grid resolution does not result in significant bed level change differences. Especially when comparing the changes in Figure 4.33 with the larger differences in bed level change observed for the two simulations with varying model domain schematization (Figure 4.18).

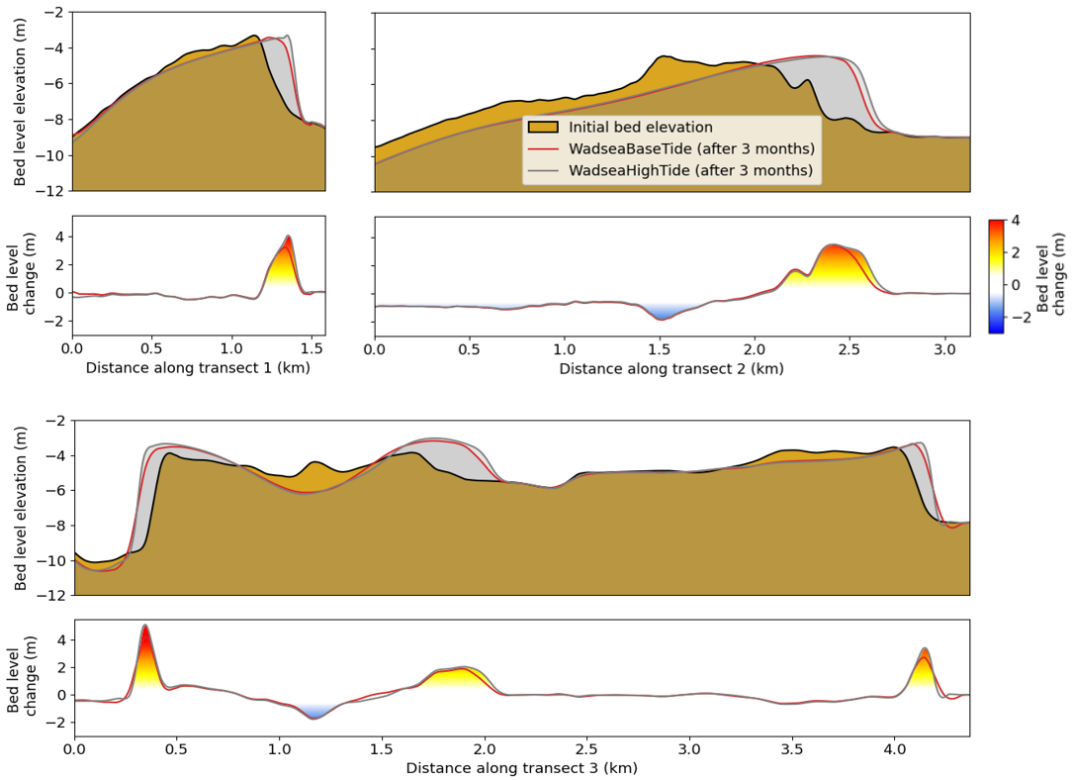

Figure 4.33: Transect analyses of bed level change for three distinct transects. Comparison of simulation results for two different grid resolution: base and high-resolution. Figures 1A, 2A and 3A show the initial bed level and bed level for the two simulations after 3 months. Figures 1B, 2B and 3B provide quantified sedimentation and erosion values. The transect numbering is consistent with those presented in Figure 4.7

5

Synthesis and discussion

In the previous chapter, transport dynamics through the Ameland tidal inlet, interactions between the Ameland basin and neighboring basins, (spatial) asymmetry in ebb and flood flow velocities and sediment transport and morphological change of the Ameland inlet region have been documented and analysed for various model simulations. This chapter combines that information into a synthesis (5.1 and comments on the results in the discussion (5.2).

5.1. Synthesis

The synthesis is divided into three parts: transport overview (5.1.1), transport dynamics (5.1.2) and morphological change (5.1.3).

5.1.1. Transport overview

Figures 5.1, 5.2 and 5.3 illustrate the average residual sediment transport across different cross-sections for each tidal cycle, lasting 12 hours and 25 minutes. These averages are calculated over a simulation period of three months. Residual transport is represented as an absolute value, while the direction of transport is indicated by grey arrows. Additionally, the figures break down the proportion of transport occurring during ebb and flood periods for both discharge and sediment transport, using percentage values to show the distribution across the cross-section.

Figure 5.1 displays data for the baseline simulation with a Wadden Sea domain, base grid resolution and tide-only forcing. Furthermore, two supplementary figures provide transport overviews: one showcases a model domain variation (Ameland domain: Figure 5.2) and the other a grid resolution variation (high-resolution grid: Figure 5.3). Average transport overview figures for simulation with wind forcing conditions are not included due to the highly temporal nature of wind effects.

All three overview figures show that there is relatively minimal residual discharge through the tidal inlet, moderate residual discharge over the cross-section at the landside of the barrier islands and substantial residual discharge at the seaside of the barrier islands. This changes when analysing the residual sediment transport. The sediment transport through the tidal inlet is substantial, while there is limited transport over the landside cross-sections and moderate transport over the seaside cross-sections.

These transport overview figures are also used to accompany Section 5.1.2.

Comparing AmelandBaseTide (Figure 5.2) to WadseaBaseTide (Figure 5.1)
The residual discharge over the sea-side cross-sections increases slightly in magnitude and the residual discharge through the inlet reduces slightly for AmelandBaseTide compared to WadseaBaseTide. The residual sediment transport decreases at the seaside TerschellingE cross-section, while increasing at the seaside AmelandC and the tidal inlet cross-sections.

Also note that there are two contrary directions for the residual transport when comparing discharge to sediment transport. For both the Ameland and Wadden Sea models, there is net import of water, while

there is net export of sediment for the tidal inlet. In the Wadden Sea model, the landside Ameland cross-section experiences a net export of water and a net import of sediment, though the latter is negligibly minimal.

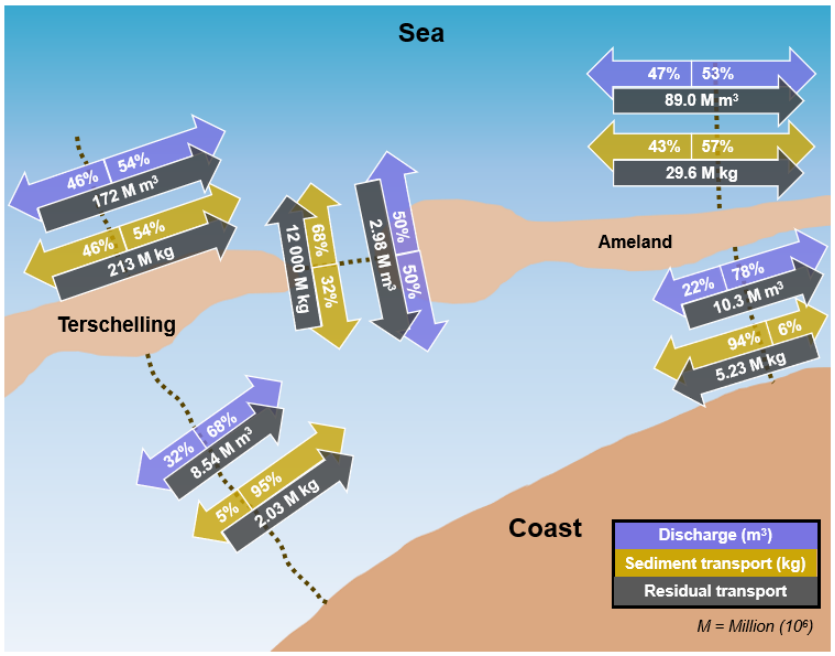

Figure 5.1: Sketch of the Ameland inlet region including a quantitative description of average discharge and sediment transport per tidal cycle (12 hours and 25 minutes) for the simulation with Wadden Sea domain, base resolution grid and tide-only forcing.

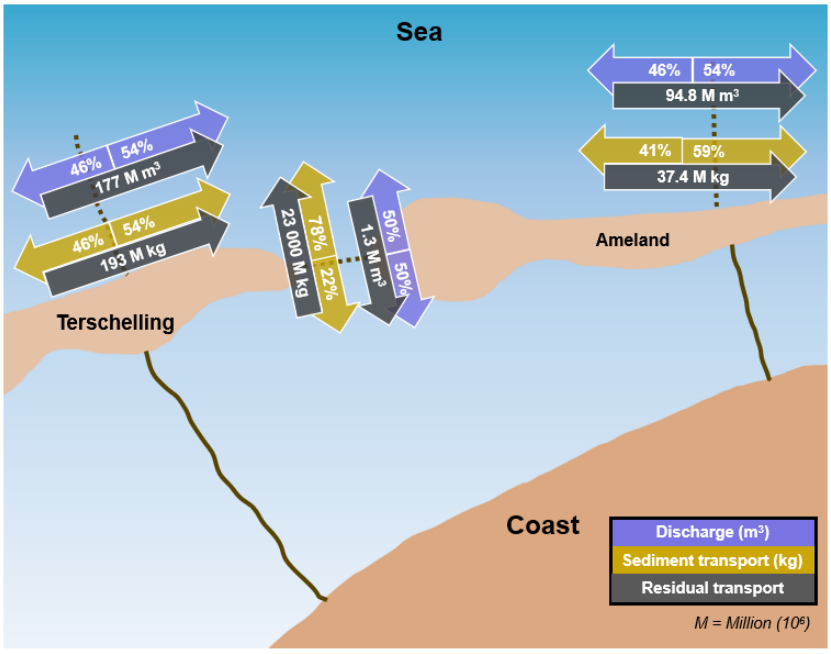

Figure 5.2: Sketch of the Ameland inlet region including a quantitative description of average discharge and sediment transport per tidal cycle (12 hours and 25 minutes) for the simulation with Ameland domain, base resolution grid and tide-only forcing.

Comparing WadseaHighTide (Figure 5.3) to WadseaBaseTide (Figure 5.1)
There are no significant changes in transport dynamics when using the base or high resolution grid, apart from slight changes in magnitudes.

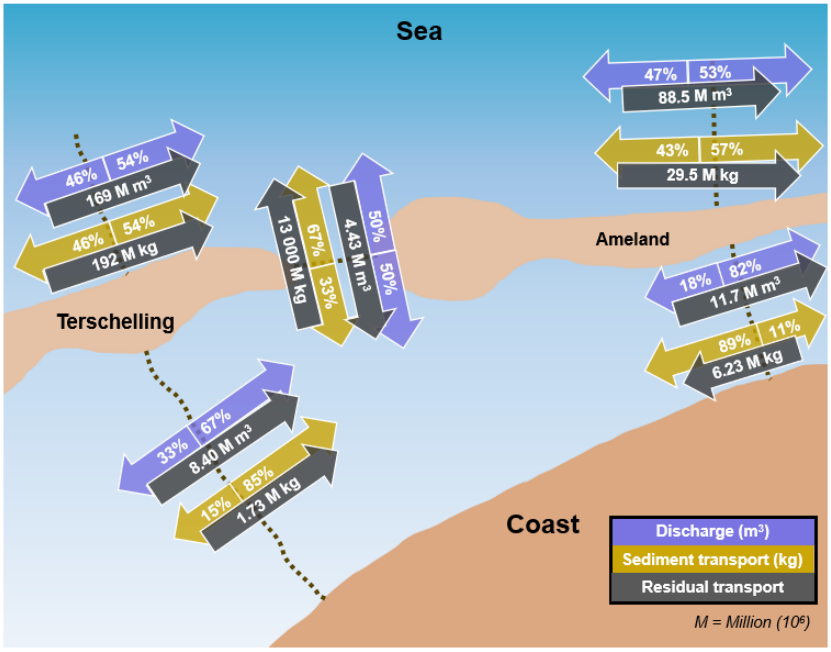

Figure 5.3: Sketch of the Ameland inlet region including a quantitative description of average discharge and sediment transport per tidal cycle (12 hours and 25 minutes) for the simulation with Wadden Sea domain, high resolution grid and tide-only forcing.

5.1.2. Transport dynamics

Single inlet vs. multi-inlet domain schematization

The main observation from the grid domain analysis is that a single-inlet schematization is not a valid schematization when interested in the morphological development of the Ameland tidal inlet. This is because there is significant discharge over the ”theoretical” tidal divides at Terschelling and Ameland. These transport dynamics influence morphological development of the Ameland tidal inlet, as there is a significant difference in residual sediment transport for the tidal inlet between the two simulations. This was expected for the situation with strong western wind, but it is already the case for the simulations with tide-only forcing. Thus, modeling practises that exclude transport dynamics between tidal basins are at risk of misrepresenting natural processes that are at play. It is also noteworthy that flow of water and sediment at the seaward-located cross-sections are affected by placing thin dams on landward-located cross-sections.

Cumulative discharge had a relatively linear trend for tide-only forcing simulations, while the cumulative sediment transport is dependent on the spring-neap tidal cycle. Periods with stagnant cumulative sediment transport can be distinguished from periods with substantial residual sediment transport. There is a more extreme spring tide followed consecutively by a milder one. Near the end of the less intense spring-tide periods, the variation in average ebb and flood velocities across the cross-sections AmelandC and TerschellingE are greater, leading to a more pronounced divergence in residual sediment transport. For the tidal inlet cross-section, significant net sediment transport occurs during periods characterized by a more pronounced spring-tide.

Other observations include that the Wadden Sea schematization shows approximately half the net export of sediment compared to the Ameland schematization. Additionally, the relative size of residual discharge is very small, while the relative size of residual sediment transport is more than half of the size of the dominant (ebb or flood) transport direction.

Another captivating difference between the Ameland and Wadden Sea schematization is that for the Ameland inlet cross-section, the export of sediment shows significant changes in magnitude between the two domain schematizations. The import of sediment during flooding stays relatively of the same magnitude for both models. The bar charts further demonstrate that despite similar magnitudes of sediment transport during flooding, the ebb-dominance is far more pronounced in the single-inlet simulation, primarily due to its greater sediment export. This directly influences the changes observed in residual sediment transport, resulting in the Ameland schematization having more net export of sediment. The slightly more import of water for the Wadden Sea model could be the inhibiting factor for the reduction in ebb transports observed in that particular simulation compared to the simulation of with the Ameland domain schematization.

The average velocity signal for the Wadden Sea schematization trails behind that of the Ameland schematization. Moreover, differences are observed in the peaks and troughs of both signals. These variations might contribute to the differing sediment transport behaviors seen between the two model domain schematizations. The differences in average velocity signals between the two schematizations further underscore the need for careful considerations of model schematizations.

Influence of forcing components

In the simulation with tide-only forcing, the Wadden Sea model shows a slight net import of water in the Ameland basin, as there is more outflow at Ameland than inflow at Terschelling resulting in flood dominance of the Ameland inlet. When adding wind forcing, there is great export of water through the Ameland inlet due to (south-)westerly wind, resulting from increased water exchange from the Terschelling basin to the Ameland basin.

While the discharge parameter shows significant flood residual transport during periods of south-westerly blowing wind, the sediment transport trend stays relatively linear. Sediment transport through the inlet is more influenced by the spring-neap tidal cycle than by changing wind patterns. The wind forcing actor does influence the cumulative sediment transport trends over the other cross-sections.

Other observations made are that when using more inclusive forcing, the (residual) sediment transport magnitudes increases. Additionally, the peaks and troughs of the average flow velocities for the tidal inlet cross-section for the three simulations have variances in their patterns. This can be one of the reasons for divergent sediment transport behaviors between the model schematizations.

Increased grid resolution

Two areas that attract attention when analysing differences between the initial bathymetries are the Dantziggat (largest channel in the flood delta) and at the Koffiebonenplaat (shoal left of main channel at flood delta side). Here the initial bathymetry between the base resolution and high resolution simulations already differ significantly. This should be taken into account when comparing bed level change. Overall, simulations with the higher grid resolution showed slightly increased dynamics.

Spatial flow velocities and sediment transport asymmetry

The position of a cross-section relative to the ebb jet significantly influences the observed sediment transport asymmetry. Cross-sections closer to the ebb jet typically result in a more pronounced ebb dominance. To clarify these dynamics, spatial maps were created to indicate areas characterized by either flood or ebb dominance.

Velocity data observations indicate that the marginal flood channel and the outer side of the ebb-tidal delta tend towards flood dominance. However, ebb dominance is more prevalent in most other areas. The primary difference between the Ameland and Wadden Sea schematizations is seen in the ebb velocities, with the Ameland simulation demonstrating higher ebb velocities. Meanwhile, flood velocities are relatively consistent between the two models.

The Ameland domain schematization, in particular, shows a more pronounced asymmetry in both velocity and sediment transport compared to the Wadden Sea domain schematization, indicating a stronger ebb dominance in sediment movement.

5.1.3. Morphological change

The magnitudes of sedimentation and erosion vary depending on model schematization, however all simulations show relatively similar patterns of morphological change. This suggests a robustness in the system its response to certain driving forces for short-term simulations. The two ebb shields at the ebb-tidal delta are expanding seaward. The seaward expansion signifies a dominance of ebb-tidal currents. The transect analysis illustrated not only the expansion but also the variations in slope steepness and the lateral smoothing of the ebb chutes. There is significant sedimentation and erosion observed at the secondary inlet channels to the west of the Borndiep main channel, indicating a highly morphodynamic environment. On the other hand, the ebb-delta margin and the Bornrif platform show little or no changes. There is modest bed level change in the flood basin in all simulations. There is limited to no change in wave-dominated areas. This is as expected as waves are not included in the simulations performed in this research.

Simulations with the Ameland domain schematization had most extreme sedimentation and erosion. Morphological changes are less pronounced at the secondary inlet channels under varied tide-only forcing. Varying forcing conditions had relatively low effect on differences in morphological development compared to changing model domain schematization. The initial bed level for the simulations with different grid resolution already differed up to 2.5 meters at the Dantziggat and the Koffiebonenplaat. Despite these initial discrepancies, morphological changes between baseline and high-resolution grid simulations do not vary greatly in other regions, such as the ebb-tidal delta, except where initial bed elevations already differed.

5.2. Discussion

The relationship between observations and their underlying causes can be obscured by the complexity of interacting variables in models of tidal inlets. In coastal systems, variables such as tide, wind action and sediment supply intertwine dynamically, making it difficult to attribute changes to a single cause. Moving forward, it is essential to acknowledge that the accuracy of predictive models is largely dependent upon the understanding of the processes they aim to simulate. Achieving accuracy and reliable morphological forecasts is a task that demands precise data collection, data (post-)processing, model schematizations that accurately represent the real-world complex processes and interactions and sufficient computational power.

Overall, focus should be on having a more inclusive approach to setting up models. The sketch of most important features and processes of a tidal inlet system from De Swart and Zimmerman (2009) in Figure 2.2 lacks the important process of tidal basin interaction. This research indicated significant water transport from the Terschelling basin to the Ameland basin, even in simulation with tide-only forcing. Figure 5.4 is a modification of the figure form De Swart and Zimmerman (2009), which includes the tidal basin interaction process. The generic representation of a tidal inlet system has been adapted to the specific geographic context of the barrier islands Terschelling and Ameland. This research also shows that the tidal current parallel to the barrier island is influenced by model domain schematization. Additionally, a sediment transport arrow in the tidal inlet channel has been added, as it proved to be a parameter greatly influenced by model schematization. This indicates that each tidal inlet possesses distinct characteristics, enabling models to be designed to the specific morphological and hydrodynamic conditions of the specific inlet and modeling goals. For instance, while basin interactions prove critical in the Ameland tidal inlet model, the same may not necessarily apply to models focused on the development of different tidal inlets.

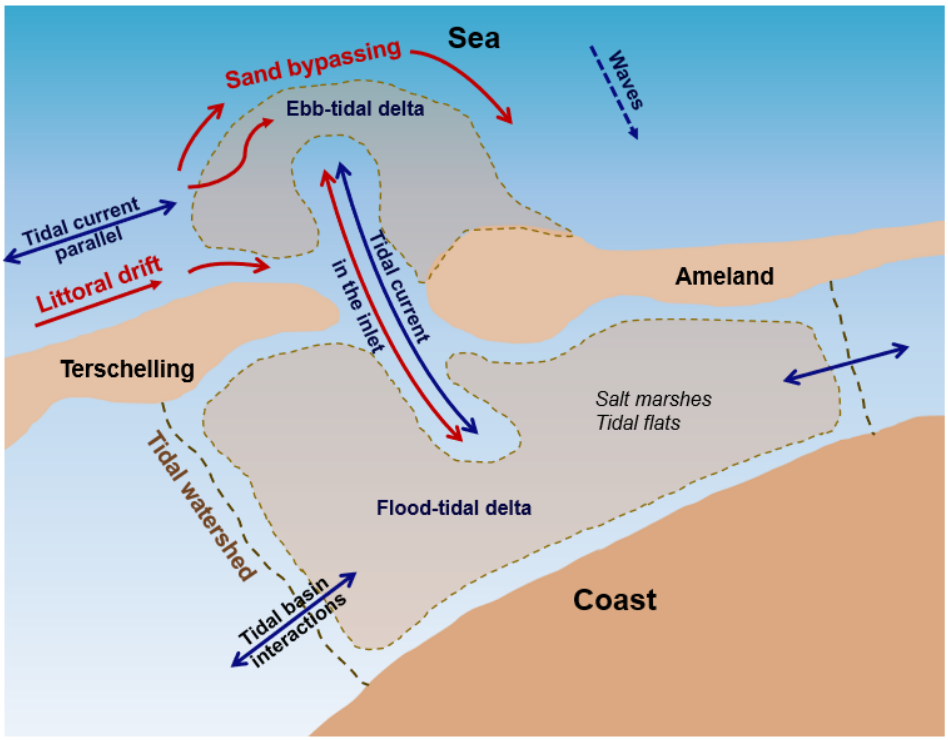

Figure 5.4: Schematic representation of the water and sediment transport dynamics at the Terschelling and Ameland barrier islands. Adapted from De Swart and Zimmerman (2009), see Figure 2.2.

5.2.1. Reflections on using high-performance computing

Using high-performance computing (HPC) for executing Delft3D-FM models leads to either a reduction in computational time, an extension of the simulation period, or both. Using larger models or extending the simulation period results in larger data output. Therefore, it is essential for HPC users to invest considerable effort in the post-processing phase, as the management and analysis of vast data sets can be challenging. Effective strategies for data handling, visualization and interpretation are crucial to unlock the full potential of the computational power at hand.

The scalability of Delft3D-FM on HPC clusters opens up new uncharted fields for discovery. With the ability to enhance computational capacity by orders of magnitude, there is a exciting prospect of achieving unprecedented levels of resolution and forecasting accuracy in simulations. Nonetheless, this study has highlighted a limitation: an addition of more computing power does not always result in better output. A profound understanding of the physical processes that drive these models is essential, especially for in the process of setting up adequate model schematizations.

The balance between the advantages and costs of employing high-performance computing should be carefully evaluated. Enhanced computational capacity enables more detailed simulations, however, the associated financial and energy costs must not be overlooked.

HPC has the potential to greatly improve coastal engineering and management by making predictions more accurate and faster. However, using HPC is complicated and adds complexity to modeling tasks. Therefore it is important for modellers to fully understand what these sophisticated models can do and what their limits are to make sure that the benefits of HPC can be fully leveraged.

5.2.2. Recommendations for future research

This study has expanded knowledge of the morphological behavior at the Ameland tidal inlet by analysing simulation outcomes derived from simulations with varying model schematizations. To further build upon and improve the predictive performance of process-based models for morphological forecasting at tidal inlets, several recommendations for future research are put forward.

First, leveraging the extensively available measurement data from the Ameland inlet region offers the opportunity to validate the simulation results for various model schematizations.

Simulations performed in this research yielded comparable bed level change patterns when varying model schematizations. A longer simulation period extending beyond the 3-month timeframe used in this study would probably yield in more pronounced pattern differences. An extended analysis could provide valuable insights into longer-term morphological changes.

The sensitivity of morphological forecasts to the placement of thin dams or cross-sections within the model should be analysed. This could aid in determining optimal schematization strategies and gain insight into their influence on hydrodynamic and sediment transport processes.

While the current research used two grid resolutions, examining a broader range of resolutions (predominantly coarser resolution) could provide more information on the trade-offs between computational efficiency and forecast accuracy. Instead of increasing the grid resolution for the entire model domain, efforts on increasing local resolution (e.g., at the littoral drift zone) might benefit the models accuracy. This could lead to a more informed choice of grid resolution based on the specific objectives of the morphological study.

Further going into the schematization of individual forcing components are recommended to increase knowledge on the impact of forcing schematization on morphological forecasts. For example, comparing the impacts of simulations that incorporate a spring-neap tidal cycle with those that use a morphological tide could provide deeper insights into the effects of different tidal forcing schematizations on sediment transport and morphological changes. Similarly, evaluating the differences between continuous timeseries wind forcing and simulations with a limited set of wind conditions could provide insights on various wind schematization methods on morphological outcomes.

Lastly, implementing validation and calibration processes using a range of model schematizations might also be beneficial for enhancing the reliability and accuracy of morphological forecasts.

6

Conclusions

6.1. Main conclusion

To what extent can improved model schematizations enhance short-term morphological forecasts of the Ameland tidal inlet?

Improved model schematizations can significantly enhance short-term morphological forecasts of the Ameland tidal inlet by providing a more accurate and comprehensive representation of the complex hydrodynamic and sediment transport processes. A multi-inlet schematization, which encompasses the entirety of the Wadden Sea, allows for the inclusion of hydrodynamic interactions between the Ameland basin and adjacent basins, thereby capturing the impact of these interactions on sediment transport in the Ameland inlet. This approach provides a more realistic representation of the real-world system, resulting in more accurate morphological forecasts. Additionally, it is important to consider the influence of various forcing processes. The spring-neap tidal cycle pattern emerged as a crucial component, as it directly influences discharge and sediment transport over time. Furthermore, wind stands out as an important forcing actor, influencing water and sediment transport dynamics and having its effect vary depending on the severity and direction from which it blows. Finally, increasing grid resolution to represent small-scale morphological features and flow patterns in more detail can lead to modest improvements in forecast accuracy. However, the benefits of increased grid resolution may not always justify the additional computational resources required.

6.2. Sub-conclusions

What is the influence of single-inlet schematization?

A single-inlet schematization does not capture hydrodynamic interactions between the Ameland basin and adjacent basins. These transport dynamics between basins do, however, impact sediment transport in the Ameland inlet and thus affect morphological development of the Ameland tidal inlet. Even the dynamics at the seaside of the barrier islands Terschelling and Ameland were affected by cutting of the model grid at the theoretical tidal divides at the landside of Terschelling and Ameland. Consequently, using a multi-inlet schematization (i.e., a grid domain encompassing the entirety of the Wadden Sea) provides a more inclusive model representation of the real-world complex system. The single-inlet schematization resulted in a factor ~ 2 larger sediment transport through the Ameland inlet compared to a multi-inlet Wadden Sea model and had more extreme bed level change, while having similar sedimentation and erosion patterns.

What is the influence of various forcing processes?

Tidal dynamics predominantly influence sediment transport through the tidal inlet, as sediment transport trends follow the spring-neap tidal cycle more than wind patterns. The existence of more extreme spring tides followed by milder ones significantly affects sediment transport. Wind forcing, particularly from a southwesterly direction, does result in meaningful transport of water between the Terschelling

and Ameland basin and results in export of water through the Ameland inlet. Lastly, the inclusion of more comprehensive forcing, for example incorporating both tidal and wind influences, increases the magnitudes of transports during both periods of ebb and flooding.

What is the added value of increasing grid resolution?

The added value of increasing grid resolution from having cells of 60 by 60 meter near the Ameland inlet to cells with dimensions of 30 by 30 meter is limited. The refinement in the representation of small-scale morphological features and flow patterns, leads to only modest changes in hydro- and morphodynamics. Representing processes in more detail for 3-month simulations is only endorsed when having abundant computational resources on hand.

How does residual sediment transport vary across the various model schematizations?

Ebb dominance is present in most areas for all simulations, however with notable exceptions such as the marginal flood channel and the outer area of the ebb-tidal delta. The Ameland schematization is distinguished by higher ebb flow velocities, which are evident across the ebb-tidal delta, the main inlet channel and the western side of the Ameland basin. This increased ebb flow is associated with a corresponding increase in sediment transport during ebb periods. Furthermore, the Ameland model shows greater sediment transport at the main tidal channel and inlet throat during ebb, as well as increased flood transport in westward-extending tidal channels from the main inlet channel. However, the flood transport is significantly less than ebb transport, resulting in a ebb-dominant character. Conversely, the Wadden Sea schematization, while also exhibiting ebb dominance, does not show the same extent of ebb-favoring sediment transport as observed in the Ameland model.

Bibliography

Davis, R. A. and Hayes, M. O. (1984). What is a wave-dominated coast?

De Swart, H. and Zimmerman, J. (2009). Morphodynamics of tidal inlet systems.

Dean, R. (1988). Sediment interaction at modified coastal inlets: processes and policies.

DelftBlue (n.d.). Delftblue documentation.

Elias, E. (2020). Technisch advies rol en mogelijkheden buitendelta's voor het kustbeheer.

Elias, E. (2021). Morfologische analyse buitendelta ameland en de rol van de pilotsuppletie.

Elias, E., Pearson, S., and Van der Spek, A. (2020). Understanding the morphological processes at ameland inlet.

Elias, E., Van der Spek, A., Pearson, S., and Cleveringa, J. (2019). Understanding sediment bypassing processes through analysis of high-frequency observations of ameland inlet, the netherlands.

Elias, E., Van der Spek, A., Wang, Z., and De Ronde, J. (2012). Morphodynamic development and sediment budget of the dutch wadden sea over the last century.

Escoffier, F. (1940). The stability of tidal inlets.

Harlequin, D. (2020). A heuristic investigation into methods to model medium-term meso-scale morphological features in tidal and estuarine environments.

Harlequin, D. (2021). Morphodynamic modelling of the ameland ebb-tidal delta.

Hersbach, H. (2019). The era5 global reanalysis.

Hillen, M., Geleynse, N., Storms, J., Walstra, D., , and Stive, M. (2009). Morphology and stratigraphy of a degrading delta.

Laan, S., Wang, Z., Van Prooijen, B., Luijendijk, A., Nederhoff, K., and Zijlstra, R. (2019). Understanding coastal dynamics at an ebb-tidal delta in the wadden sea.

Lambregts, P. (2021). Sediment bypassing at ameland inlet.

Roelvink, J. (2006). Coastal morphodynamic evolution techniques.

Stive, M., De Schipper, M., Luijendijk, A., Ranasinghe, R., and Van Thiel de Vries, J. (2013). The sand engine: A solution for vulnerable deltas in the 21st century?

Stive, M. and Wang, Z. (2003). Morphodynamic modeling of tidal basins and coastal inlets.

Van Weerdenburg, R., Pearson, S., Van Prooijen, B., and Laan, S. (2021). Field measurements and numerical modelling of wind-driven exchange flows in a tidal inlet system in the dutch wadden sea.

Vroom, J. and Wang, Z. (2012). Tidal divides.

Zijl, F., Verlaan, M., and Gerritsen, H. (2013). Improved water-level forecasting for the northwest european shelf and north sea through direct modelling of tide, surge and non-linear interaction.

A

Spatial transport asymmetry

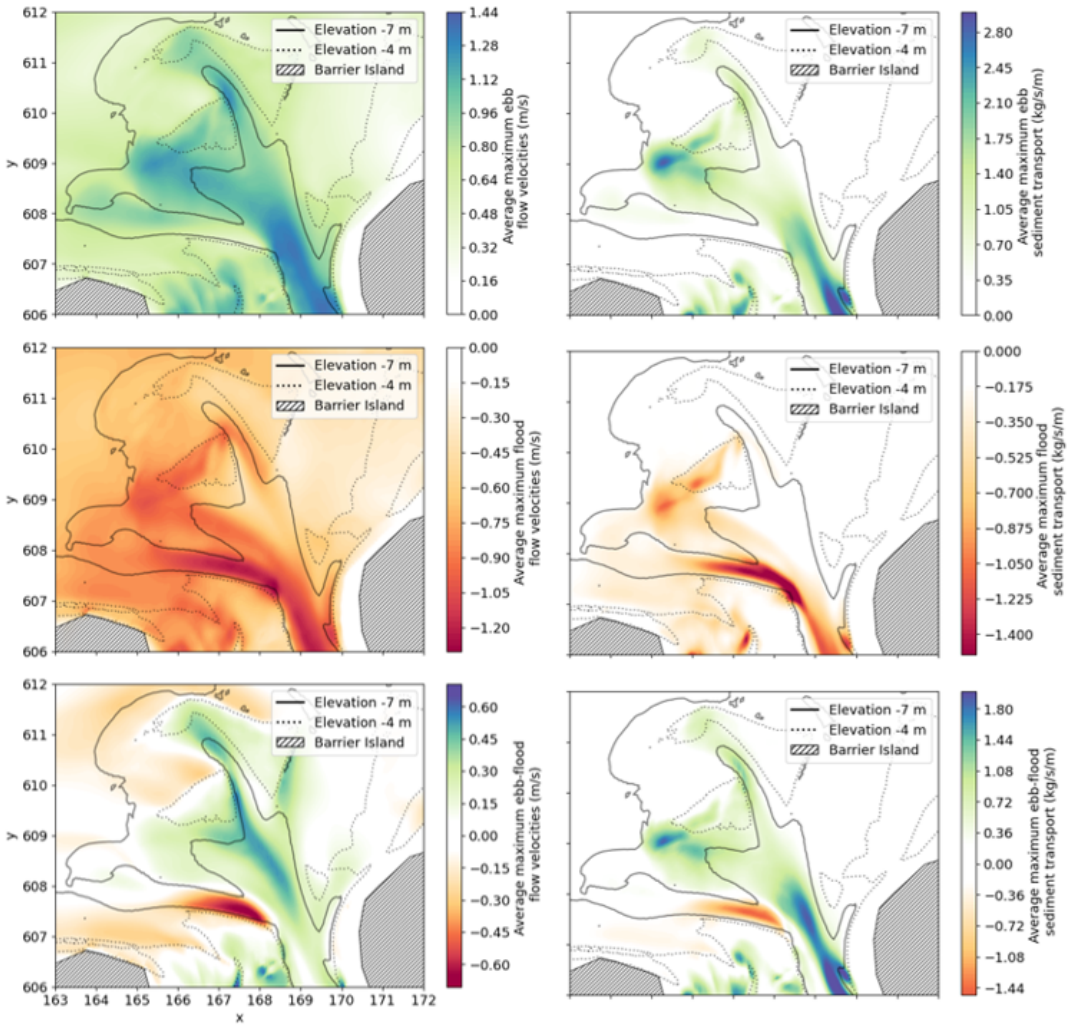

Figure A.1: Spatial representation of flow velocities (left column) and sediment transport (right column), zoomed-in version of figure 4.6. Top row: averaged values per tidal cycle (12 hrs, 25 mins) for maximum ebb velocity/transport over a 7-day simulation; middle row: corresponding data for flood velocity/transport; bottom row: the difference between the ebb and flood values.

B

Variation in domain

B.1. Tide-only forcing

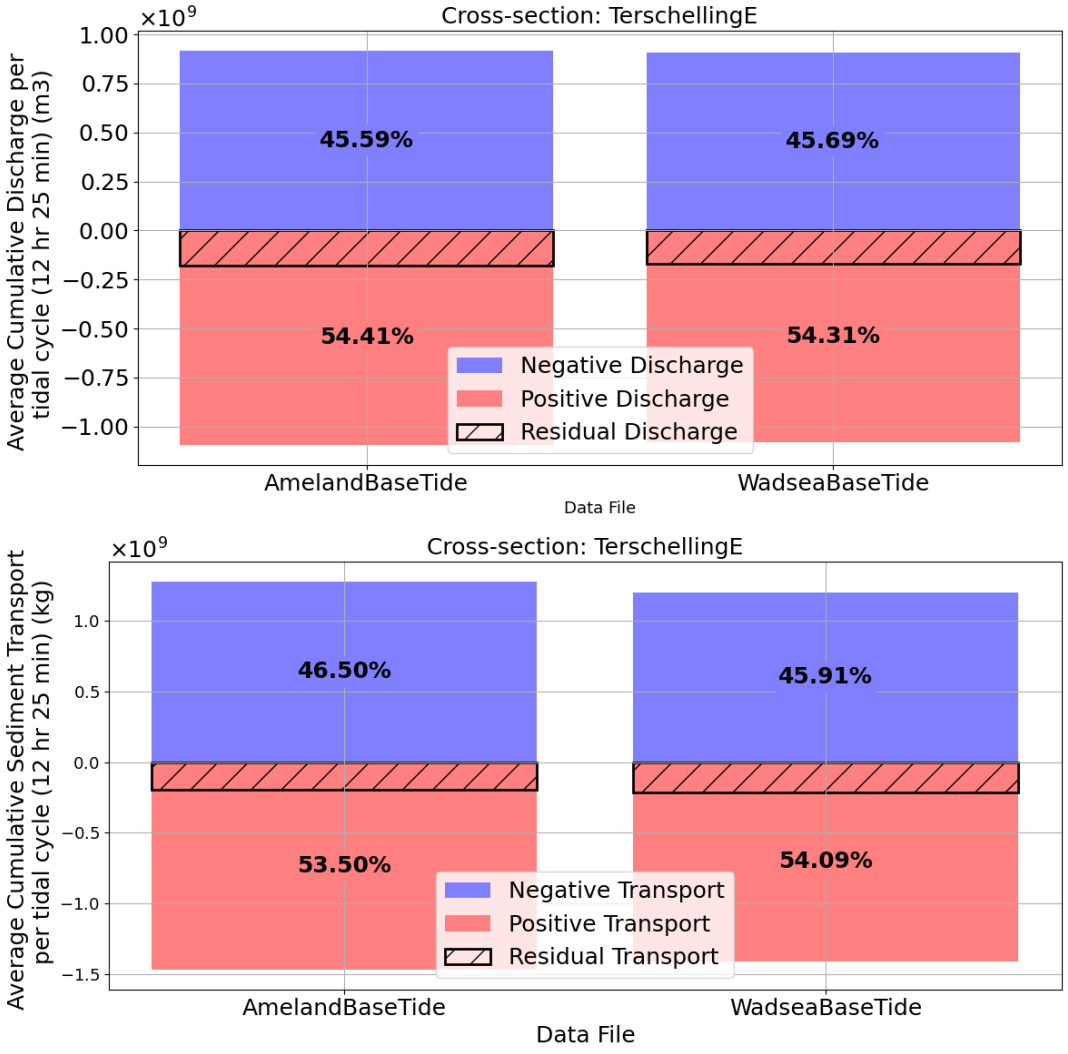

Figure B.1: Comparison of cumulative discharge (top figure) and sediment transport (lower figure) under tide-only forcing per tidal cycle (12 hrs, 25 mins) averaged over a 3-month simulation across the tidal inlet cross-section. Positive discharge and transport indicate westward and northward flow, while negative values represent southward and eastward flow.

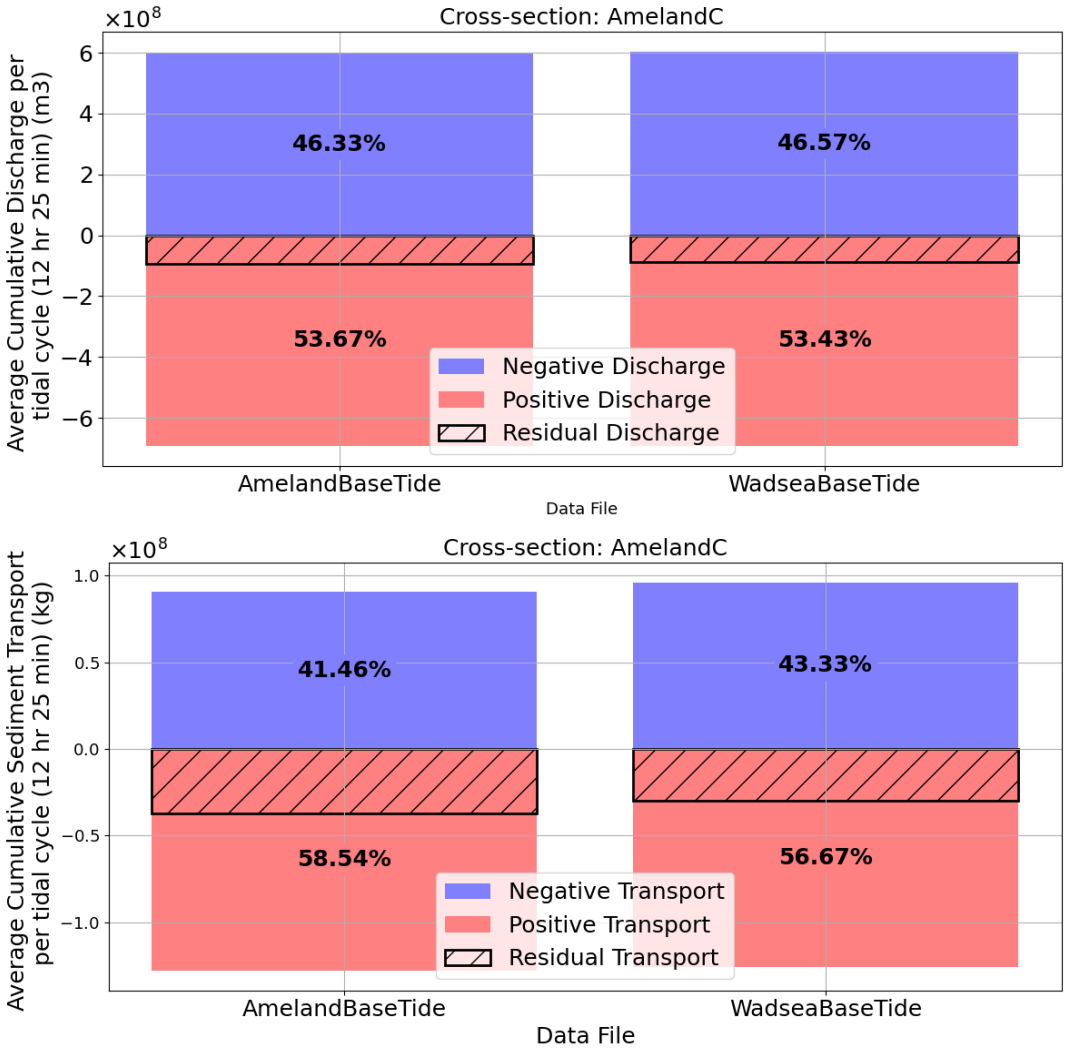

Figure B.2: Comparison of cumulative discharge (top figure) and sediment transport (lower figure) under tide-only forcing per tidal cycle (12 hrs, 25 mins) averaged over a 3-month simulation across the tidal inlet cross-section. Positive discharge and transport indicate westward and northward flow, while negative values represent southward and eastward flow.

B.2. Wind-inclusive forcing

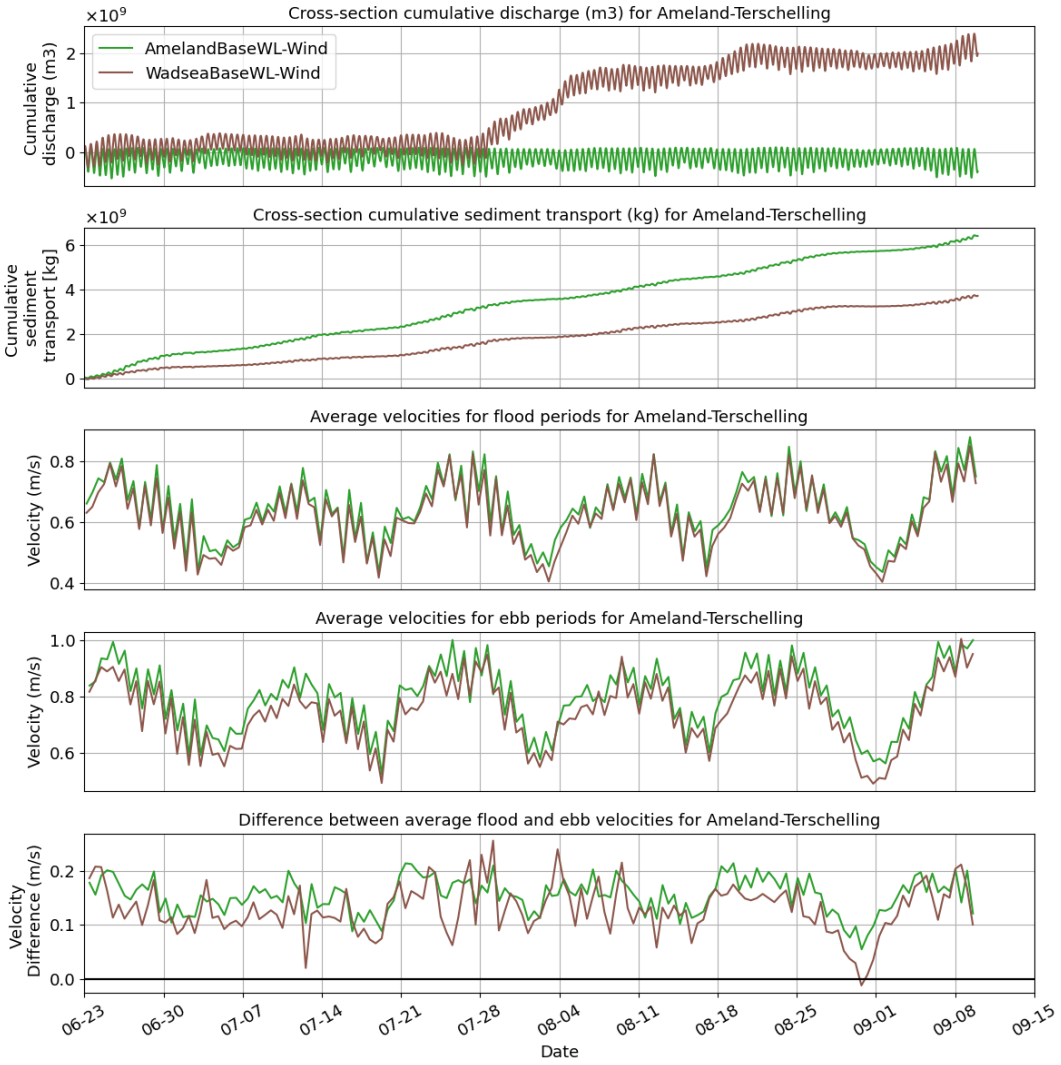

Figure B.3: Comparison of simulation results for the tidal inlet cross-section for two different model domains: Ameland and Wadden Sea. The figure showcases five subplots: the topmost plot shows the cumulative discharge for both domains, followed by a plot on cumulative sediment transport. The third and fourth plots illustrate average velocities during flood and ebb periods, respectively. The bottommost plot highlights the difference between the average flood and ebb velocities (ebb-flood).

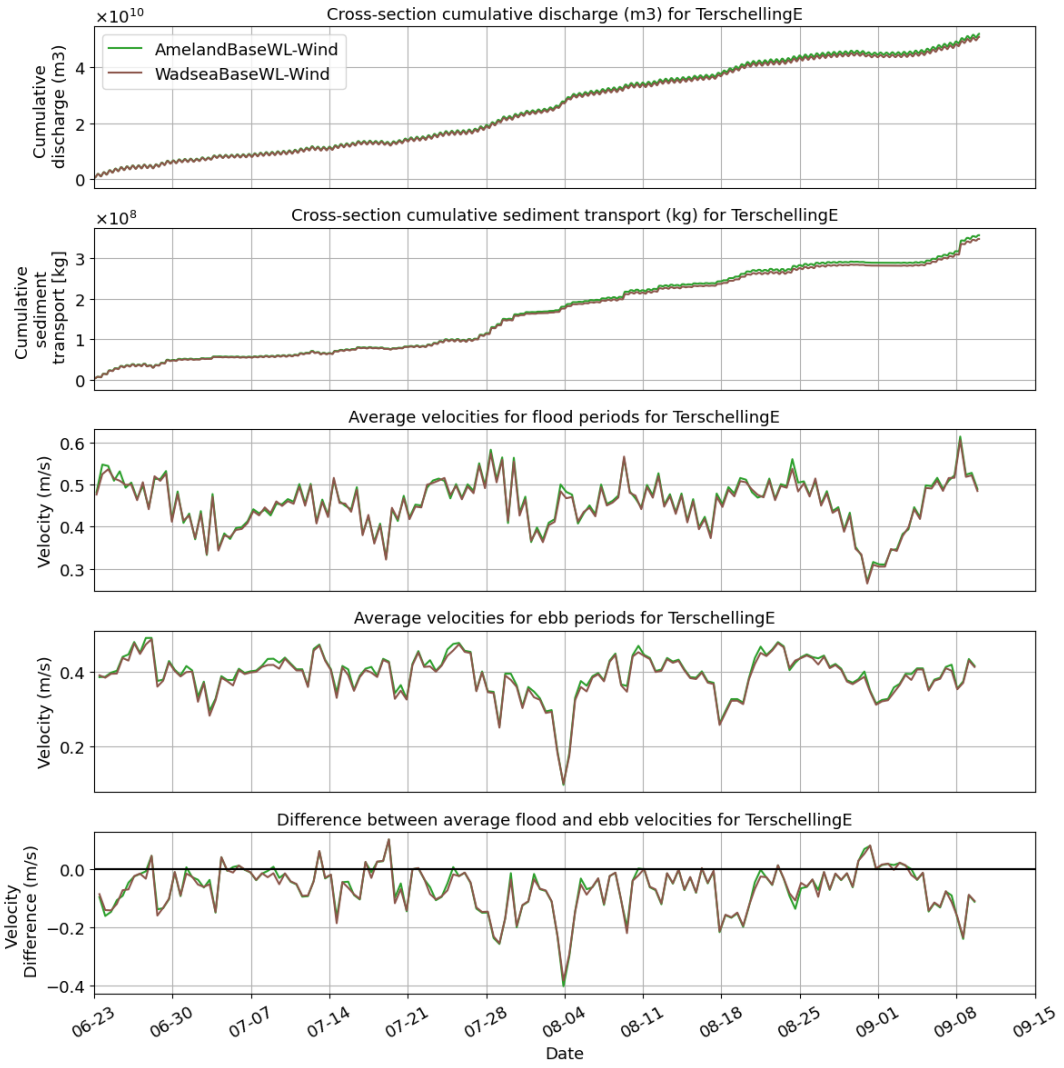

Figure B.4: Comparison of simulation results for the seaside Terschelling cross-section for two different model domains: Ameland and Wadden Sea. The figure showcases five subplots: the topmost plot shows the cumulative discharge for both domains, followed by a plot on cumulative sediment transport. The third and fourth plots illustrate average velocities during flood and ebb periods, respectively. The bottommost plot highlights the difference between the average flood and ebb velocities (ebb-flood).

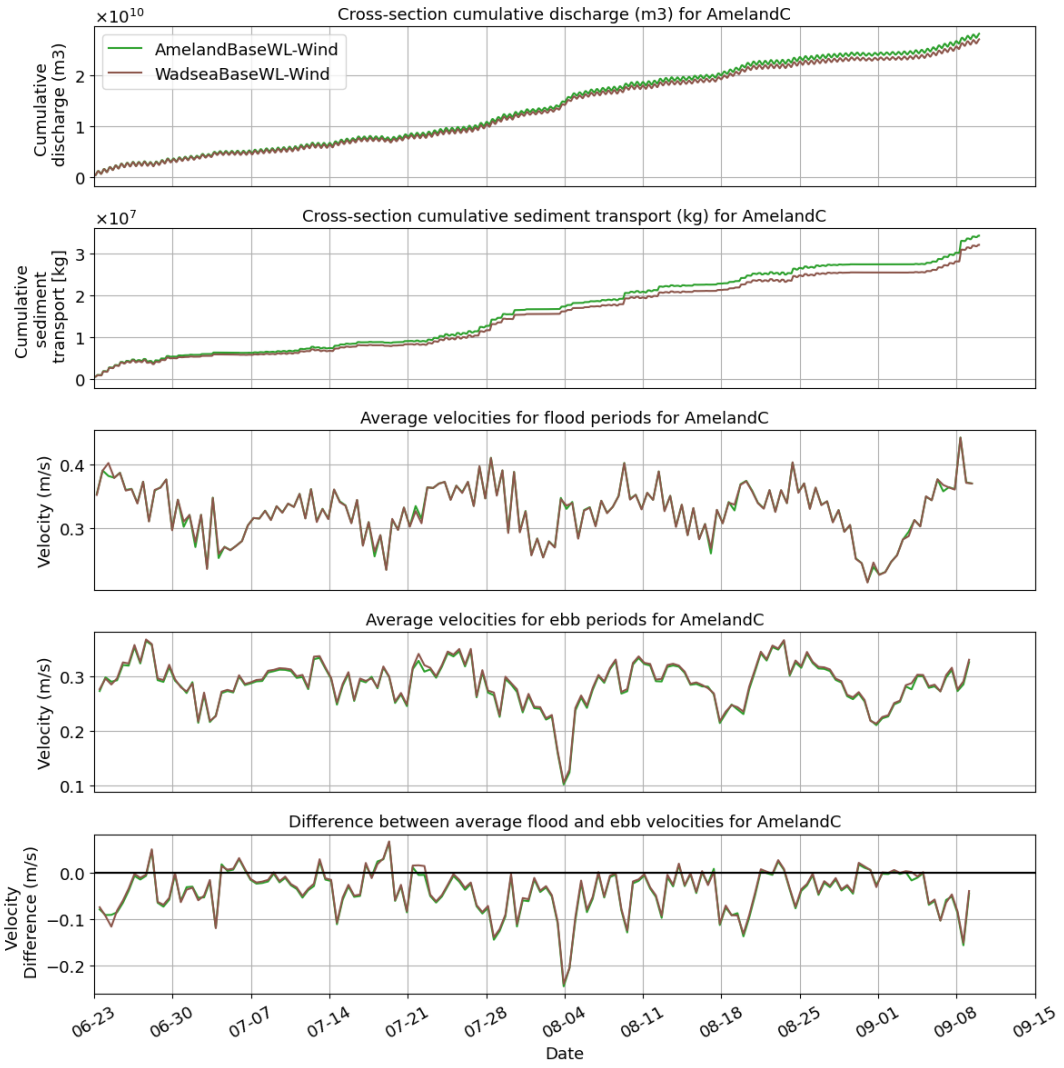

Figure B.5: Comparison of simulation results for the seaside Ameland cross-section for two different model domains: Ameland and Wadden Sea. The figure showcases five subplots: the topmost plot shows the cumulative discharge for both domains, followed by a plot on cumulative sediment transport. The third and fourth plots illustrate average velocities during flood and ebb periods, respectively. The bottommost plot highlights the difference between the average flood and ebb velocities (ebb-flood).

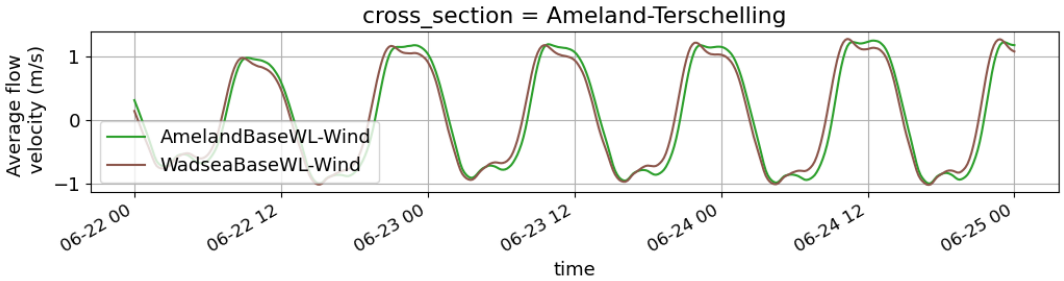

Figure B.6: Comparison of simulation results for two different model domains: Ameland and Wadden Sea. The graph represents average water flow velocities across the tidal inlet cross-section over a 3-day period.

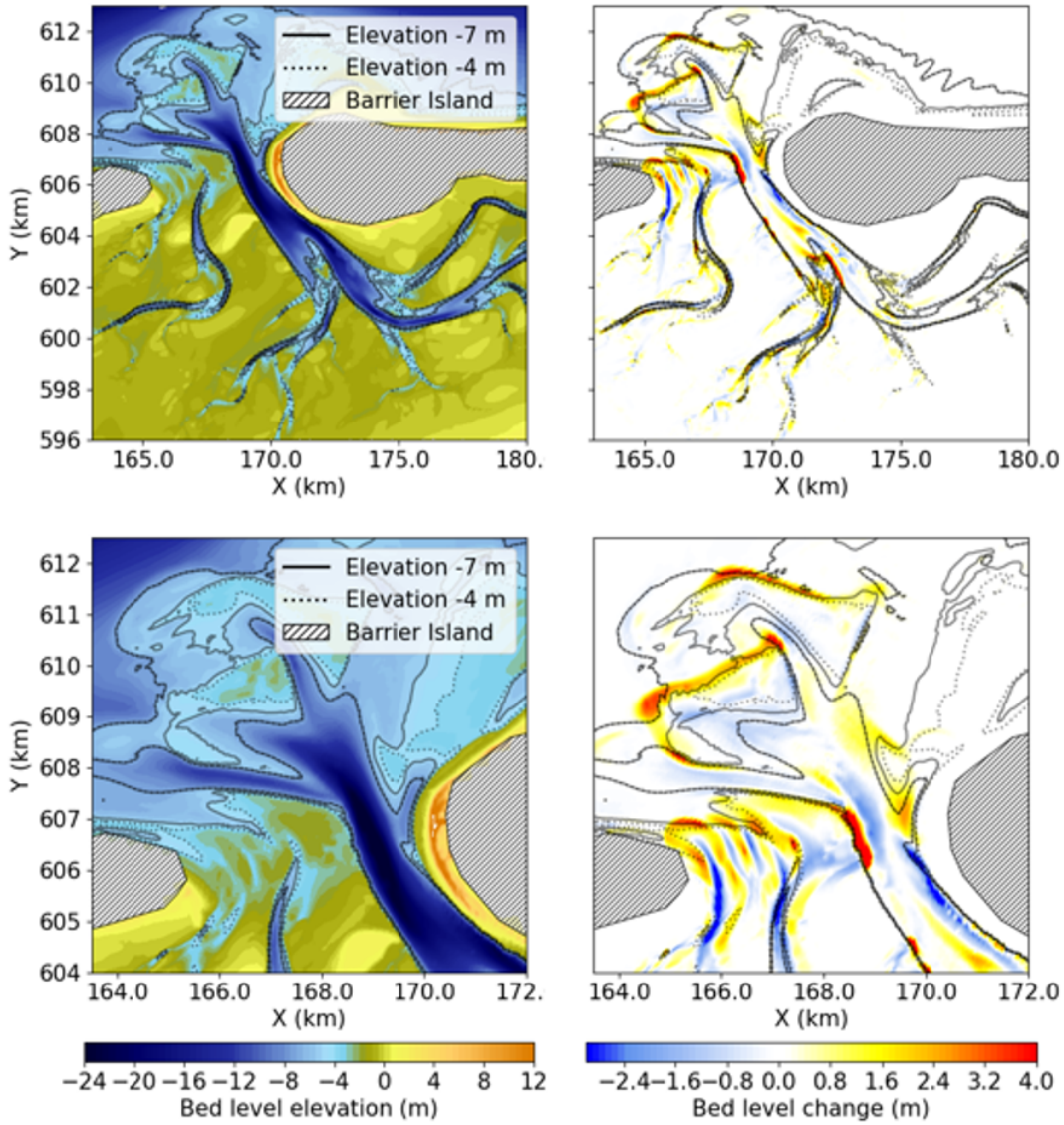

Figure B.7: Top row: Ameland inlet initial bed level (left column) and bed level change (right column) after a 3-month simulation (Ameland domain, wind-inclusive forcing, baseline grid resolution). Bottom row: Zoomed-in version of top row focusing on the ebb-tidal delta.

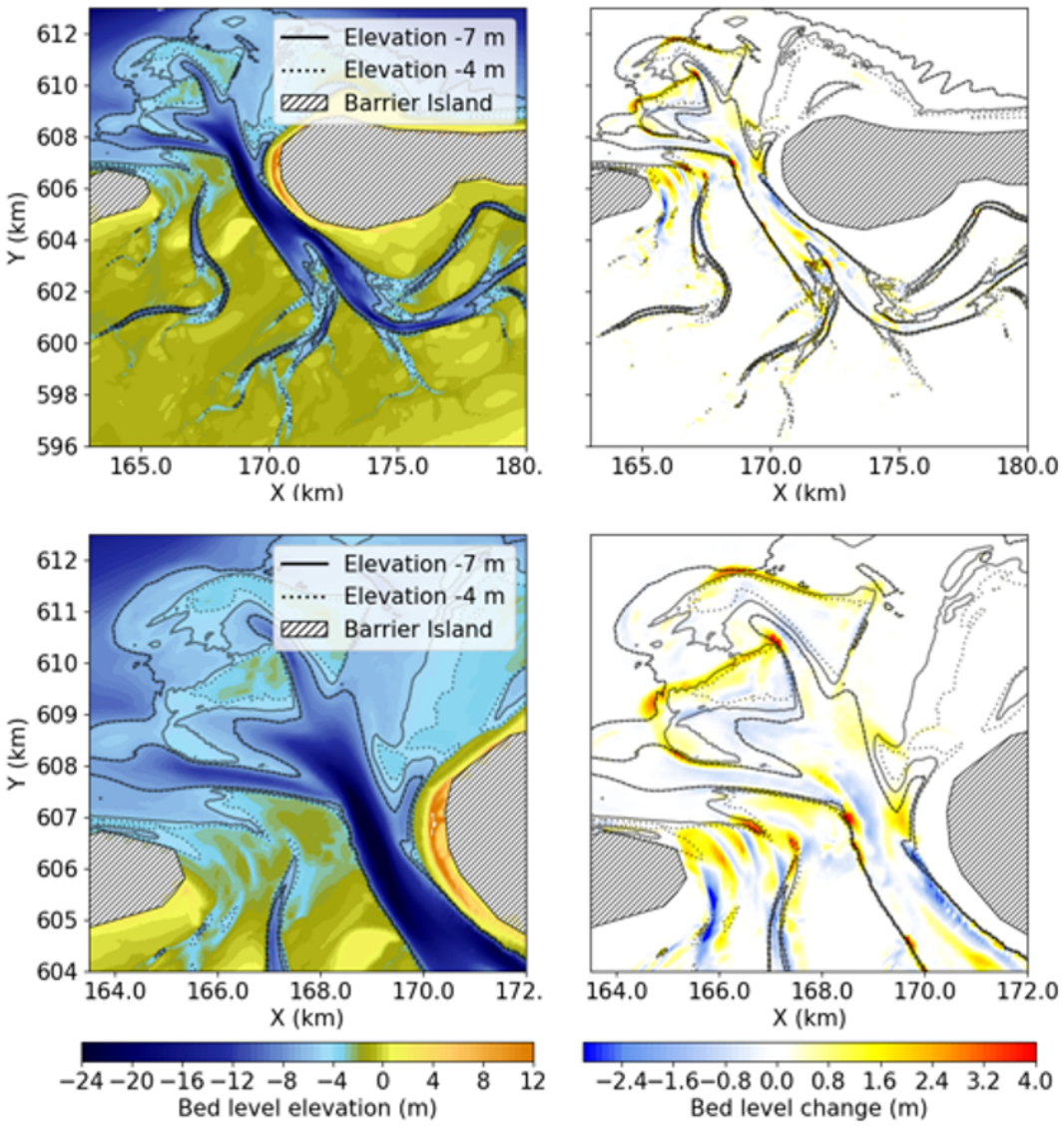

Figure B.8: Top row: Ameland inlet initial bed level (left column) and bed level change (right column) after a 3-month simulation (Wadden Sea domain, wind-inclusive forcing, baseline grid resolution). Bottom row: Zoomed-in version of top row focusing on the ebb-tidal delta.

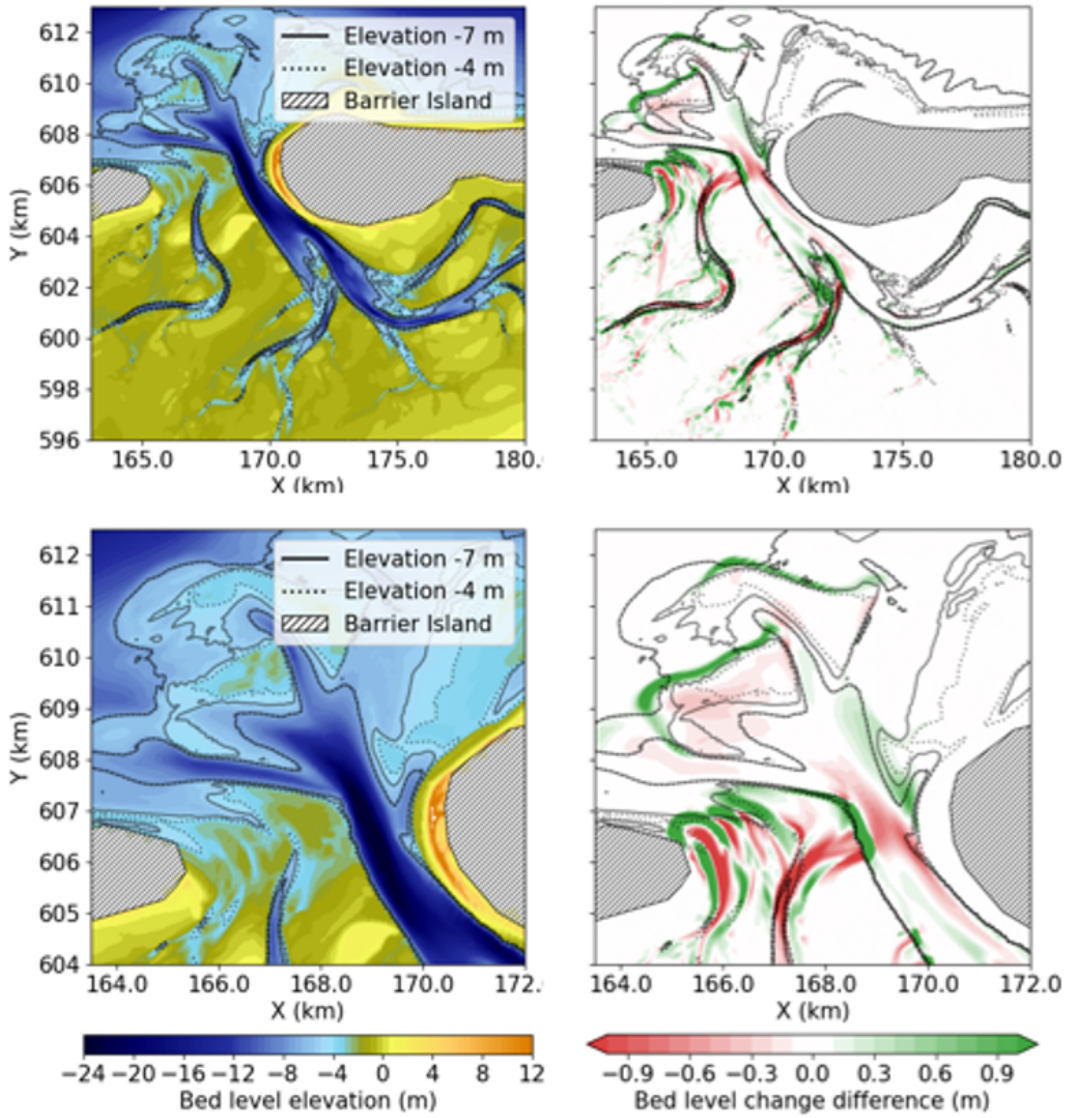

Figure B.9: Top row: Initial bed level of the Ameland inlet (left) and bed level change difference between the Ameland and Wadden Sea models after a 3-month simulation (right), under wind-inclusive forcing and baseline grid resolution. Positive values indicate larger positive bed level changes in the Ameland simulation. Bottom row: Zoomed-in version of the top row focusing on the ebb-tidal delta.

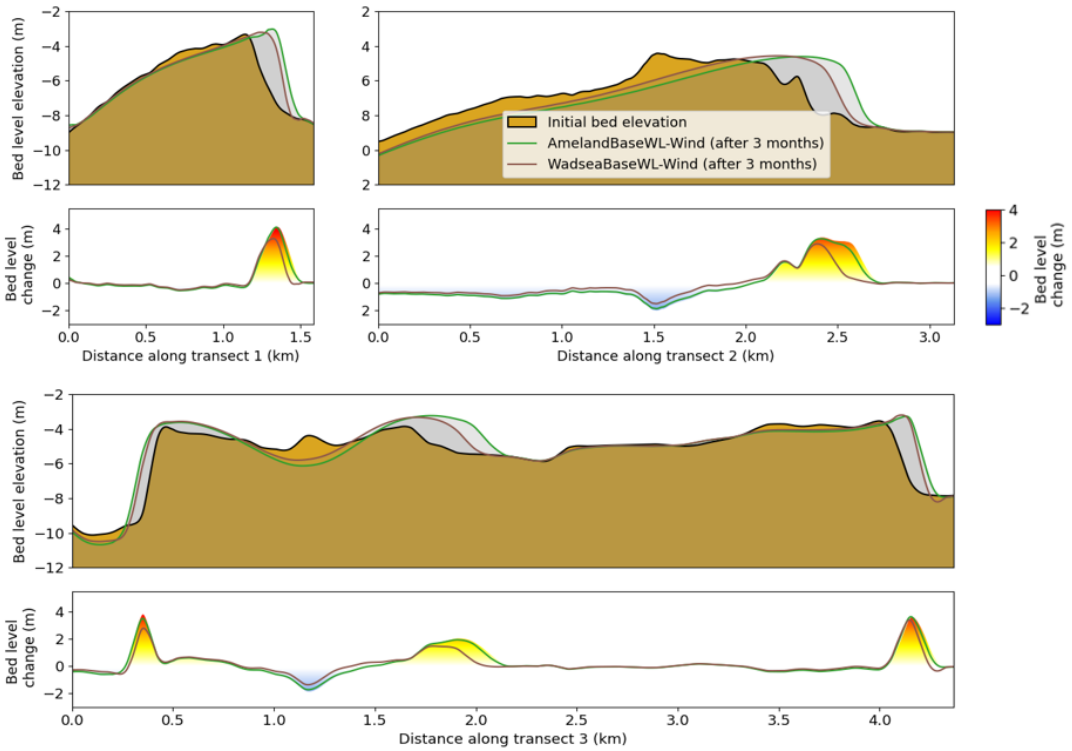

Figure B.10: Transect analyses of bed level change for three distinct transects. Comparison of simulation results for two different model domains with wind-inclusive forcing. Figures 1A, 2A, and 3A show the initial bed level and bed level for the three simulations after 3 months. Figures 1B, 2B, and 3B provide quantified sedimentation and erosion values. The transect numbering is consistent with those presented in Figure 4.7.

C

Variation in resolution

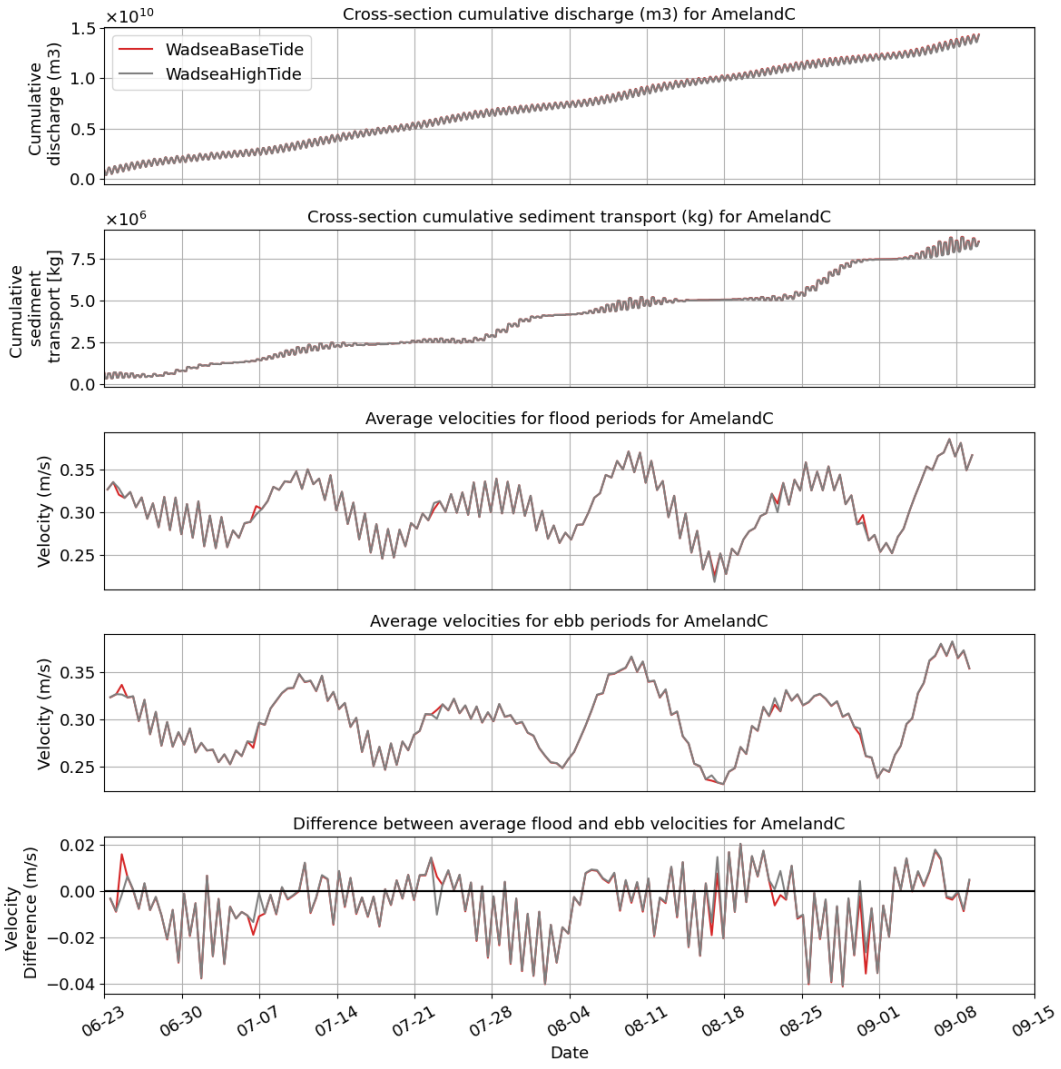

Figure C.1: Comparison of simulation results for the seaside Ameland cross-section for two different grid resolution: 30x30 m cells and 60x60 m cells. The figure showcases five subplots: the topmost plot shows the cumulative discharge for both domains, followed by a plot on cumulative sediment transport. The third and fourth plots illustrate average velocities during flood and ebb periods, respectively. The lower plot highlights the difference between the average flood and ebb velocities (ebb-flood).

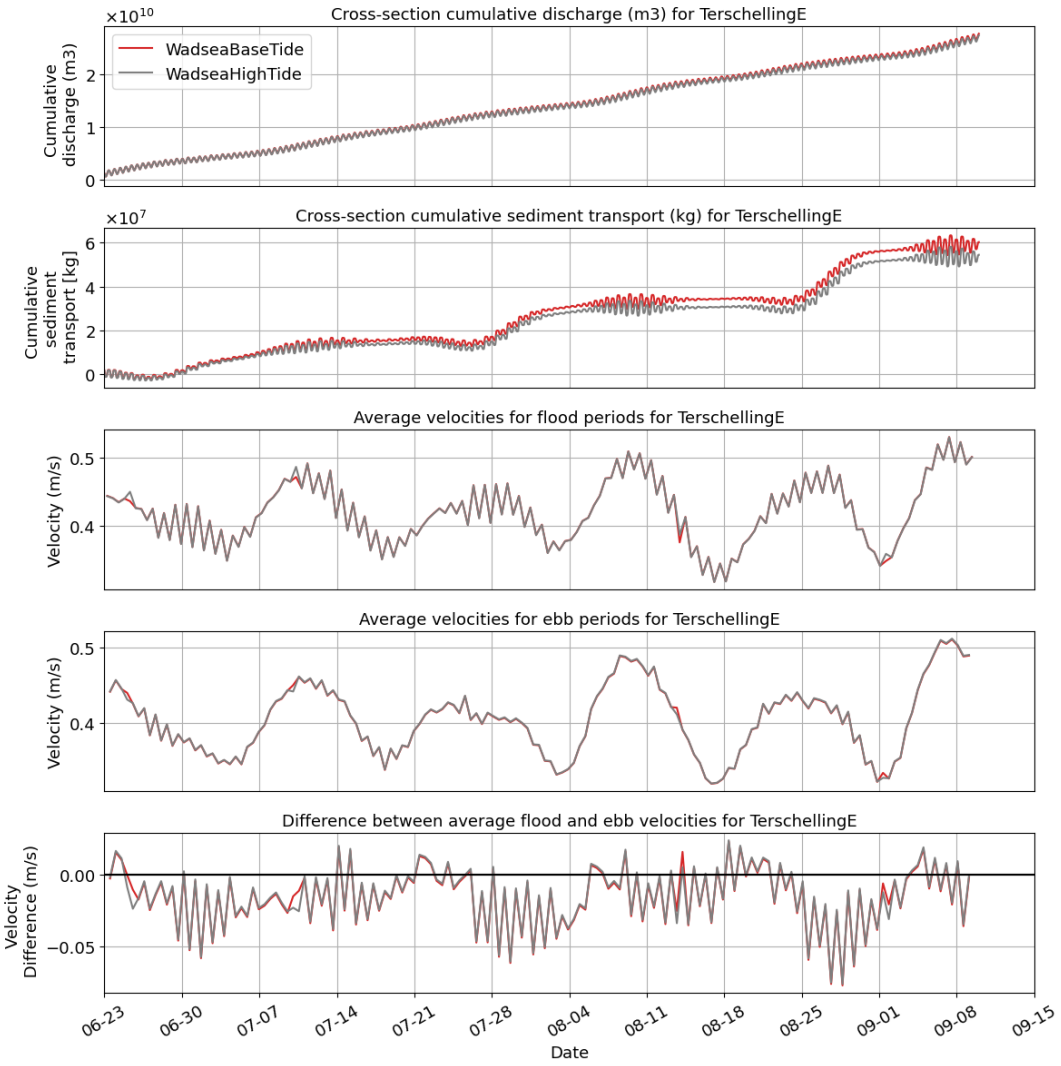

Figure C.2: Comparison of simulation results for the seaside Terschelling cross-section for two different grid resolution: 30x30 m cells and 60x60 m cells. The figure showcases five subplots: the topmost plot shows the cumulative discharge for both domains, followed by a plot on cumulative sediment transport. The third and fourth plots illustrate average velocities during flood and ebb periods, respectively. The lower plot highlights the difference between the average flood and ebb velocities (ebb-flood).

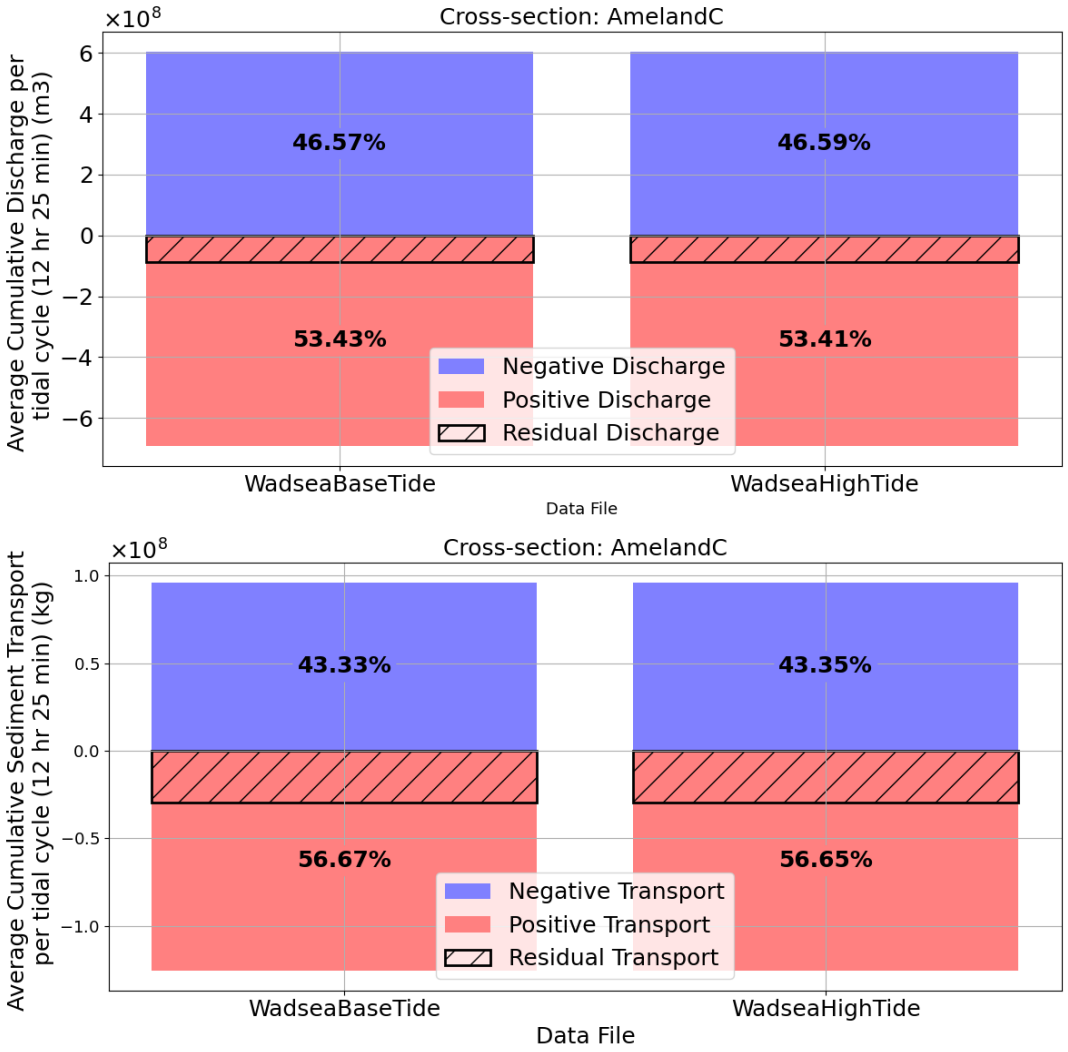

Figure C.3: Comparison of cumulative discharge (top figure) and sediment transport (lower figure) for simulations with different grid resolution under tide-only forcing averaged per tidal cycle (12 hrs, 25 mins) over a 3-month simulation across the seaside AmelandC cross-section. Positive discharge and transport indicate westward and northward flow, while negative values represent southward and eastward flow.

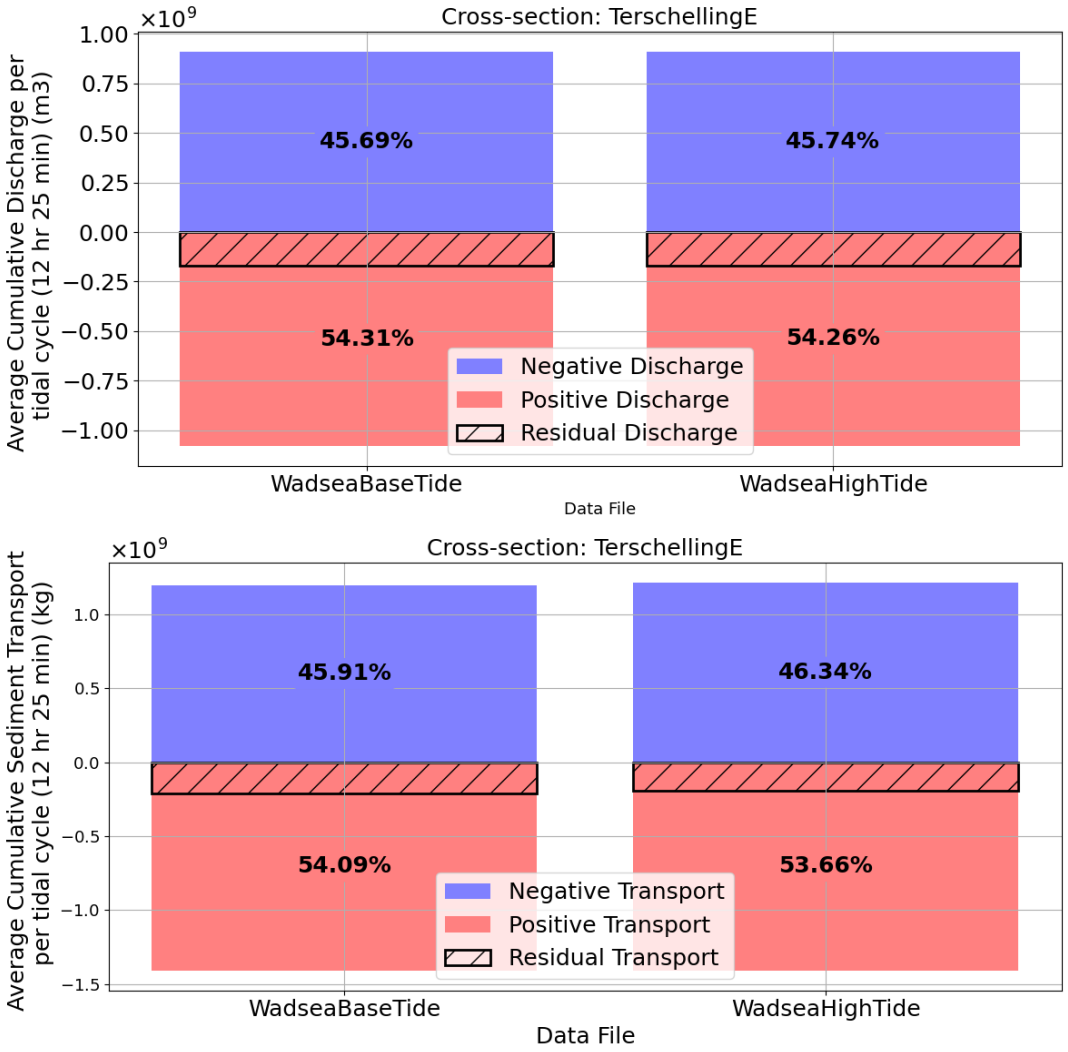

Figure C.4: Comparison of cumulative discharge (top figure) and sediment transport (lower figure) for simulations with different grid resolution under tide-only forcing averaged per tidal cycle (12 hrs, 25 mins) over a 3-month simulation across the seaside TerschellingE cross-section. Positive discharge and transport indicate westward and northward flow, while negative values represent southward and eastward flow.

D

Temporal and spatial visualization of wind flow

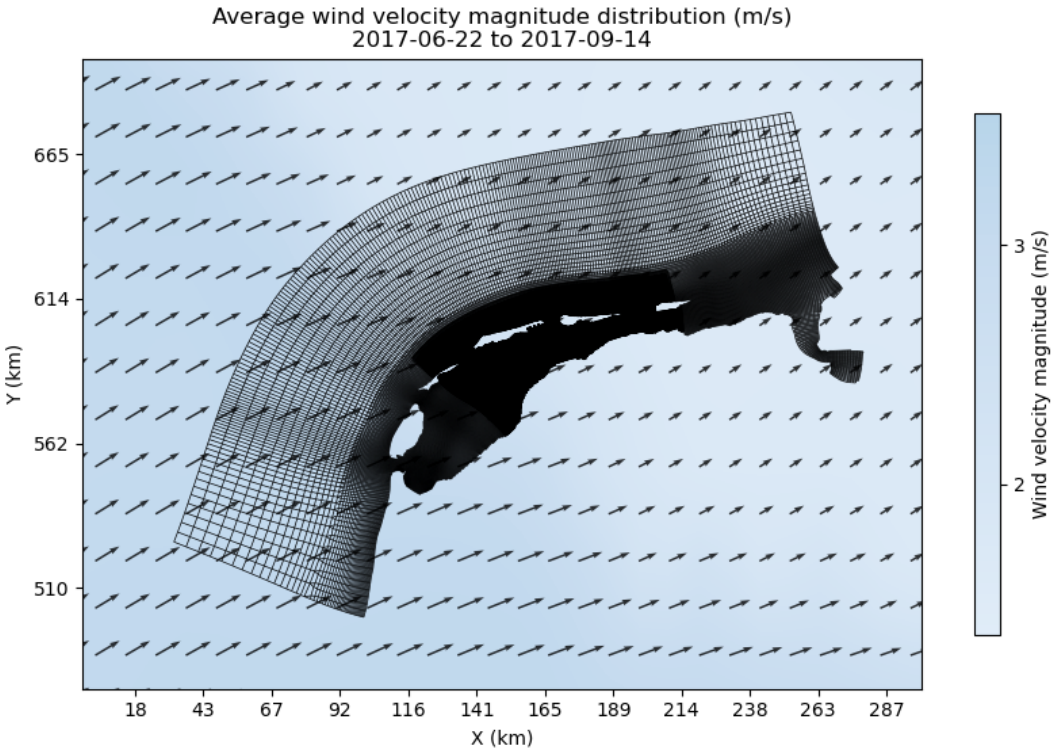

Figure D.1: Average wind flow from 22-6-2017 to 14-9-2017.

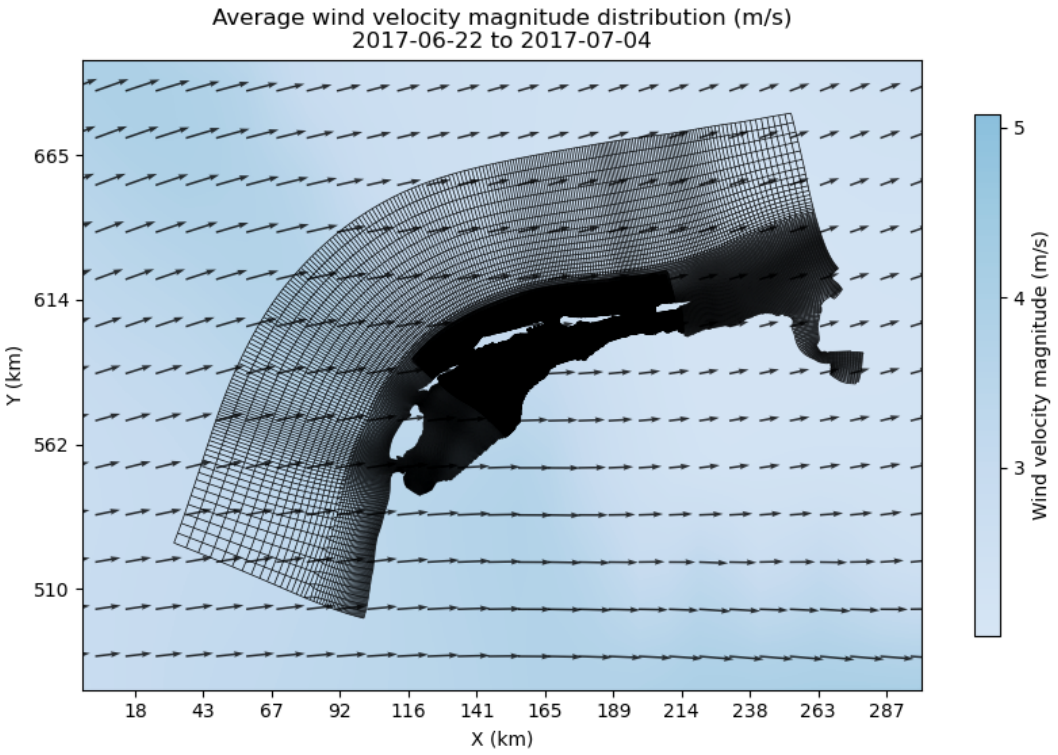

Figure D.2: Average wind flow from 22-6-2017 to 4-7-2017.

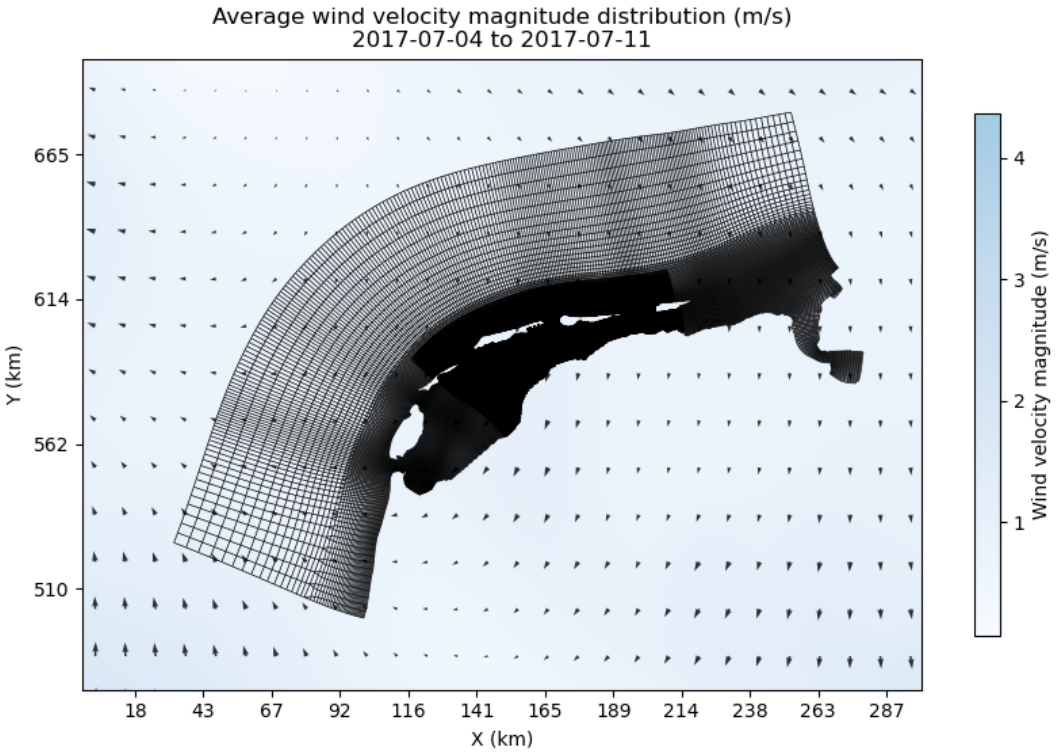

Figure D.3: Average wind flow from 4-7-2017 to 11-7-2017.

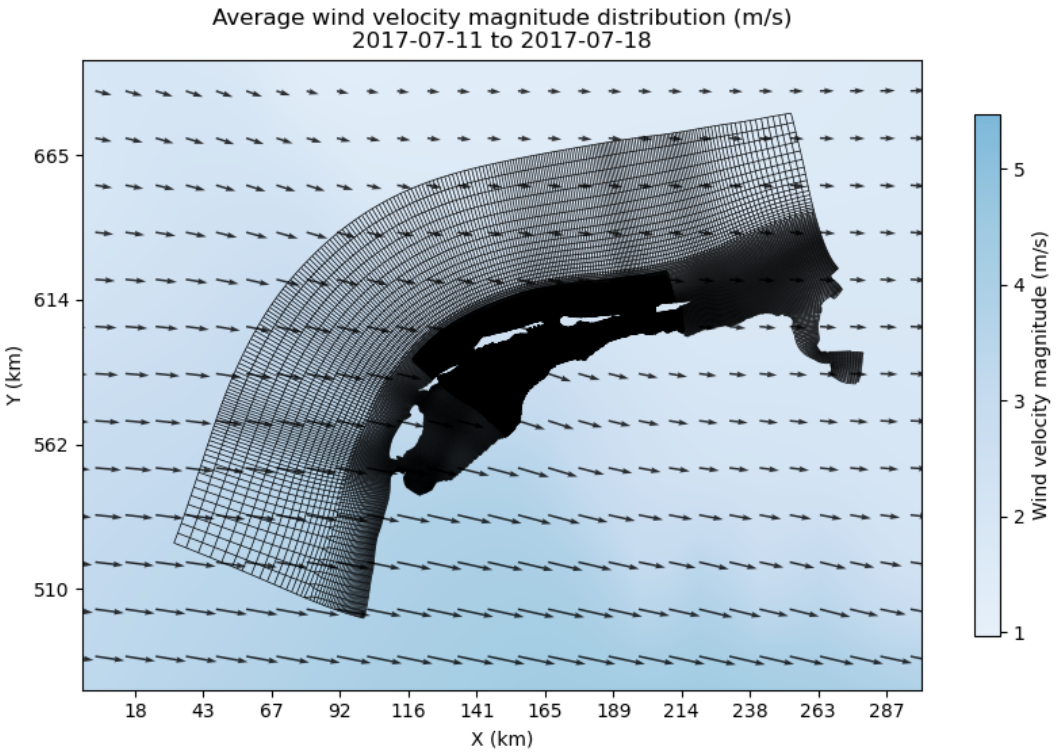

Figure D.4: Average wind flow from 11-7-2017 to 18-7-2017.

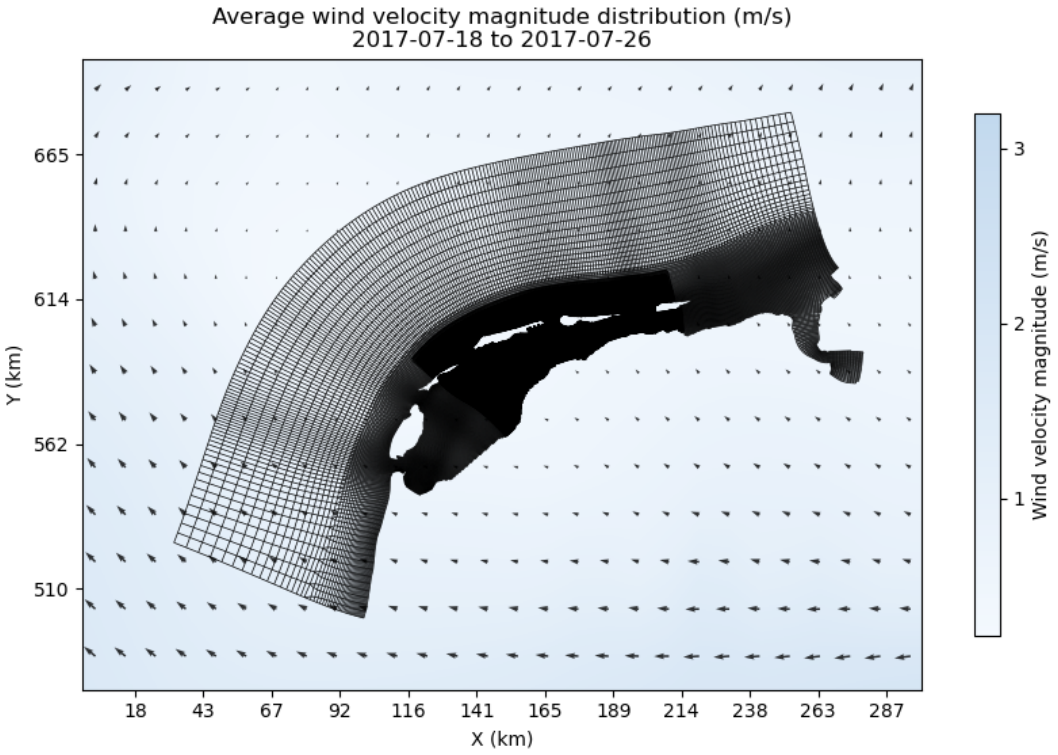

Figure D.5: Average wind flow from 18-7-2017 to 26-7-2017.

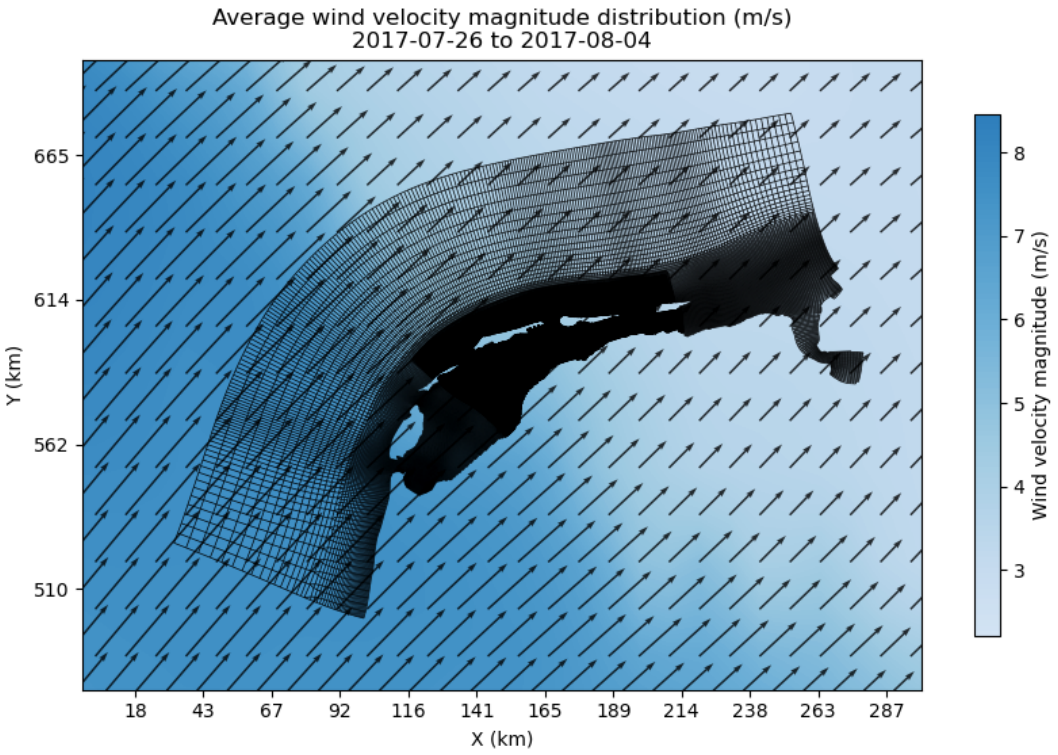

Figure D.6: Average wind flow from 26-7-2017 to 4-8-2017.

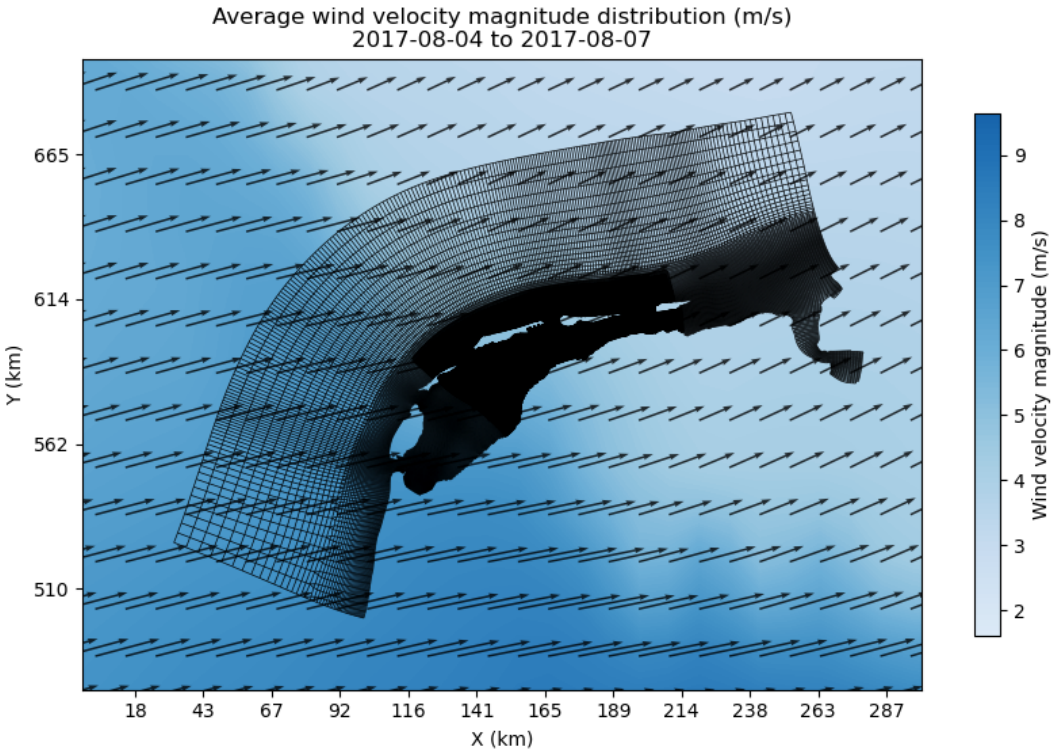

Figure D.7: Average wind flow from 4-8-2017 to 7-8-2017.

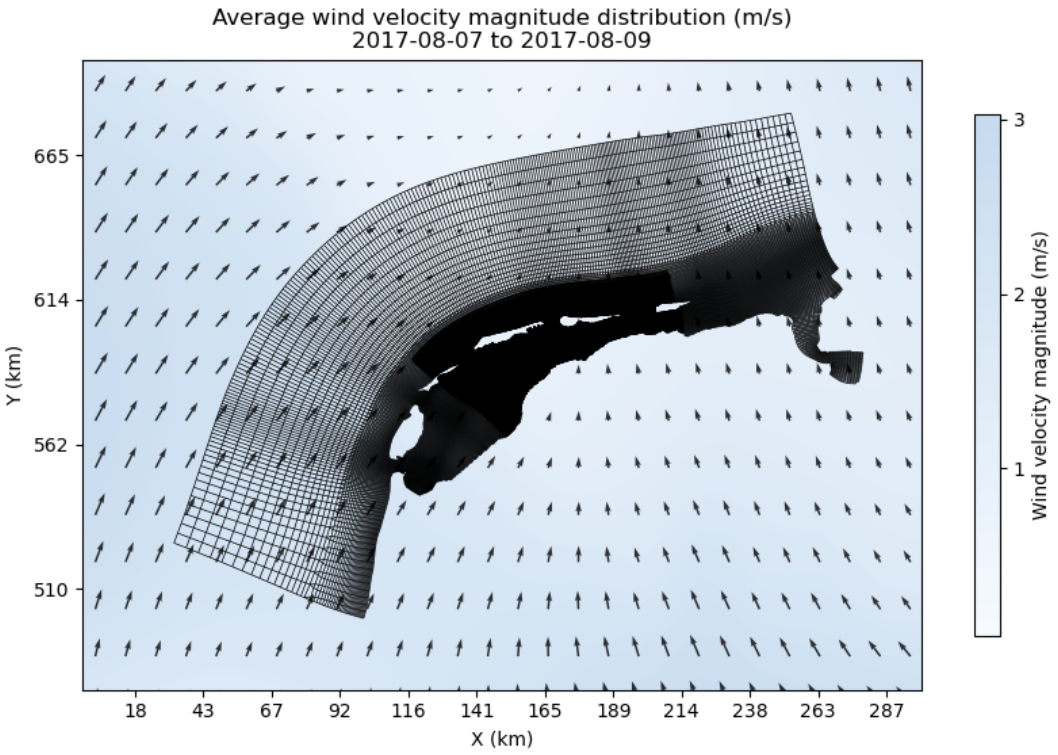

Figure D.8: Average wind flow from 7-8-2017 to 9-8-2017.

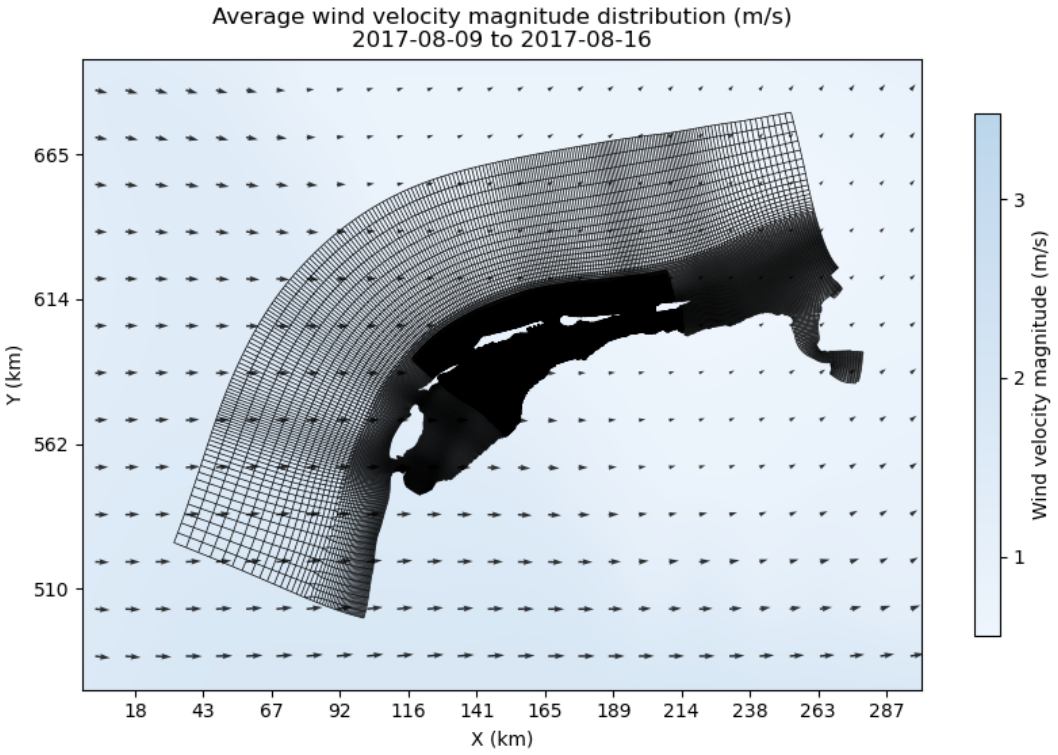

Figure D.9: Average wind flow from 9-8-2017 to 16-8-2017.

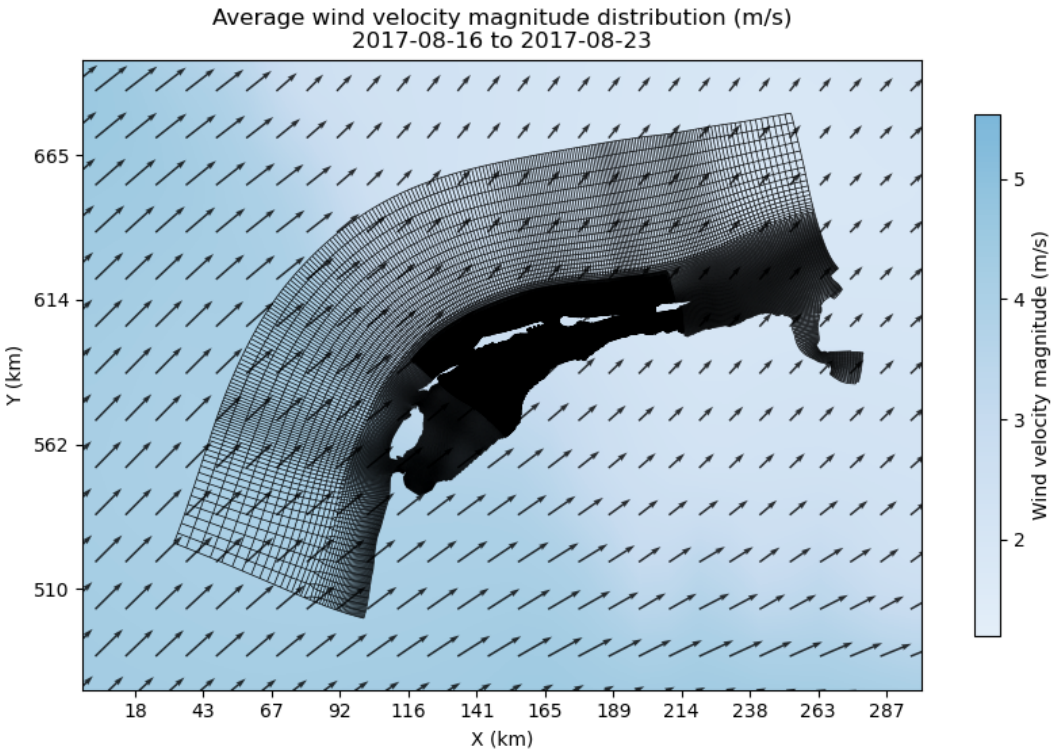

Figure D.10: Average wind flow from 16-8-2017 to 23-8-2017.

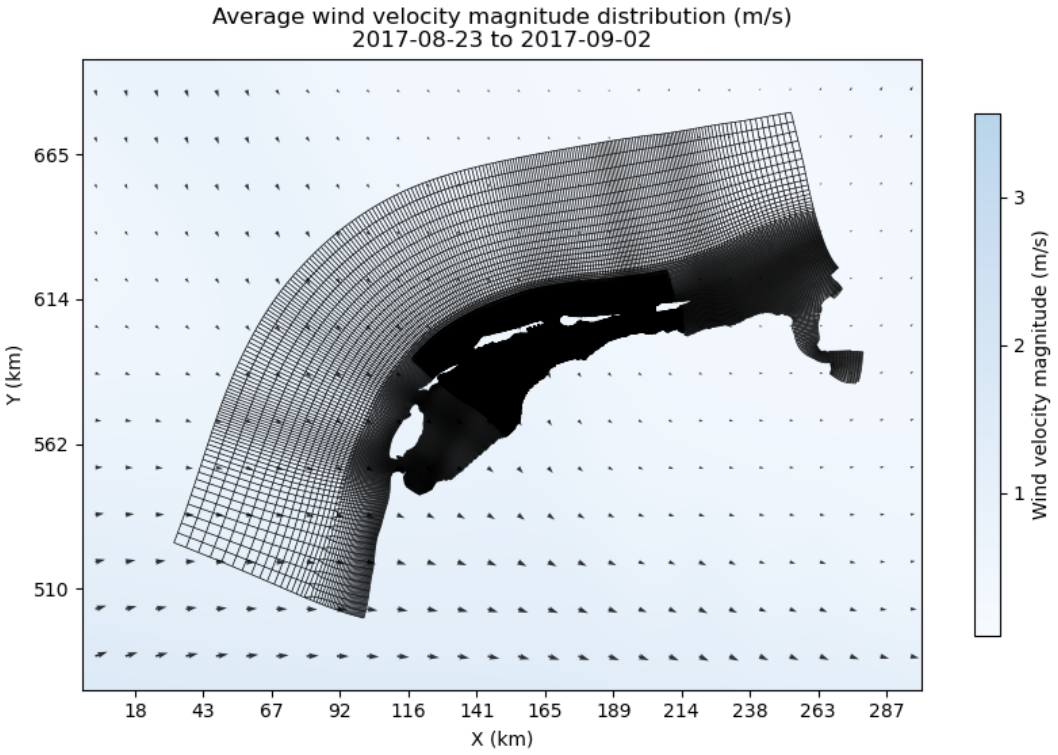

Figure D.11: Average wind flow from 23-8-2017 to 2-9-2017.

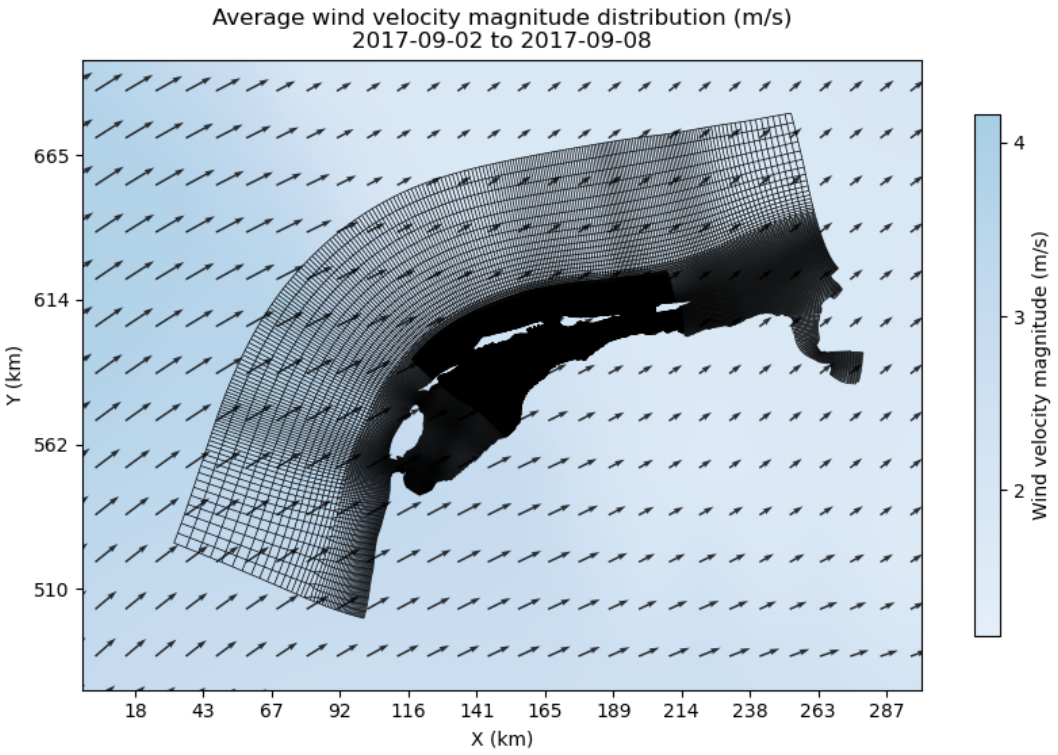

Figure D.12: Average wind flow from 2-9-2017 to 8-9-2017.

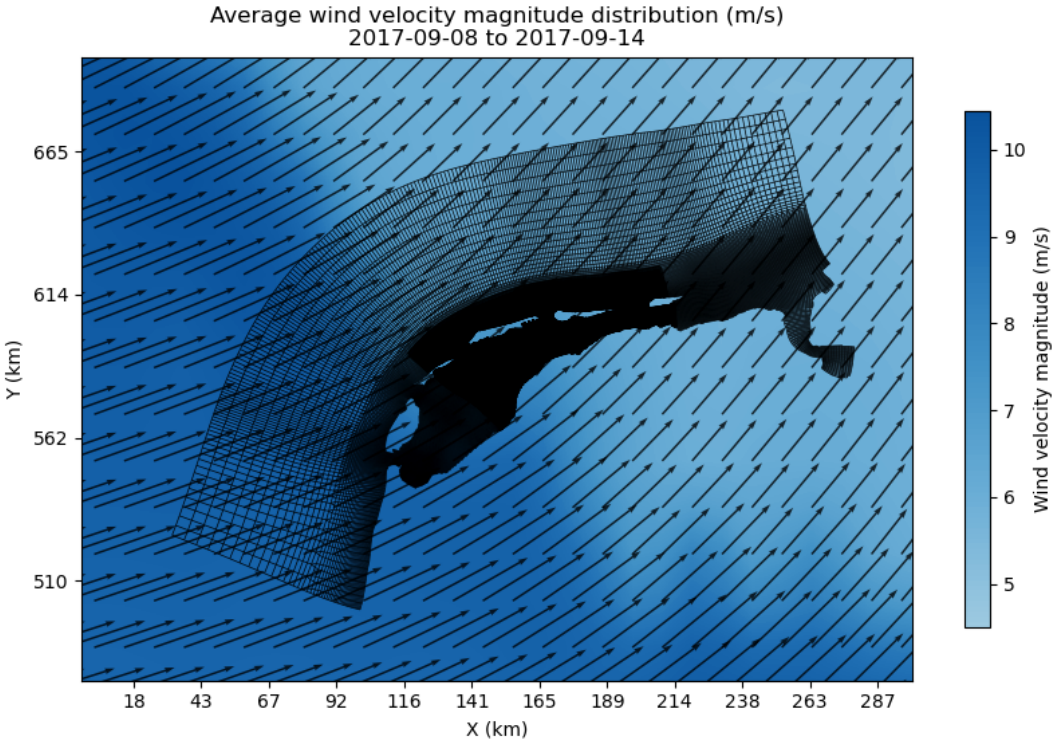

Figure D.13: Average wind flow from 8-9-2017 to 14-9-2017.

E

DelftBlue configuration

Delft High Performance Computing Centre (DHPC) is a department from Delft University of Technology responsible for the use and operation of the DelftBlue supercomputer (figure E.1). The information presented here is based on the official DelftBlue documentation from September 2023 (DelftBlue, nd). This research was conducted during Phase 1 of DelftBlue configuration, which means that there were, among other types of nodes, 228 Intel Xeon compute nodes with each 48 cores. Each faculty and institution of the university can access a share of the supercomputer. As this is a research for a Civil Engineering master study, the education share of CEG-MSC-CE (Civil Engineering and Geosciences, Master, Civil Engineering) has been used. The use had some limits, most notably a run-time per submission of 24 hours and a maximum of 48 CPUs. The base resolution grid and FLOW-only runs took about 8 hours while utilizing 48 CPUs and the high-resolution grid with FLOW-only runs took about double that time.

As the Delft3D-FM software is not installed on DelftBlue, singularity containers of Delft3D-FM were transferred to the DelftBlue worker environment. A singularity container is a portable environment, which includes all the dependencies, libraries and configuration files needed to run Delft3D-FM. The singularity container version used for this research is 2021-04. The reason for not using the most recent version is because model settings were based on older versions of Delft3D-FM, which meant newer singularity container version gave errors when executing the model.

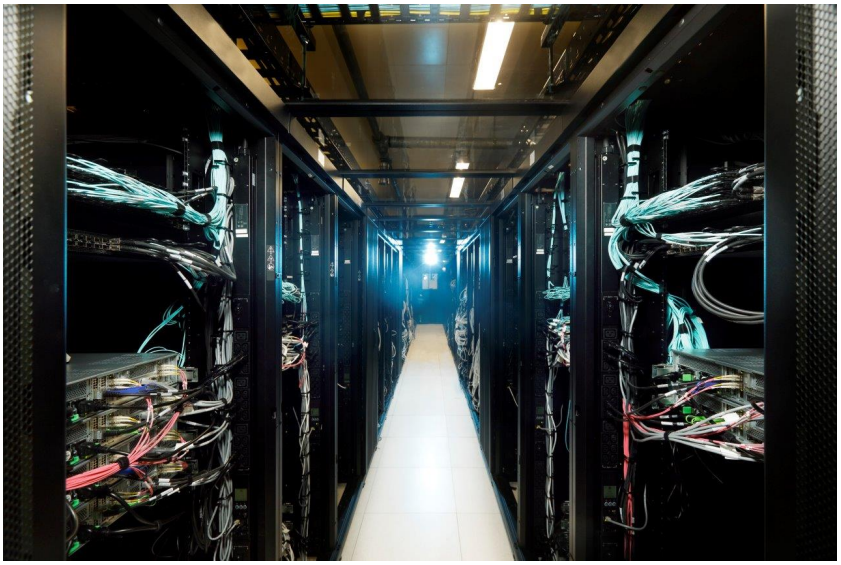

Figure E.1: DelftBlue supercomputer at TU Delft